PhD Thesis

Mathematical programming-based models for the distribution networks' decarbonization

Fernando García Muñoz

Departament d'Enginyeria Elèctrica

Universitat Politècnica de Catalunya

Advisors

Dra. Cristina Corchero
Dr. Francisco Díaz González

Barcelona 2022

To my parents

Acknowledgements

This thesis has been financially supported by the National Agency for Research and Development (ANID) through the Scholarship Program / DOCTORADO BECA CHILE /2018 72190443 and by the Energy System Analytic (ESA) area of Catalonia Institute for Energy Research (IREC).

First of all, I would like to express my most sincere gratefulness to my advisors, Francisco and Cristina, for their supervision, dedication, encouragement and for giving me the freedom to address the topics presented in this work. Many thanks also to Dr. Fei Teng and Dr. Adrià Junyent at the Department of Electrical and Electronic Engineering of Imperial College London for their supervision and collaboration in the last topic. Equally, I am grateful to Dr. Franco Quezada and Dr. Sebastián Dávila at the Department of Industrial Engineering of the Universidad Santiago de Chile to collaborate on the Bender topics.

I would like to thank my parents and brothers for their unconditional support, who from a distance have given me their love in all these years away from home. Many thanks also to my Bilbao family, who have given me all the family warmth during my years living in Spain.

Finally, I would like to thank my girlfriend Mar for being with me every day, supporting me, and making me understand that the essential thing in life is to do what we like.

Abstract

Climate change is pushing to decarbonize worldwide economies and forcing fossil fuel-based power systems to evolve into power systems based mainly on renewable energies sources (RES). Thus, increasing the energy generated from renewables in the energy supply mix involves transversal challenges at operational, market, political and social levels due to the stochasticity associated with these technologies and their capacity to generate energy at a small scale close to the consumption point. In this regard, the power generation uncertainty can be handled through battery storage systems (BSS) that have become competitive over the last few years due to a significant price reduction and are a potential alternative to mitigate the technical network problems associated with the intermittency of the renewables, providing flexibility to store/supply energy when is required. On the other hand, the capacity of low-cost generation from small-scale power systems (distributed or decentralized generation (DG)) represents an opportunity for both customers and the power system operators. i.e., customers can generate their energy, reduce their network dependency, and participate actively in eventual local energy markets (LEM), while the power system operator can reduce the system losses and increase the power system quality against unexpected external failures. Nevertheless, incorporating these structures and operational frameworks into distribution networks (DN) requires developing sophisticated tools to support decision-making related to the optimal integration of the distributed energy resources (DER) and assessing the performance of new DNs with high DERs penetration under different operational scenarios.

This thesis addresses the distribution networks' decarbonization challenge by developing novel algorithms and applying different optimization techniques through three subtopics. The first axis addresses the optimal sizing and allocation of DG and BSS into a DN from deterministic and stochastic approaches, considering the technical network limitation, the electric vehicle (EV) presence, the users capacity to modify their load consumption, and the DG capability to generate reactive power for voltage stability. Besides, a novel algorithm is developed to solve the deterministic

and stochastic models for multiple scenarios providing an accurate DERs capacity that should be installed to decrease the external network dependency. The second subtopic assesses the DN capacity to face unlikely scenarios like primary grid failure or natural disasters preventing the energy supply through a deterministic model that modifies the unbalance DN topology into multiple virtual microgrids (VM) balanced, considering the power supplied by DG and the flexibility provided by the storage devices (SD) and demand response (DR). The third axis addresses the emerging transactive energy (TE) schemes in DNs with high DERs penetration at a residential level through two stochastic approaches to model a Peer-to-peer (P2P) energy trading. To this end, the capability of a P2P energy trading scheme to operate on different markets as day-ahead, intraday, flexibility, and ancillary services (AS) market is assessed, while an algorithm is developed to manage the users' information under a decentralized design.

Nomenclature

Global nomenclature

$i \in \mathcal{B}$	Set of buses.
$k \in \Omega$	Set of type of generation source.
$l \in \Psi$	Set of type of batteries.
$d \in \mathcal{D}$	Set of type of demand response.
$i \in \mathcal{A}$	Set of agents/users that trade energy in the LEM, such that $\mathcal{A} \subset \mathcal{B}$
$t \in \mathcal{T}$	Set of time slots.
$s \in \mathcal{S}$	Set of scenarios.
$(i,j) \in \mathcal{L}$	Set of lines, such that $\mathcal{L} = \{(i,j); i,j \in \mathcal{B}\}$.
$PG_{i,t}^{max}$	Maximum active power output of bus i at period t in [%].
$PG_{i,t}^{min}$	Minimum active power output of bus i at period t in [%].
$QG_{i,t}^{min}$	Minimum reactive power output of bus i at period t in [%].
$QG_{i,t}^{max}$	Maximum reactive power output of bus i at period t in [%].
$PL_{i,t,s}$	Active load of bus i at period t in scenario s [kW].
$QL_{i,t,s}$	Reactive load of bus i at period t in scenario s [kVAr].
V^{min}	Minimum voltage allowed [p.u.].
V^{max}	Maximum voltage allowed [p.u.].
$Bs_{i,j}$	Non-zero upper diagonal bus admittance matrix elements [p.u.].
$S_{i,j}^{max}$	Allowed maximum apparent power of the line between buses i and j [kVA].
$G_{i,j}, B_{i,j}$	Conductance and susceptance of the line between buses i and j such that $i \neq j$ [p.u.].
G_i, B_i	Conductance and susceptance of the line between buses i and j such that $i = j$ [p.u.].

DG_i PV system capacity in bus i [%].

SOC^{min} Minimum state of charge of battery [%].

SOC^{max} Maximum state of charge of battery [%].

φ^{ch} Charging battery efficiency [%].

φ^{ds} Discharging battery efficiency [%].

PB Maximum charge/discharge power for battery i in a period [kW].

BT Battery capacity [kWh].

Δt Time slot (1 h in the models).

M Big M.

$v_{i,t,s}$ Voltage of bus i at period t in scenario s [p.u].

$\theta_{i,t,s}$ Angle of bus i at period t in scenario s, such that $\Delta\theta_{t,s}^{i,j} = (\theta_{i,t,s} - \theta_{j,t,s})$ is a summary expression of the angle difference between bus i and bus j.

$p_{t,s}^{i,j}$ Active power in line between buses i and j at period t in scenario s [kW].

$q_{t,s}^{i,j}$ Reactive power in line between buses i and j at period t in scenario s [kVAr].

Nomenclature for location and sizing problems

Cb_l Capacity cost of storage type l [€k/kWh].

Cp_k Capacity active power cost of generator type k [€k/kW].

Cq_k Capacity reactive power cost of generator type k [€k/kW].

Ds_t^{ev} Discharging EV unplugged at the time t [kWh].

E_i^{ev} Binary parameter for EV location at bus i.

Fl_i^d Maximum number of load type d active in bus i.

H_t Binary parameter for EV connected at the time t.

I_l^{bt} Installation cost of storage type l [€k].

I_k^{gn} Installation cost of generator type k [€k].

M^l Maximum charge/discharge power for battery type l in a period [kW].

OMG_i^k Operational and maintenance cost for generation type k of bus i [€k/kW/yr].

OMB_i^l Degradation cost for battery type l of bus i [€k/kWh].

ψ^{ev} EV storage capacity [kWh].

$Pf_{i,t}$	Fixed active load in bus i at the time t.
Pv_i^d	Variable load of type d in bus i.
$\overline{SOC}_t^{ev}$	Maximum state of charge of the EV at time t [%].
$\underline{SOC}_t^{ev}$	Minimum state of charge of the EV at time t [%].
U_k^g	Maximum generator capacity type k [kW].
U_l^b	Maximum battery capacity type l [kWh].
$\lambda_{t,s}$	Energy price from the grid at the time t in scenario s [€/kWh].
$\gamma_{k,i}^p$	Active power capacity of generator k in bus i [kW].
$\gamma_{k,i}^q$	Reactive power capacity of generator k in bus i [kVAr].
$\gamma_{l,i}^b$	Storage power capacity of battery l in bus i [kWh].
x_i^k	Binary variable: 1 if the generator type k is installed in bus i, 0 otherwise.
y_i^l	Binary variable: 1 if the battery type l is installed in bus i, 0 otherwise.
$pg_{i,t,s}^k$	Active power of generator type k of bus i at period t in scenario s [kW].
$qg_{i,t,s}^k$	Reactive power of generator type k of bus i at period t in scenario s [kVAr].
$gp_{i,t,s}$	Active power from the Grid in bus i at period t in scenario s [kW].
$gq_{i,t,s}$	Reactive power from the Grid in bus i at period t in scenario s [kVAr].
$pl_{i,t,s}$	Active load of bus i at period t in scenario s [kW].
$ch_{i,t,s}^l$	Power absorbed for the storage type l of bus i at period t in scenario s [kW].
$ds_{i,t,s}^l$	Power injected for the storage type l of bus i at period t in scenario s [kW].
$ch_{i,t,s}^{ev}$	Power absorbed for the EV in bus i at period t in scenario s [kW].
$ds_{i,t,s}^{ev}$	Power injected for the EV in bus i at period t in scenario s [kW].
$soc_{i,t,s}^l$	State of charge of battery type l of bus i at period t in scenario s [kWh].
$soc_{i,t,s}^{ev}$	State of charge of EV in bus i at period t in scenario s [kWh].
$w_{i,t,s}^l$	Binary variable: 1 if the battery type l is charging in bus i at period t in scenario s, 0 otherwise.
$w_{i,t,s}^{ev}$	Binary variable: 1 if the EV is charging in bus i at period t in scenario s, 0 otherwise.
$\tau_{i,t,s}^d$	Binary variable: 1 if the load type d is active in bus i at time t in scenario s, 0 otherwise.

Nomenclature for microgrids clustering problem

U_k^g	Active power capacity installed of generator type k [MW].
U_k^q	Reactive power capacity installed of generator type k [MW].
U_l^b	Active power capacity installed of battery type l [MWh].
Y_i^l	Binary parameter representing if a battery type l is installed in node i.
$\lambda_{i,t}$	Virtual active and reactive power of bus i at period t [MW].
$\gamma_{i,t}$	Active and reactive power supplied on bus i at period t [MW].
$\delta_{i,t}$	Active and reactive power not-supplied on bus i at period t [MW].

Nomenclature for P2P energy trading problems

κ^{max}	Maximum substation power.
$\lambda_{t,s}^{bg}$	Price of the energy bought from the grid at time t in scenario s.
λ^{sg}	Feed in Tariff or net metering price.
ρ_s	Probability of the scenario s.
κ_t^{bg}	Energy bought from the grid through the substation at period t [kW]
κ_t^{sg}	Energy sold to the grid through the substation at period t [kW]
$\Delta p_{i,t,s}$	Difference between the energy self-generated and the consumption in bus i at period t in scenario s [kW].
$pg_{i,t,s}$	Energy self-generated in bus i at period t in scenario s [kW].
$p_{i,t,s}^{bg}$	Energy bought from the grid by the bus i at the period t in scenario s [kW].
$p_{i,t,s}^{sg}$	Energy sold to the grid by the bus i at the period t in scenario s [kW].
$p_{i,t,s}^{bm}$	Energy bought from the market by the bus i at the period t in scenario s [kW].
$p_{i,t,s}^{sm}$	Energy sold to the market by the bus i at the period t in scenario s [kW].
$q\kappa_{i,t,s}^{bg}$	Reactive power bought from the grid through the substation of bus i at period t in scenario s [kVAr].
$ch_{i,t,s}$	Power absorbed for the storage of bus i at period t in scenario s [kW].
$ds_{i,t,s}$	Power injected for the storage of bus i at period t in scenario s [kW].
$soc_{i,t,s}$	State of charge of battery of bus i at period t in scenario s [kWh].

$\varepsilon_{i,t,s}$ Losses of bus i at period t in scenario s [kWh].

$q\kappa_t^{as}$ Total reactive power injected to the main grid at period t [kVAr].

$\Delta ch_{i,t,s}$ Additional power absorbed by the battery in bus i at period t in scenario s to face the community electricity consumption uncertainty. [kW].

$\Delta ds_{i,t,s}$ Additional power injected by the battery in bus i at period t in scenario s to face the community electricity consumption uncertainty.

$ch_{i,t,s}^{cb}$ Power absorbed by the community battery in bus i at period t in scenario s [kW].

$ds_{i,t,s}^{cb}$ Power injected from the community battery in bus i at period t in scenario s [kW].

$qds_{i,t,s}^{cb}$ Reactive power dispatched from the community battery in bus i at period t in scenario s [kVAr].

$qds_{i,t,s}$ Reactive power dispatched from the storage in bus i at period t in scenario s [kVAr].

$qg_{i,t,s}$ Reactive power generated in bus i at period t in scenario s [kVAr].

$w_{i,t,s}$ Binary variable: 1 if the battery is charging in bus i at period t in scenario s, 0 otherwise.

$y_{i,t,s}$ Binary variable: 1 if the agent in bus i at period t in scenario s has an energy surplus, 0 otherwise.

List of acronyms

ADMM	Alternating direction method of multipliers
ADN	Active distribution network
BD	Benders algorithm
BSS	Battery storage system
CB	Community batteries
CDA	Continuous double-auction
CM	Community manager
DEP	Distribution expansion planning
DER	Distributed energy resource
DG	Distributed generation
DN	Distribution network
DR	Demand response
DSO	Distribution system operator
DSR	Demand side response
EC	Energy community
ENS	Energy not-supplied
ESS	Energy storage system
EV	Electric vehicle
FF	Fitness function
FIT	Feed-in tariff
GA	Genetic algorithm
LEM	Local energy market

LP	Linear problem
LVF	Losses-Voltage-Factor
MG	Microgrid
MILP	Mixed-integer linear problem
MINLP	Mixed-integer non-linear problem
MISOCP	Mixed-integer second-order conic programming
MP	Master problem
OF	Objective function
OPF	Optimal power flow
P2P	Peer-to-peer
PEV	Plug-in electric vehicle
PSO	Particle swarm optimization
PV	Photovoltaic system
QC	Quadratic convex
QP	Quadratic programming
RES	Renewable energy source
SDP	Semi-definite programming
SOC	State of charge
SOCP	Second-order cone programming
SP	Subproblem
TE	Transactive energy
TSO	Transmission system operator
TSS-MINLP	Two-stage stochastic mixed-integer non-linear problem
VM	Virtual microgrid
VMTS	Virtual microgrids topology scheduling
WT	Wind turbine system

Contents

1 Introduction **1**

1.1 Context and motivation 1
1.2 Thesis objectives 3
1.3 Thesis contributions 4
1.4 Thesis outline 6

2 An algorithm to solve the optimal sizing and location of DERs problem **8**

2.1 Introduction 8
2.2 Literature review 9
2.3 Location and sizing optimization model for a DN 11
2.3.1 Islanded mode 11
2.3.2 Grid-connected mode 14
2.4 Linear optimization model 15
2.5 Algorithm for sizing & location of DGs and BSS 17
2.5.1 Proposal 17
2.5.2 Operation 17
2.5.2.1 Chromosome structure 17
2.5.2.2 Set initial parameters 18
2.5.2.3 Create an initial population 18
2.5.2.4 GA and LP model 20
2.5.3 Convergence 20
2.6 Case study and computational results 21
2.6.1 Case study 21
2.6.2 Model validation 22
2.6.3 Worst-case scenario and parameters 22
2.6.4 Algorithm performance 23
2.6.5 Case: Off-grid operation 25

2.6.6 Case: grid-connected . . . 26
2.7 Chapter conclusions . . . 28

3 On the optimal sizing and location of DERs: A two-stage stochastic approach including EVs and DR 30
3.1 Introduction . . . 30
3.2 Literature review . . . 31
3.3 Mathematical Formulation . . . 33
3.4 Methodology . . . 36
3.4.1 DER units and loads modelling . . . 37
3.4.2 Scenarios creation . . . 38
3.4.3 Linearization method . . . 39
3.4.4 Algorithm description . . . 40
3.4.5 Reactive power capacity . . . 40
3.4.6 Cost modelling . . . 41
3.5 Case study and computational results . . . 42
3.5.1 Network and data parameters . . . 42
3.5.2 Case studies . . . 44
3.5.3 Computational results . . . 45
3.5.4 Flexible demand and electric vehicles . . . 48
3.6 Discussion and model limitations . . . 50
3.7 Chapter conclusions . . . 54

4 A virtual microgrids scheduling model 55
4.1 Introduction . . . 55
4.2 Literature review . . . 56
4.3 Problem definition and methodology . . . 58
4.4 Optimal model for scheduling virtual microgrids topology . . . 59
4.4.1 Model without flexible demand . . . 60
4.4.2 Model with flexible demand . . . 63
4.5 Case study . . . 64
4.5.1 Model performance . . . 65
4.5.2 Mathematical model operation . . . 66
4.5.3 Weakest nodes . . . 68
4.5.4 Energy for flexibility market . . . 68
4.5.5 Dynamic topology . . . 70
4.6 Chapter conclusions . . . 70

5 A Benders decomposition approach for solving a P2P energy trading problem under uncertainty 75
5.1 Introduction . . . 75
5.2 Literature review . . . 76
5.2.0.1 Deterministic approaches . . . 76
5.2.0.2 Stochastic approaches . . . 78
5.3 Problem definition . . . 80
5.3.1 Market design . . . 80
5.3.2 Two-stage stochastic approach . . . 81
5.3.3 Centralized model . . . 82
5.3.3.1 Network technical constraints . . . 83
5.3.3.2 Battery modelling . . . 85
5.3.3.3 Local energy market rules . . . 85
5.4 Decentralized approach . . . 86
5.4.1 Preliminaries . . . 86
5.4.2 The Benders decomposition approach (BD) . . . 88
5.4.2.1 Master Problem . . . 88
5.4.2.2 Subproblems . . . 89
5.4.2.3 Strengthened Benders' cuts . . . 89
5.4.3 Cut strategy . . . 91
5.4.4 Summary . . . 92
5.5 Computational results . . . 93
5.5.1 Case study parameters . . . 93
5.5.2 Algorithm convergence and scalability assessment . . . 95
5.5.3 Numerical results . . . 98
5.5.4 Model assessment under different assumptions . . . 99
5.5.5 Local energy market and batteries behavior . . . 100
5.5.6 Local energy market pricing . . . 101
5.5.7 Agents profits . . . 101
5.5.8 Future research and discussion . . . 102
5.6 Chapter conclusions . . . 104

6 A stochastic model to measure the reactive power supplied by DERs under a P2P energy trading scheme 105
6.1 Introduction . . . 105
6.2 Literature review . . . 106

6.3 System description . . . 110
6.3.1 Two-stage stochastic programming approach . . . 110
6.3.2 Market framework . . . 111
6.3.3 Pricing . . . 112
6.3.4 Assumptions . . . 113
6.4 Mathematical formulation . . . 114
6.4.1 Local energy market constraints . . . 114
6.4.2 Agents battery modeling . . . 116
6.4.3 Community battery modeling . . . 116
6.4.4 Battery flexibility detection . . . 117
6.4.5 Network technical limitation . . . 117
6.5 Computational results . . . 118
6.5.1 System data . . . 119
6.5.2 Numerical results . . . 119
6.5.2.1 Case A and B analysis . . . 120
6.5.2.2 Case A' and B' analysis . . . 121
6.5.2.3 Local energy market share . . . 122
6.5.2.4 Reactive power capability . . . 123
6.5.2.5 Community battery role . . . 124
6.5.3 Individual profit . . . 124
6.6 Chapter conclusions . . . 126

7 Conclusions **128**
7.1 Further work . . . 130

Bibliography **132**

A List of Publications **151**
A.1 Journal articles . . . 151
A.2 Conference articles . . . 152
A.3 Other publications . . . 152

List of Figures

1.1 Summary thesis structure and scope 7

2.1 Algorithm for sizing & location of DGs and BSS 19
2.2 Example of a chromosome structure 20
2.3 The hypothetical worst-case scenario of 192 consecutive hours. 23
2.4 Algorithm convergence 24
2.5 DERs location into the distribution network for off-grid operation case 26
2.6 Energy seasonality for off-grid case. The curves have been normalized considering, for each one of them, the highest values over the 12 months 26
2.7 Energy seasonality for grid-connected case. Battery charge has been discounted from the energy generated by the WT 28

3.1 Methodology scheme 37
3.2 Modified IEEE 69-bus distribution network 44
3.3 Total capacity installed of WT, PV, lead-acid battery (BT 1), and Li-ion battery (BT 2) for every case study. 45
3.4 Normalized curves of Wind Turbine (WT), Photovoltaic system (PV), Aggregate Load (Load), and Energy Price for every scenario belonging to every case study 46
3.5 Annual aggregate energy in a 24-hour view 48
3.6 Annual aggregate energy in a monthly view 49
3.7 Aggregate charge (Ch) and discharge (Ds) by hour of the electric vehicles compared with their aggregated state of charge (SOC). 50
3.8 Flexible demand uses by hour for every scenario and case study . . . 51

4.1 Methodology structure for self-adaptive distribution networks 60
4.2 Capacity and location for DERs in the PG&E 33-bus radial distribution network. 64

4.3 The four consecutive scenarios of 72 hours. The vertical axis is the percentage of the total capacity that can be used by the WT/PV or the percentage of the energy demand for every hour. 65
4.4 Scenario 4: electricity demand fulfillment behavior 67
4.5 Scenario 4: SOC of batteries vs. load, and wind/irradiation resources available 67
4.6 PG&E 33-bus radial DN partitioning for the second scenario at 46h. Red balls indicate the loads reduced to zero, without considering DSR into the model 72
4.7 PG&E 33-bus radial DN partitioning for the second scenario at 46h. Considering DSR into the model 72

5.1 P2P energy trading schematic diagram modeled 81
5.2 Modified IEEE 69-bus distribution network. 94
5.3 Residential load profiles for three different scenarios. 96
5.4 Scenarios for the energy prices, the PV power generation, and the aggregated residential loads. 96
5.5 Algorithm convergence 98
5.6 Energy share for a case (A) under a P2P energy trading scheme, (B) without Energy trading, (C) considering energy trading but linear batteries, and (D) Energy trading such as batteries and the market trading are linear variables. 100
5.7 Hourly market and battery behaviour 101
5.8 Local energy market pricing compared with the FIT and the grid price, corresponding to the third scenario 102
5.9 Agents profit comparison between using P2P energy trading or not for different scenarios 103

6.1 P2P energy trading scheme considering community battery bank and reactive power 110
6.2 P2P energy trading frameworks. A: P2P energy trading with CB, B: P2P energy trading without CB, A': P2P energy trading with CB and detecting the flexibility provided by the agents' batteries, and B': P2P energy trading detecting the flexibility provided by the agents' batteries. 113
6.3 Test system 119
6.4 Energy share by agents 123
6.5 Reactive power supplied with and without ASs 123

6.6 Community batteries effect on the second stage variables 125
6.7 Agents profit comparison when they operate under P2P energy trading providing ASs and when they not 126

Chapter 1

Introduction

1.1 Context and motivation

Decarbonizing the worldwide economies to reduce greenhouse emissions is forcing the electric power systems to rethink their current operational and structure schemes to include more renewable technologies into the energy supply mix. In this regard, the RES cost reduction and the constant BSS improvements become these technologies in a powerful alternative to boost their penetration in the current energy matrix and speed up the energy transition. Expressly, the IRENA report [1] declares a cost reduction of utility-scale solar photovoltaics (PV) and onshore wind (WT) of 85% and 56%, respectively, between 2010 and 2020, while according to [2], the lithium-ion batteries showed a drastic drop in prices around 87% from above 1100 $/kWh in 2010 to 156 $/kWh in 2019. In this way, following the objectives and guidelines established in the Paris agreement, renewables are expected to represent two-thirds of energy consumption and 86% of power generation in 2050 [3].

However, according to the above context, renewables expansion in transmission and distribution systems requires proper planning to handle the new operational and market management opportunities in highly decarbonized networks to allow a flexible, secure, and sustainable integration. For example, in the DNs field, one of the challenges from the planning perspective corresponds to the optimal location and sizing of DERs to reduce the system losses and increase the DN autonomy and resilience [4]. The problems related to the optimal location and sizing are not new in the optimization field; however, their application in the electricity networks planning field brings some challenges related to the network technical limitation and stochasticity associated with the electricity load and the power generated through the DG. Specifically, the constraints to properly represent the physical and technical network limitations are non-linear and non-convex, which may significantly increase the model

execution time under a multiperiod context. On the other hand, the multiperiod scenarios required to include the stochasticity of renewable sources representatively must be extensive and consider multiple different periods to obtain the optimal DERs capacity while the investment and the main grid dependency are minimized. Besides, the formulation must consider the trade-off between the expected power provided by the DERs and the power supplied by the main grid since higher installed capacity implies high autonomy but a significant investment. Thus, the optimal location and sizing of DERs have received increased research attention in the last few years, and it is one of the problems addressed in this thesis.

From the operational perspective, one of the challenges of DNs with high DERs penetration is the capacity to face unexpected main grid failures in electricity provision. However, it is worth noting that one of the consequences of the problem mentioned in the previous paragraph corresponds to that meeting 100% of the electricity demand with DERs requires a high investment due to their stochasticity. Thus, the main grid must supply part of the electricity demand not covered by the DERs, and any failure in the main grid provision or natural disasters could prevent a regular network operation causing balance problems and supply cuts to the DN. Under these failure scenarios, microgrids (MG) appear as a potential alternative to increase reliability and resiliency due to their capacity to operate in islanded or grid-connected mode. MGs usually are applied into DNs through multiple-MG interconnected; however, over the last few years, some researchers have introduced the concept of virtual or dynamic MGs (VMs), which consist of MGs with dynamic boundaries that can expand or shrink their boundaries depending on available local DERs [5]. This new dynamic operational mode may increase the DN and microgrids' efficiency, autonomy, and resiliency while minimizing the load not supplied by the network under inspected scenarios. Thus, some researchers have considered this new concept of VM to face unexpected scenarios in the last few years, turning it into the second topic managed in this thesis.

Another operational challenge is the new market structures that have emerged as an alternative to face an increasing penetration of DERs in low-voltage DN in the hands of more empowered, aware, and active residential consumers. These new prosumers have opted for self-consumption supported by BSS to reduce the electricity bill, and their dependence on the grid [6] forcing the DNs to restructure their traditional unidirectional electricity supply to a more flexible structure. P2P energy trading belongs to this new structure that seeks to increase the efficiency of the energy self-generated by selling and buying the prosumers' energy surplus within a local

energy market (LEM). Thus, the residential areas or energy communities composed of prosumers and consumers willing to exchange energy surplus are the baselines of this trading scheme [7], which possesses some modeling challenges. For example, a suitable model should include the DN limitations, the DGs stochasticity, the storage devices operation, and some market rules, i.e., that the LEM does not allow simultaneous energy selling and buying by the users, among others. In this regard, the models that allow representing P2P energy trading have become the focus of many research works over the last few years, and it is the third problem addressed in this thesis.

The three situations described above emerge as a consequence of the energy transition to decarbonize the current power systems and from DNs with high DERs penetration. Likewise, the optimization techniques provide a suitable mathematical framework to address these three problems, allowing the decision-makers proper assessment. Therefore, this thesis pretends to contribute to the DN transition process, presenting deterministic and stochastic optimization approaches to address i) the optimal placement and sizing of DERs into DNs, ii) the optimal scheduling of VM to face unexpected main grid failures in the electricity provision, and iii) the optimal scheduling for community energies operating under transactive energy (TE) schemes.

1.2 Thesis objectives

The main objectives addressed in this thesis, considering the context and the motivation described above, are pointed out below:

- **O1:** To formulate a deterministic and stochastic optimization model to address the optimal location and sizing of DG and BSS into a DN considering the investment, operation costs, and network limitations.

- **O2:** To develop an algorithm to solve the deterministic and stochastic optimal DERs location and sizing problem defined in the O1 for multiples scenarios or scenarios greater than 24 hours, considering characteristics of highly decarbonized networks, such as the heterogeneity of distributed consumption, generation, and energy storage assets.

- **O3:** To assess the potentialities of demand flexibility and the electric vehicles in mathematical optimization tools for the location and sizing of DG into a DN.

- **O4:** To review the current partitioning methods applied to DNs that increase network resilience under main grid failures and create an optimization-based tool to manage the DN partitioning in multiple VMs while the load curtailment is minimized and the use of DERs is maximized.
- **O5:** To model a P2P energy trading scheme under a distributed market design that reduces the information shared by the DERs users' by implementing a decomposition algorithm.
- **O6:** To model a P2P energy trading scheme under a centralized market design to quantify the users' DERs' capability to provide reactive power as an ancillary service to the distribution system operator (DSO).

1.3 Thesis contributions

The central thesis contributions have been separated by topic as follows:

Contributions related to the optimal integration of DERs into DNs

- A deterministic model to address the optimal integration of DG and BSS into DNs in terms of location and capacity, considering the network technical limitation and economic indicators as CapEx and OpEx.
- An algorithm capable of assessing the deterministic problem related to the optimal capacity and location of DERs considering scenarios from 24 hours to 8760 hours, improving the existing models and algorithms.
- A methodology framework for DSO to measure the economic effort to integrate renewable resources into the DN.
- A two-stage stochastic programming model for managing the optimal integration of DG and BSS into DN considering EV and DR while the network constraints are respected.
- A stochastic formulation that includes the DERs' capability to generate reactive power to self-satisfied the internal network requirement in a planning problem for the optimal integration of DERs under uncertainty.
- An optimization model to measure the effect on the DG and BSS capacity problem when the DN possesses a high EV penetration.

Contributions related to the VMs application on DN to face primary grid unexpected failures

- Addresses unexpected failures in the energy provision from the primary grid to an active distribution network (ADN) through a deterministic model, which provides a dynamic MGs topology minimizing the load curtailment.

- An optimization-based partitioning method using the DR, the flexibility provided by BSS, and the power generated by the distributed resources to pass from an unbalanced ADN to multiple balanced VMs.

- An optimization model to identify the nodes with the highest probability of not meeting the electricity demand and quantify the energy that may not be supplied when unexpected failures in the energy provision from the primary grid occur.

Contributions related to the DN operation under a P2P energy trading scheme

- A new two-stage stochastic model to address the P2P energy trading operation considering i) prosumers and consumers, ii) the network technical limitations, iii) BSS modeled through binary variables to avoid the simultaneous charging and discharging, iv) agents that cannot sell or buy energy simultaneously, and v) keep the users' information.

- The implementation of new Benders cuts to decompose the P2P energy trading model into a master problem that preserves the DN balanced and subproblems that manage the energy trading between peers while the agents' private information is respected.

- A numerical analysis to identify the effect of the i) binary variables over the total energy traded in the LEM, ii) the battery operation over the individual profit when the global community cost is minimized in a two-stage P2P energy trading context, and iii) the batteries capacity to support a two-stage approach where the EC compromises the entire energy buying and selling from/to the grid under unknown self-generation scenarios.

- A model scalability assessment in terms of the method convergence concerning the time considering until 39 agents trading active power in DN of 69 nodes.

- A two-stage stochastic P2P energy trading model to address an energy community's day-ahead and intraday market schedule, considering the active/reactive power provided by DERs, and minimizing the total community cost while the technical constraints are respected.

1.4 Thesis outline

A summary thesis structure and scope is presented in Fig. 1.1 to guide the reader about the main topics and frameworks addressed in this work. Thus, the thesis has been divided into seven chapters as follows:

Chapter 2 presents an algorithm based on the AC optimal power flow (OPF) constraints and the genetic algorithm (GA) to obtain an optimal local solution for the network planning process related to the optimal integration of different RES and different BSS into a DN.

Chapter 3 addresses the optimal DERs allocation and sizing into an DN considering DR and high penetration of plug-in electric vehicles (PEV) under a two-stage stochastic programming framework.

Chapter 4 presents a mathematical optimization-based model for partitioning an unbalance active distribution network (ADN) due to unexpected failures in the energy provision from the primary grid into multiple balanced MGs with dynamic boundaries.

Chapter 5 presents a two-stage stochastic programming model to address a scheduling day-ahead problem of an EC operating under a P2P energy trading scheme. Besides, a new type of Bender cuts is used in the Benders decomposition algorithm to solve the stochastic problem.

Chapter 6 a two-stage stochastic energy trading model is presented to measure the DERs capability to provide reactive power as ASs to the DSO under a day-ahead and intraday markets considering community batteries to study the effect on the global cost under a collaborative scheme.

Chapter 7 presents the conclusions and future research lines arising from the topics managed in the previous chapters.

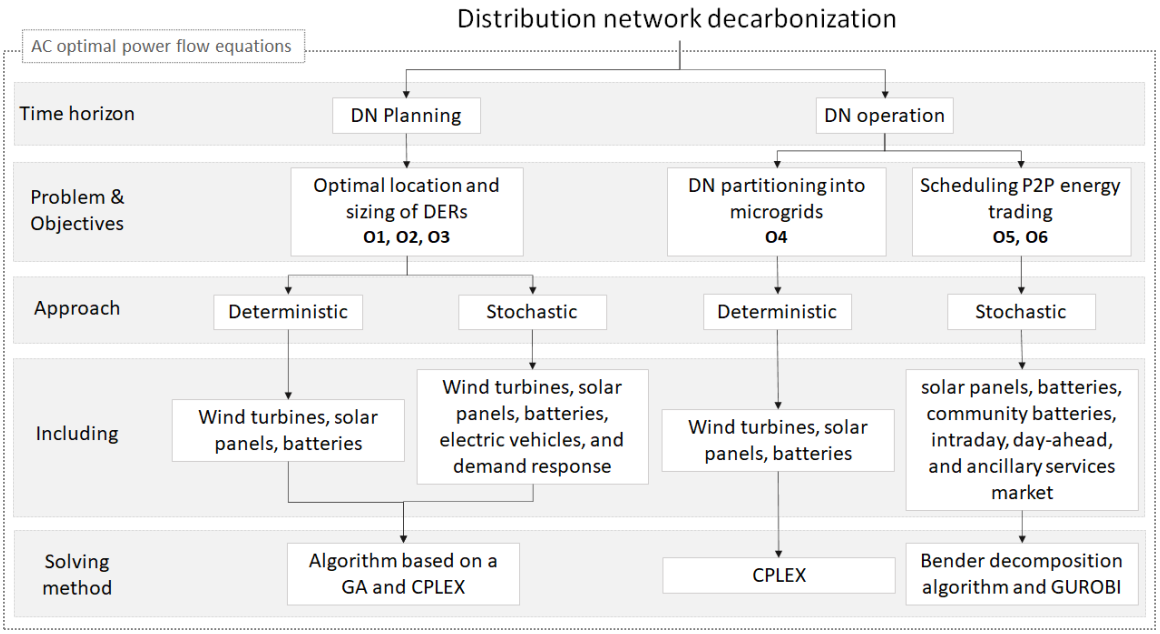

Figure 1.1: Summary thesis structure and scope

Chapter 2

An algorithm to solve the optimal sizing and location of DERs problem

2.1 Introduction

A global transition to 100% renewable energy is feasible [8]. New energy efficiencies and technologies are allowing a decline in renewable energy costs, improving the competitiveness regarding the traditional power plants. Besides, the transition process from the traditional centralized system towards a clean and sustainable energy system is being promoted by different countries worldwide through new policies on renewables, opening new energy market opportunities [9]. Under this global context, work in [4] supports the idea that to achieve a successful transition and to be aligned with the Paris agreement, it is required optimal planning of different types of DG and BSS into DN that involves the sizing and location simultaneously, and that takes into consideration realistic constraints and the stochastic behaviour of RES for a period greater than 24 hours.

This chapter proposes an algorithm to obtain an optimal local solution for the network planning process related to the optimal integration of different RES and different BSS into a DN. The algorithm provides strategic information related to investment and operation costs regarding the type of technology, location, and sizing. The mathematical formulation is based on an AC OPF to ensure the network's minimal stability conditions. Besides, through the use of linearization and a modified version of a GA, the algorithm proposed breaks the 24 hours wall, used until now in the literature, and extend it to 8760 hours, which represents a much more realistic scenario to define the storage and power generation capacity of a DN in a planning

context. The algorithm has been tested in a modified version of the IEEE 33-bus considering two cases of study: an off-grid case and grid-connected case, to measure the CapEx and OpEx variability, achieving to show that a grid-connected system reduces the installed capacity of DG and BSS in 37.4% and the CapEx 22.8%.

The chapter is organized as follows. Section 2.2 provides a literature review. Then, Section 2.3 describes the non-linear formulation for the optimal integration of DG and BSS into a DN, which by itself does not allow a time horizon of more than 12 hours due to its high computational burden. Section 2.4 presents a linearization to tackle the non-linearity of the original problem, establishing the MILP that is used in the algorithm. In section 2.5, the novel algorithm is explained, which uses a modified GA for handling binary variables. In section 2.6, the algorithm is tested in two different study cases. And finally, the results are discussed in section 2.7.

2.2 Literature review

The AC OPF model appears as a proper alternative to include realistic constraints in the DN planning process. However, its formulation is a mixed-integer non-linear and nonconvex problem, which means a high computational burden to solve, even for a concise time horizon [10, 11]. Unfortunately, to address long-term planning, a long-time-interval must be taken into account to include RES's stochastic behaviour. Therefore, two issues are considered in this chapter to achieve a model for the optimal planning to transform a centralized network into an active network; i) to create a mathematical formulation for the simultaneous integration of different DG and BSS in terms of location and sizing, and ii) to reduce the computational times of AC OPF to include stochasticity of the RESs behaviour properly.

The first problem has been widely addressed in different publications [12, 13, 14, 15, 16, 17, 18]. Work in [12] presents a mixed-integer linear problem (MILP) based on DC OPF to obtain storage devices' capacity and location. In [13], the impedance matrix is used to observe the voltage variation and define the optimal placement and sizing of a BSS. Work in [14] proposes a mixed-integer non-linear problem (MINLP), which maximizes the battery lifespan to obtain its location and capacity. In [15], an optimal allocation model is proposed to minimize the investment and operational cost of integrating batteries in a DN, considering a stochastic model. The authors in [16] proposes planning based on K-means clustering for the location and sizing of PV generation in a DN. Likewise, [17] uses an ant-lion optimization algorithm to solve the optimal allocation and sizing of PV panels and wind energy based on a loss sensitive

factor. The non-dominated sorting genetic algorithm (NSGA) and the NSGA-II are introduced by [19] and [20] respectively, to manage the optimal location and sizing of DERs. In the same research line, the method presented in [18] obtains the optimal placement and sizing of DG through Monte Carlo simulation to model the renewable resources' behaviour and use a NSGA-II to solve an OPF applied for DC.

The previous literature shows that few researches address the location and sizing of different types of BSS and DG simultaneously. For example, [21] proposes a formulation to obtain the optimal sizing of DG and BSS simultaneously, however, the location is not part of the model, and the time period is 24h. A two-stage approach is used by [22] to manage the sizing and location problem, where the sizing is addressed in the first stage and the location through the power flow equation in the second stage. Likewise, the particle swarm optimization algorithm and the GA are used in [23] to manage the same problem, but the master problem solves the location and sizing problem simultaneously, and the subproblem validates the operational constraints. On the contrary, authors in [24] manage the two-stage approach through a cooperative Game Theory-based model, while [25, 26] use an artificial bee colony algorithm. Work in [27] presents a methodology to obtain the optimal placement and capacity of DG and BSS, also for 24h, considering a Losses-Voltage-Factor (LVF) to ensure the right voltage limits, but not based on the power flow equations; hence, some critical variables like the reactive power, and offset angle are not considered. The same issue is tackled in [28] to apply it for a large-scale DN, the formulation is based on an OPF, and the time interval is the same as the previous articles except that here the model uses the worst 24h. However, this hypothetical case does not guarantee a feasible solution for other time periods. A stochastic multi-objective framework to face optimal planning is presented by [29] with a long-term vision. The formulation in [29] generates multiple scenarios for the DERs and a time step of one year (not by hours), making it possible to develop planning for ten years, using a particle swarm optimization to reduce the computational burden. Thereby, the related literature possesses a common factor; the formulation is applied for a short time interval due to its high complexity.

Regarding the second problem, OPF difficulty comes from non-convexity and nonlinearity; therefore, deleting one of these issues through a convex relaxation or a linearization, respectively, the time execution could decrease considerably. Recent studies have suggested several techniques and methodologies to provide formulations that guarantee convergence in large-scale DN. Works [30, 31] present different convex relaxation methods to tackle this issue. An improving successive linear programming

(SLP) is done by [11] to reduce the number of iterations. In [30], the approach combines quadratic programming (QP) with second-order cone programming (SOCP) to solve a multiperiod AC OPF. The authors in [31] provides a comparison between the use of a quadratic convex (QC) relaxation with semi-definite programming (SDP) and second-order cone relaxation. The works in [32, 33] present a summary of the different techniques applied to power system planning, including the interior point method, Newton method, quadratic programming, and a hybrid version of linear programming and integer programming.

Therefore, in this chapter, through the use and modification of existing techniques, a novel algorithm is constructed to find the optimal capacity and location for different types of DG and different types of BSS considering 8760 h, which represents a time horizon much bigger than the 24 h used until now in the related literature. The information in terms of placement and sizing of DERs provided by the algorithm is relevant when DN planning is developed. This is a strategic decision because the capacity installed cannot be modified every year. In this way, both the CapEx and OpEx, given by the algorithm, correspond exclusively to the installed capacity and operational cost, which are significant *input* for a proper economic evaluation, and therefore for a planning process. However, the economic analysis (through NPV, IRR, and payback) is out of this thesis's scope because it would require a proper explanation about financing, amortization, taxes, revenue/savings, discount rate, load and pricing forecast, among others, and must be addressed in detail in a separate study.

2.3 Location and sizing optimization model for a DN

2.3.1 Islanded mode

The MINLP presented in [34] is explained as follows:

$$Minimize\ F = B_I + B_C + DG_I + DG_C. \tag{2.1}$$

Where:

$$B_I = \sum_{l\in\Psi}\sum_{i\in\mathcal{B}} y_i^l I_l^{bt} + \gamma_{l,i}^b Cb_l, \tag{2.2}$$

$$DG_I = \sum_{k\in\Omega}\sum_{i\in\mathcal{B}} x_i^k I_k^{gn} + \gamma_{k,i}^p Cp_k, \tag{2.3}$$

$$B_C = \sum_{l\in\Psi}\sum_{i\in\mathcal{B}}\sum_{t\in\mathcal{T}} OMB_i^l(ds_{i,t}^l \Delta t \varphi^l), \tag{2.4}$$

$$DG_C = \sum_{k\in\Omega}\sum_{i\in\mathcal{B}}\sum_{t\in\mathcal{T}} OMG_i^k(pg_{i,t}^k). \tag{2.5}$$

The objective function (OF) goal in (2.1) is to minimize the investment and operation cost of DG and BSS into a low-voltage DN such that the system operates in islanded mode, using storage devices to maximize the electricity generated through the RES. Thus, the OF does not optimize the use of DG or BSS in electricity market terms, i.e., it is not intended to maximize the benefits of the battery operator to demonstrate the viability of its business model, based on market variables, for example, the price of electricity or the provision of ASs.

The DERs investment has been addressed in Eqs. (2.2) and (2.3) for BSS and DG, respectively, separating the location and sizing variables into two different terms with their respective cost associated (to avoid the non-linearity of multiply these variables). The cost related to the location is an installation cost that does not depend on generation or storage capacity. Thus, for BSS, the location costs include the power electronics and plant balance system and are related to the maximum power absorbed or injected into the grid (M^l). On the other hand, BSS's and DG's capacities variables have associated their respective capital cost in €/MWh, and €/MW. Therefore, the capital cost at a certain point is determined by the capacity installed γ^b/γ^p (obtained through the model) multiplied by their respective capital cost, plus the installation cost. The degradation cost for batteries is represented in Eq. (2.4), including only the energy injected from the battery and not the energy absorbed to promote energy storage into the BSS and avoid much charging/discharging cycles since the battery discharge only when is strictly necessary and charge always when is possible, without cost. Eq. (2.5) considers an equal structure as Eq. (2.4) but for DG operations.

The formulation of the constraints are as follows: Eq. (2.6) and (2.7) correspond to reactive and active nodal power flow equations, therefore; $\forall i \in \mathcal{B}, \forall t \in \mathcal{T}$,

$$-v_{i,t}^2 B_i + v_{i,t} \sum_{(i,j)\in\mathcal{L}} v_{j,t}[G_{i,j} sin(\Delta\theta_t^{i,j}) - B_{i,j} cos(\Delta\theta_t^{i,j})] = \sum_{k\in\Omega} qg_{i,t}^k - QL_{i,t}, \tag{2.6}$$

$$v_{i,t}^2 G_i + v_{i,t} \sum_{(i,j)\in\mathcal{L}} v_{j,t}[G_{i,j}cos(\Delta\theta_t^{i,j}) + B_{i,j}sin(\Delta\theta_t^{i,j})] = \sum_{k\in\Omega} pg_{i,t}^k - PL_{i,t} + \sum_{l\in\Psi}(ds_{i,t}^l - ch_{i,t}^l). \quad (2.7)$$

Constraints (2.8) and (2.9) correspond to the active and reactive power flow equations, therefore; $\forall(i,j) \in \mathcal{L}, \forall t \in \mathcal{T}$,

$$v_{i,t}v_{j,t}[G_{i,j}cos(\Delta\theta_t^{i,j}) + B_{i,j}sin(\Delta\theta_t^{i,j})] - G_{i,j}v_{i,t}^2 = p_t^{i,j}, \quad (2.8)$$

$$v_{i,t}v_{j,t}[G_{i,j}sin(\Delta\theta_t^{i,j}) - B_{i,j}cos(\Delta\theta_t^{i,j})] + v_{i,j}^2(B_{i,j} - Bs_{i,j}) = q_t^{i,j}. \quad (2.9)$$

Active and reactive power limits are considered in constraints (2.10) - (2.12), therefore; $\forall i \in \mathcal{B}, \forall k \in \Omega$,

$$\gamma_{k,i}^p PG_{k,t}^{min} \leq pg_{i,t}^k \leq \gamma_{k,i}^p PG_{k,t}^{max}, \quad (2.10)$$

$$\gamma_{k,i}^q QG_{k,t}^{min} \leq qg_{i,t}^k \leq \gamma_{k,i}^q QG_{k,t}^{max}, \quad (2.11)$$

$$\gamma_{k,i}^p \leq x_i^k U_k^g. \quad (2.12)$$

Eq. (2.10) establishes that the active power injected must be bounded by the generation capacity installed multiplied by the maximum power that can be generated in a given period. This maximum power corresponds to the RES's generation's normalized curve under certain weather conditions (see section 2.6.3 for an example). Eq. (2.11) follows the same structure as Eq. (2.10). Eq. (2.12) indicates that the capacity installed is less or equal to a maximum capacity allowed multiplied by the binary variable associated with whether the RES is installed. These sets of equations allow introducing DGs' stochastic behaviour into a modified version of AC OPF model [34].

The voltage and apparent power limits are represented by the following constraints; $\forall i \in \mathcal{B}, \forall t \in \mathcal{T}, \forall l \in \Psi$,

$$V_i^{min} \leq v_{i,t} \leq V_i^{max}, \quad (2.13)$$

$$\sqrt{p_{i,j,t}^2 + q_{i,j,t}^2} \leq S_{i,j}^{max}. \quad (2.14)$$

To model the behaviour of the batteries, the following constraints are added. There-

fore; $\forall i \in \mathcal{B}, \forall t \in \mathcal{T}, \forall l \in \Psi$,

$$soc^l_{i,t+1} = soc^l_{i,t} + [\varphi^l ch^l_{i,t} - \frac{1}{\varphi^l} ds^l_{i,t}]\Delta t, \tag{2.15}$$

$$(\gamma^b_{l,i}) SOC^{min}_l \leq soc^l_{i,t} \leq SOC^{max}_l (\gamma^b_{l,i}), \tag{2.16}$$

$$\gamma^b_{l,i} \leq y^l_i U^b_l, \tag{2.17}$$

$$ch^l_{i,t} \leq w^l_{i,t} M^l, \tag{2.18}$$

$$ds^l_{i,t} \leq M^l(1 - w^l_{i,t}) - M^l(1 - y^l_i), \tag{2.19}$$

$$w^l_{i,t} \leq y^l_i. \tag{2.20}$$

Constraint (2.15) represents the $soc^l_{i,t+1}$ for the next period of the battery, which is in MWh and not in percentage, as usual, to keep the linearity in Eqs. (2.16) and (2.17). Eq. (2.16) represents the upper and lower bound for the $soc^l_{i,t}$ in MWh, where the limits depend on the one hand, of the installed capacity, and on the other hand, of the maximum/minimum operational limits allowed in the battery ($SOC^{max}_l / SOC^{min}_l$) in percentage. Thus, for a capacity of 10 MWh and 90%/10% as operational limits, the $soc^l_{i,t+1}$ will not be less than 1 MWh or greater than 9 MWh. Eq. (2.17) restricts the installed capacity to a maximum capacity allowed, multiplied by the binary variable whether the battery is installed. Constraints (2.18)-(2.20) define the charging/discharging process through a binary variable $w^l_{i,t}$ which is bounded by the battery whether it is installed, and where M^l represents the maximum energy injected/absorbed for a battery in a certain period. In the case that the battery is not installed (Eq. 2.20), constraints (2.15)-(2.19) are zero; otherwise, if the battery is charging, the discharging process is modeled through Eq. (2.19).

2.3.2 Grid-connected mode

If the model proposed is used for a grid-connected mode, the main grid's reactive (gq) and active (gp) power must be included as variables in the right-side of Eq. (2.6) and (2.7), respectively, as follows:

$$- v^2_{i,t} B_i + v_{i,t} \sum_{(i,j)\in\mathcal{L}} v_{j,t}[G_{i,j} sin(\Delta\theta^{i,j}_t) - B_{i,j} cos(\Delta\theta^{i,j}_t)] = \sum_{k\in\Omega} qg^k_{i,t} - QL_{i,t} + gq_{i,t}, \tag{2.21}$$

$$v_{i,t}^2 G_i + v_{i,t} \sum_{(i,j)\in\mathcal{L}} v_{j,t}[G_{i,j}cos(\Delta\theta_t^{i,j}) + B_{i,j}sin(\Delta\theta_t^{i,j})]$$
$$= \sum_{k\in\Omega} pg_{i,t}^k - PL_{i,t} + \sum_{l\in\Psi}(ds_{i,t}^l - ch_{i,t}^l) + gp_{i,t}. \quad (2.22)$$

Furthermore, the power provided by the grid is included in Eq. (2.1) as follows:

$$F = B_I + B_C + DG_I + DG_C + \sum_{i\in\mathcal{B}}\sum_{t\in\mathcal{T}}(\Lambda\lambda_t)(gq_{i,t} + gp_{i,t}). \quad (2.23)$$

λ represents the energy price and Λ, a penalization parameter to handle the trade-off between RES assets and the energy bought to the grid. Thus, the bigger is Λ, the bigger is the willingness to install DERs, and the less is the grid dependence.

2.4 Linear optimization model

The linearization method presented in [10] is used in this chapter because it does not require new information about the network, considers the reactive power and voltage as variables, and guarantees the convergence of the OPF, which is applied over the non-linear constraints present in the power flow equations and the apparent power limit. Therefore, the left sides of Eq. (2.6) and (2.7) are modified and expressed, respectively $\forall i \in \mathcal{B}, \forall t \in \mathcal{T}$, as follows:

$$-vs_{i,t}[B_i + \sum_{(i,j)\in\mathcal{L}}(B_{i,j} - Bs_{i,j})] + \sum_{(i,j)\in\mathcal{L}} q_t^{i,j} = \sum_{k\in\Omega} qg_{i,t}^k - QL_{i,t}, \quad (2.24)$$

$$vs_{i,t}[G_i + \sum_{(i,j)\in\mathcal{L}} G_{i,j}] + \sum_{(i,j)\in\mathcal{L}} p_t^{i,j} = \sum_{k\in\Omega} pg_{i,t}^k - PL_{i,t} + \sum_{l\in\Psi}(ds_{i,t}^l - ch_{i,t}^l). \quad (2.25)$$

Constraints (2.24) and (2.25) represent the linear version of the balance in nodes. Specifically, the left side have been rewritten in terms of $q_{i,j,t}$ and $p_{i,j,t}$, and the voltage has been replaced by $vs_{i,t}$, which is $v_{i,t}^2 = vs_{i,t} \forall (i,j) \in \mathcal{L}, \forall t \in \mathcal{T}$. Therefore, Eq. (2.13), which limits the voltage, is expressed now as:

$$(V_i^{min})^2 \leq vs_{i,t} \leq (V_i^{max})^2. \quad (2.26)$$

Linearization of the power flow Eqs. (2.8) and (2.9) can be achieved using a Taylor series expansion for sine and cosine, considering $\theta_t^{i,j}$ is a small number and the voltage is closer to 1.0 p.u. leading to the following set of Eqs. $\forall (i,j) \in \mathcal{L}, \forall t \in \mathcal{T}$,

$$G_{i,j}\left[\frac{vs_{i,t} - vs_{j,t}}{2}\right] - B_{i,j}(\Delta\theta_t^{i,j}) + LP_{i,j} = p_t^{i,j}, \quad (2.27)$$

$$-B_{i,j}\left[\frac{vs_{i,t} - vs_{j,t}}{2}\right] - G_{i,j}(\Delta\theta_t^{i,j}) + LQ_{i,j} = q_t^{i,j}. \quad (2.28)$$

Eqs. (2.27) and (2.28) corresponds to the new active and reactive power flow equations and they are in terms of a loss factor, which are approximated through the follow expressions:

$$LP_{i,j} = G_{i,j}[\Delta\widehat{\theta}_t^{i,j}]m_{i,j} + G_{i,j}\left[\frac{\widehat{V}_{i,t} - \widehat{V}_{j,t}}{\widehat{V}_{i,t} + \widehat{V}_{j,t}}\right] - \frac{G_{i,j}}{2}[(\Delta\widehat{\theta}_t^{i,j})^2 + (\Delta\widehat{V}_{i,j,t})^2], \tag{2.29}$$

$$LQ_{i,j} = -B_{i,j}[\Delta\widehat{\theta}_t^{i,j}]m_{i,j} - B_{i,j}\left[\frac{\widehat{V}_{i,t} - \widehat{V}_{j,t}}{\widehat{V}_{i,t} + \widehat{V}_{j,t}}\right] + \frac{B_{i,j}}{2}[(\Delta\widehat{\theta}_t^{i,j})^2 + (\Delta\widehat{V}_{i,j,t})^2]. \tag{2.30}$$

Both constraints (2.29) and (2.30) are composed of a loss factor related to the angle, voltage, and offset. Furthermore, $m_{i,j}$ represents an incident vector of branch (i,j). i.e. the i^{th} node is 1, the $j^{th} - 1$ and the other values are zero. $\widehat{\theta}_t^{i,j}$ and $\widehat{V}_{i,j,t}$ are parameters associated with an angle and voltage obtained in a base case using the original model.

The apparent power limits expressed in (2.14) is the last constraint that needs to be linearized. Thus, using the method presented in [10], Eq. (2.14) is approximated by the following set of constraints $\forall(i,j) \in \mathcal{L}, \forall t \in \mathcal{T}, \forall r \in \mathcal{R}$:

$$A_{i,j}^r p_t^{i,j} + B_{i,j}^r q_t^{i,j} + C_{i,j}^r \geq 0, \tag{2.31}$$

$$-A_{i,j}^r p_t^{i,j} + B_{i,j}^r q_t^{i,j} + C_{i,j}^r \geq 0, \tag{2.32}$$

where:

$$A_{i,j}^r = -S_{i,j}^{max} cos(\beta_{i,j}^r)\ ;\ B_{i,j}^r = -S_{i,j}^{max} sin(\beta_{i,j}^r), \tag{2.33}$$

$$C_{i,j}^r = (S_{i,j}^{max})^2\ ;\ \beta_{i,j}^r = \alpha + (r-1)\frac{\pi - 2\alpha}{\mathbb{R} - 1}. \tag{2.34}$$

Eq. (2.31) and (2.32) emerge as a set of constraints which represent a polygon formed by $r \in \mathbb{R}$ lines that define a feasible region approximation of the original constraint (2.14), which is a circle. Thus, the bigger the set $\mathbb{R}$, the closer will be the polygon to the circle.

Finally, the MILP to tackle the optimal integration of DGs and BSS using a multi-period AC OPF can be expressed by the following equations:

$$Min_{y_i^l, x_i^k, \gamma_{l,i}^b, \gamma_{k,i}^p, ds_{i,t}^l, pg_{i,t}^k}(F).$$

Subject to:

- Power flow equations: (2.24) (2.25) (2.27) (2.28) (2.29) (2.30).
- Limits: (2.26) (2.33) (2.34) (2.10) (2.11) (2.12).
- Battery: (2.15) (2.16) (2.17) (2.18) (2.19) (2.20).

2.5 Algorithm for sizing & location of DGs and BSS

The algorithm proposed in this section uses the logic behind the GA as a backbone, intending to reduce the complexity generated by the binary variables since the formulation presented in the previous sections by itself cannot be applied in a time horizon beyond 24 h.

2.5.1 Proposal

The GA algorithm was presented by [35] in 1975, and, until today, it has been used to solve OPF problems [36, 37]. However, the GA has not been applied in its original form because to do this; would require defining the mathematical formulation in a Fitness Function (FF), which would not allow us to include the decision variables related to the battery behaviour, capacity/location, and satisfy the network technical constraints for *multiple* periods, at the same time. In this context, it is proposed to use the GA logic and replace the FF with the formulation presented at the end of section 2.4 (the *MILP* problem). By doing this, the computational time is sacrificed, but all the variables and constraints of the original formulation are considered. Therefore, for each iteration, the algorithm proposed resolves the *MILP* model to obtain the DERs capacities, with the difference that the binary variables are replaced by parameters generated randomly, and therefore, the MILP problem becomes an *LP*. The solution to each optimization problem will be called FF to follow the same language of the GA.

2.5.2 Operation

The algorithm operation is explained in detail using as support the flowchart in Fig. 2.1

2.5.2.1 Chromosome structure

There are two sets of binary variables in our work; the first one is associated with DG and BSS location, and the second one with the charge and discharge of batteries for every hour. Both are generated randomly every iteration.

Fig. 2.2, illustrates an example of a chromosome for each case. The first one, associated with the location, is composed of DG genes in blue and BSS in red; the label is *one* when the element is installed and *zero* otherwise, thus, their dimensions

depend on the number of buses and the type of DG and BSS. On the other hand, the second chromosome's dimension depends on the number of buses, the type of battery, and the period. In this case, the red labels indicate that the value has been set to zero because there is no battery type l installed in bus i. These binary variable models the behaviour if the battery type l at period t is charging or discharging. However, if the battery is not installed in the bus i, all the values associated with that bus are zero. For example, following Fig. 2.2, the bus 1 has installed a battery type 2 ($y_1^2 = 1$) and not type 1 ($y_1^1 = 0$), thus, the binary variable for charge/discharge for the battery type 1, $w_{1,t}^1$ will be always zero, and the battery type 2 $w_{1,t}^2$ could be one or zero.

2.5.2.2 Set initial parameters

The main input parameters are described as following:

- *Load*: corresponds to two vectors; i) one for the normalized load curve, ii) a second one with the maximum load allowed of every bus.
- *Price*: refers to the price curve, which is exclusively parameters for the grid-connected case.
- *WT/PV power generation*: represents the RES's behaviour through normalized curves between [0,1].
- *Network data*: related to the technical information to run the classic OPF model.
- *Size population*: refers to the number of possible solutions for every iteration.

2.5.2.3 Create an initial population

The initial population is created through the random generation of the binary variables, where every one of these variables sets, called chromosomes, represents a candidate for the optimal solution. The LP (ex MILP) is then executed for every chromosome to obtain the optimal sizing and its respective FF value. If the LP solution is infeasible, the FF for that set of locations is penalized. The infeasibilities can emerge when the LP is solved for locations that do not satisfy the network constraints to meet the electricity load. If this occurs, the function by parts explained in section 2.5.3 is applied not to maintain the infeasibility across the while loop.

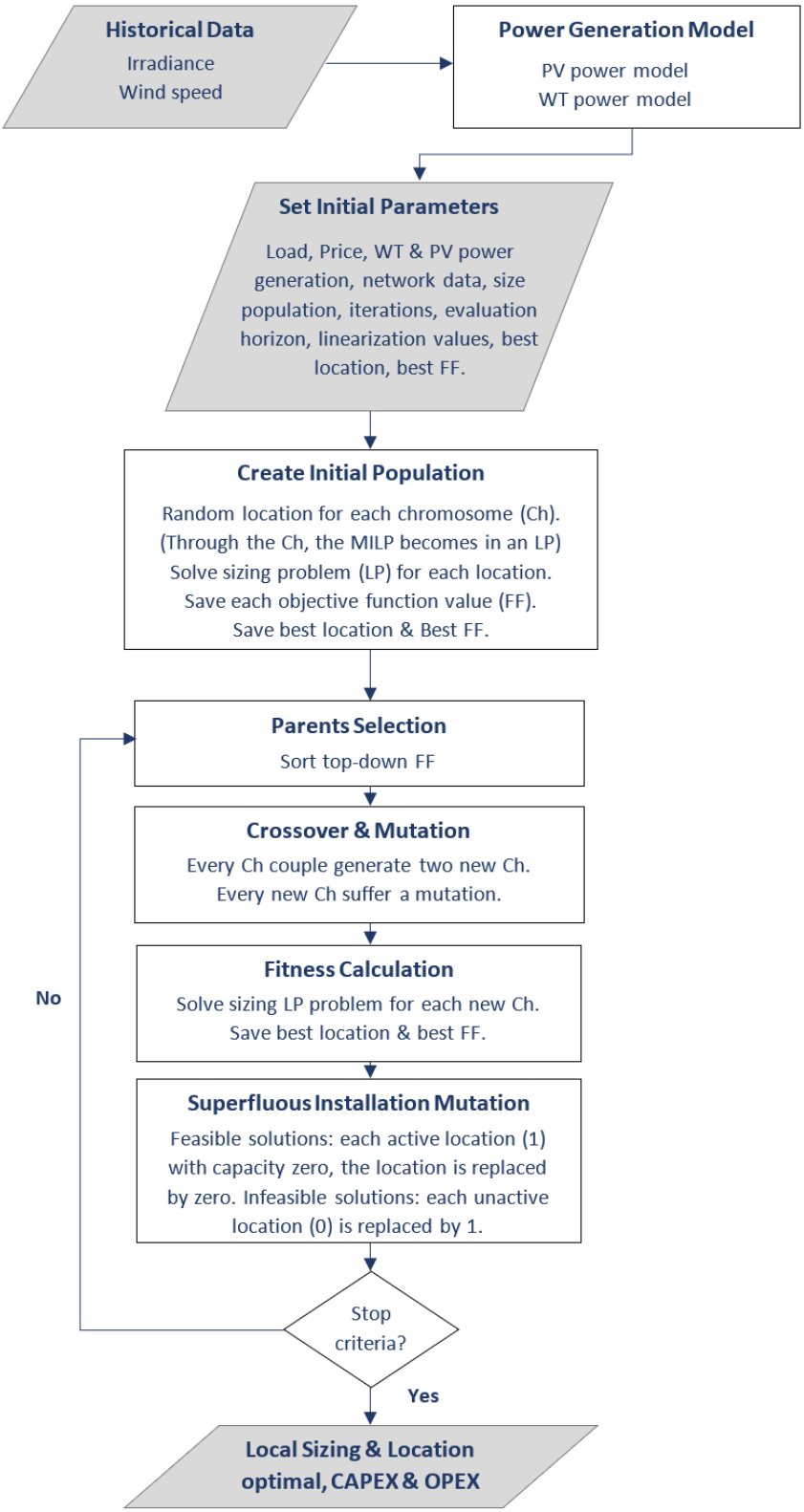

Figure 2.1: Algorithm for sizing & location of DGs and BSS

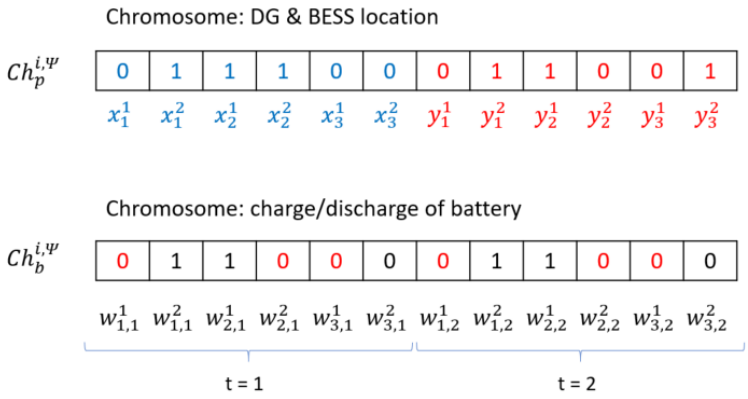

Figure 2.2: Example of a chromosome structure

2.5.2.4 GA and LP model

The while loop starts applying the classic GA steps for every chromosome belonging to the initial population; i) the chromosomes are sorted top-down depending on their FF forming couples for mating; ii) the offspring of the matings are called *New Locations* which suffer a random mutation to increase the variability; iii) for every new chromosome the LP model is executed to obtain the new FF, wherein the case of infeasibility the FF is penalized; iv) if one of these FF is better than the best FF, then its location becomes the new best location with the best FF; v) finally, an extra mutation process (see 2.5.3) is applied for all chromosomes to improve the convergence of the algorithm.

2.5.3 Convergence

In order to improve the algorithm convergence, a new *Superfluous installation mutation* is introduced to reduce some *noise* in the LP solutions (see Fig. 2.1). Due to the objective function structure of the MILP (binary variables for the locations and continuous variables for the capacities of the DERs), when the binary variables are established randomly, some DERs may have zero capacity due to the LP solution. Therefore, these superfluous locations are modified following a function by parts for two cases: feasibility and infeasibility solutions, therefore; $\forall p \in \Phi$:

$$Ch_p^{i,\psi} = \begin{cases} \frac{P(1)}{I+1} & if \quad \gamma_{\psi,i} = 0 \quad and \quad Ch_p^{i,\psi} = 1 \\ \frac{1-P(1)}{I+1} & if \quad \gamma_{\psi,i} = 0 \quad and \quad Ch_p^{i,\psi} = 0 \end{cases}$$

Where Φ represents the chromosome population. $Ch_p^{i,\psi}$ corresponds to the chromosome p at bus i and the types of DGs (k) and BSS (l) which are grouped in ψ. $P(1)$ is the probability of obtaining a *one* and I is the number of iterations.

Therefore, the previous function defined by parts means; if the *capacity* $\gamma_{\psi,i}$ obtained as the optimal solution is zero in a bus when the DG or BSS is installed ($Ch_p^{i,\psi} = 1$), that device or generator is replaced by a zero or one by the function defined by parts. For infeasible solutions, the buses without DG or BSS are changed from 0 to 1, and the random selector is applied oppositely. Note that the probability of replacing a 1 for a 0 for feasible solutions, increasing when the number of iterations rises.

Applying this criterion, the convergence speed increases, and the infeasibilities tend to disappear when the number of iterations increases.

2.6 Case study and computational results

2.6.1 Case study

Two cases are considered to observe the variability of the investment. The first case is an autonomous system, where the electricity demand is supplied only by DG and BSS, and a second case where the main grid supports the system. In the latter case, it has been used the equations presented in section 2.3.2 and to ensure that the energy obtained from the grid is only at critical hours; the Λ parameter has been set in 5 (obtained after executing the algorithm for different penalization values). Thus, the model is willing to install a higher RES capacity and buy less energy from the main grid.

WT and PV panels are considered the distributed generation resources, and Lead-acid and Li-ion batteries storage systems. The parameters associated with the RES uncertainty $PG_{i,t}^{min}$ and $PG_{i,t}^{max}$, are generated through the formulation used in [10]. The chromosome's length for the GA has 132 gens, explained by 33 buses, 2 types of DG, and 2 types of batteries. The data corresponds to the Lugo, Galicia region's historical information in the north of Spain 2018 [38, 39].

The well-known IEEE 33 Bus radial distributed system, 32 lines and 32 load buses [40] is used to test the mathematical formulation, and the algorithm set out in this chapter. The network has been extended for 8760 h, i.e., one year.

In order to estimate the DERs operational cost, the electricity load corresponds to a forecast for the next 20 years. Thus, the DERs capacity obtained through

Table 2.1: Model validation for the 5-bus test system

	Power generated [MW]			
Location	[41]	AC-OPF model	AC-OPF linearized	DC-OPF model
Bus 2	0	0	0	0
Bus 4	14.773	14.848	14.186	14.718
Bus 5	5.227	5.694	5.89	5.814

the algorithm satisfies the load requirement for a typical time horizon in a planning process.

2.6.2 Model validation

The mathematical formulation proposed in this chapter has been programmed in Python, using BONMIN and CPLEX as leading solvers for the MINLP and MILP, respectively. The non-linear and linear formulation for the AC OPF model has been validated using a 5-bus system [41] as reference taking into account the location and the capacity as fixed parameters of the model, to make the results comparable with the reference values as can be observed in Table 2.1.

2.6.3 Worst-case scenario and parameters

In order to provide a DERs capacity closer to a real case, the time horizon must be extended beyond 24 hours because there are some factors to take into account to enlarge the study period. i) if the worst-case scenario of 24 hours is considered, the algorithm could overestimate the total capacity installed because it could not harness the battery behaviour to fulfil some gap between generation and demand. Likewise, ii) if the battery starts the period fully charged, the LP result could overestimate the installed capacity for the storage devices, sizing a capacity needs to supply the 100% of the load, without considering the DGs. iii) If the weather conditions in the worst 24 hours have a suitable wind resource but not the minimum to provide solar energy, the mathematical model does not install PV panels. This situation could generate infeasibilities in other seasons with high irradiation and low wind speed. Thus, a critical scenario must be defined in which the solution (capacity) reported by this scenario, is a feasible solution for a multi-period AC OPF for 8760 h.

In this way, a hypothetical critical scenario of 192 consecutive hours (8 days) is created, uniting the worst eight days of the historical data (not necessarily consecutive), understanding *the worst* as days with a high difference between load and available generation. Fig. 2.3 shows these 192 hours, where the curves have been normalized to represent the percentage of available power generated by a WT or a PV panel. For

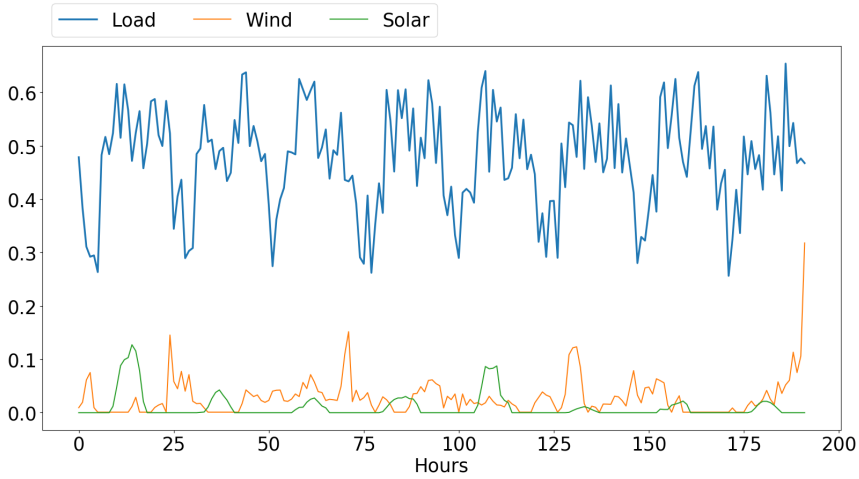

Figure 2.3: The hypothetical worst-case scenario of 192 consecutive hours.

example, in Fig. 2.3, if the capacity of PV is 1 MW, and the available power for solar generation is 0.15 at hour 13 of the first day, it implies that the *maximum* power that can be injected into the grid from the PV panel is 15% of the PV capacity, which is 0.15 MW. Thus, the most critical days belong to December, January, and February, where there are many days with more than 6 consecutive hours with a deficient generation.

The parameters used for the mathematical model include installation and capital cost for WT/ PV/ Li-ion/ Lead-acid batteries, voltages, max capacities allowed, among others. They have been set out in [34, 42] following the breakdown cost in [43, 44], and the energy prices have been taken from [45]

2.6.4 Algorithm performance

In order to size the performance of the algorithm, four components are considered: execution time, size population, number of iterations, and accuracy. The first component is measured comparing the computational burden when the mathematical formulation presented at the end of Section 2.4 is solved i) only with CPLEX, and ii) solved with the algorithm. For both cases, different time horizons are considered within the *worst-case* scenario. Table 2.2 shows these results, where for a short time horizons, the CPLEX time is lower than the time offered by the algorithm. However, for a time horizon of 24 hours or greater, the execution time of CPLEX increases much faster than the algorithm's execution time. Likewise, the FF value found by the algorithm is far from the optimal value obtained by CPLEX, only 2.5%, which is considered an acceptable value for this study.

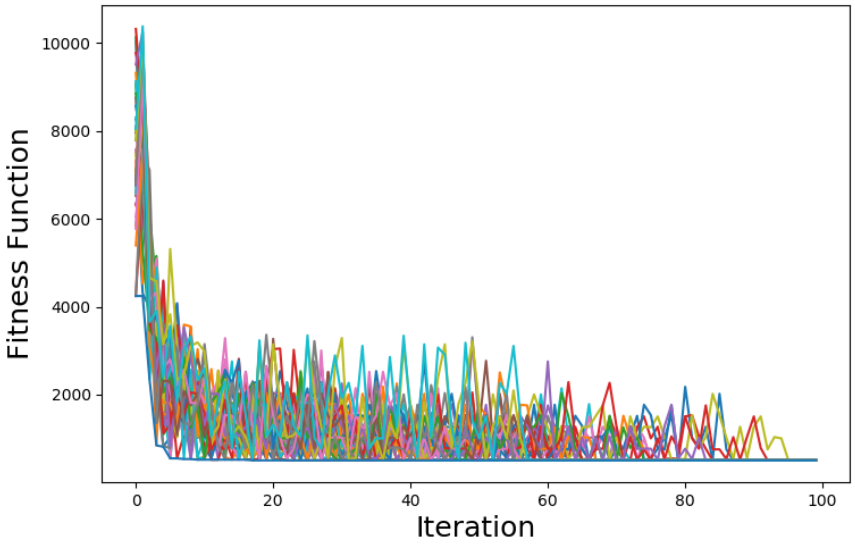

Figure 2.4: Algorithm convergence

Two considerations are established to study the effect of the size population and the number of iteration over the algorithm accuracy; i) a single hour as the time horizon, ii) an OF value like the reference (505.62 €k - solving the original MILP using CPLEX). Table 2.3 shows the results for the different population sizes and the number of iterations, where every combination of these parameters has been executed 5 times. Thus, **(A)** in Table 2.3 represents the best value obtained in the 5 executions. **(B)** the percentage of execution that reaches the best value. **(C)** corresponds to the error regarding the optimal reference value, in this case, 505.62, and **(D)** shows the average of the number of iteration that each execution required to reach the best value. Therefore, under these results, the number of iterations seems to be more relevant than the population size because when 30 iterations are considered, for every execution, no matter the population size, the algorithm reaches the optimal value. However, when the number of iterations is 15, only 40% of the executions with a population size of 16 reaches the optimal value; the remaining cases have 2.97% of error regarding the optimal reference value.

To visualize the convergence of the algorithm is required a more vast number of iterations and uses a reference value to stop the chromosome mating when it reaches this value. Thus, Fig. 2.4 shows the convergence of the algorithm when it is executed for one hour in the test system, considering a population of 50 chromosomes and 100 iterations. Each colour line represents one chromosome, which is a set of locations of DG and BSS. Close to iteration 100, every chromosome has found the optimal solution.

Table 2.2: Algorithm performance versus MILP

Period [h]	1	6	12	24	48
MILP [s]	3.61	102.5	209.1	1660.5	8516.7
FF [k€]	553.4	807.1	1132.6	1139.4	1150.7
Status	ok	ok	ok	ok	ok
Algorithm [s]	41.73	151	311.1	880	2716.6
FF [k€]	553.4	823.5	1151.8	1161	1178.1
Status	ok	ok	ok	ok	ok
D Time [s]	38.1	48.5	102.1	-780.5	-5800
D FF [%]	0%	2.0%	1.7%	1.9%	2.4%

Table 2.3: Algorithm accuracy considering an optimal value as a reference

Population	Iteration	(A)	(B)	(C)	(D)
4	15	520.63	20%	2.97%	12.8
8	15	520.63	60%	2.97%	10.8
12	15	520.63	80%	2.97%	8.6
16	15	505.62	40%	0%	10.8
4	30	505.62	100%	0%	15.6
8	30	505.62	100%	0%	19.2
12	30	505.62	100%	0%	12.8
16	30	505.62	100%	0%	18.8

2.6.5 Case: Off-grid operation

This section presents the results when the algorithm is applied in a context where DG and BSS supply 100% of the electricity load.

The *critical scenario* (see 2.6.3) is considered to provide a *feasible* solution, in terms of sizing and location of the DERs, for the 8760 hours. The GA's size population is 12, and the iterations 30, taking around 2h and 45 min (9,937 s). Fig. 2.5 shows the location into the distribution system for every DERs.

Regarding Table 2.4, 56.11% of the total capacity installed is associated with wind energy and 43.89% with solar energy. The output is within the expected values because of the location. i.e., in the Lugo region, the annual average wind speed is around 6.28 m/s [39] and the annual average irradiation 3.86 kWh/m2/year [38], which indicate that the solar energy available in the zone is weak compared with the wind energy. Likewise, 100% of the total storage capacity belongs to Lead-acid batteries, which means that the efficiency factor does not compensate for the Li-ion batteries' high cost.

The location and size obtained using the algorithm under this scenario is a *feasible* solution for the AC OPF model considering 8760 h, where the seasonality of the battery, WT, and PV panels are shown in Fig. 2.6. The curves represent the energy provided or demanded by these resources, which have been independently normalized

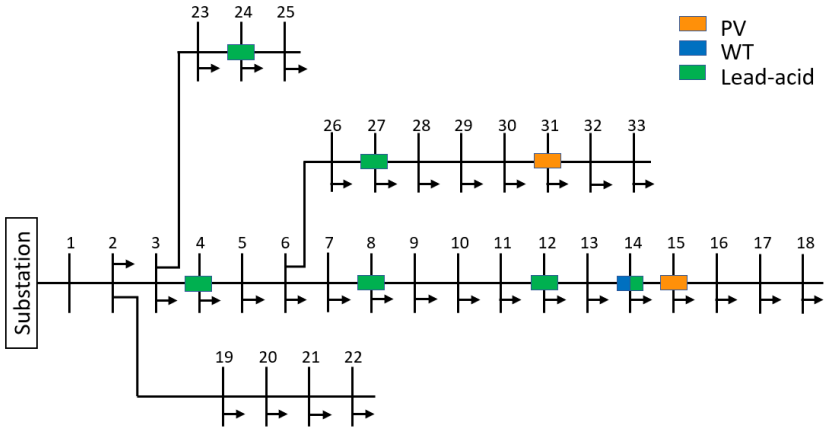

Figure 2.5: DERs location into the distribution network for off-grid operation case

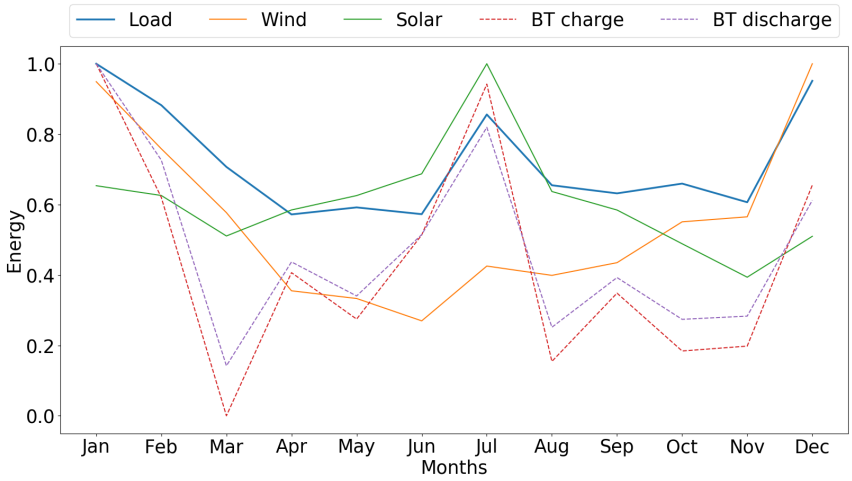

Figure 2.6: Energy seasonality for off-grid case. The curves have been normalized considering, for each one of them, the highest values over the 12 months

to remark the behaviour of each element for every month. Thus, the battery has a more significant participation in winter and summer than autumn and spring, which could be attributed to the fact that when there are more abundant resources of wind for WT (December) or irradiation for PV panels (July), there is more energy that can be stored.

2.6.6 Case: grid-connected

The same methodology used in the previous section is applied now, with the difference that in the present case, a new variable is included within the formulation, which is the power provided by the main grid in the most critical hours. Therefore, the algorithm

Table 2.4: Sizing & location for off-grid operation

Bus	Off-grid			Grid connected		
	WT	**PV**	**L-A**	**WT**	**PV**	**L-A**
4	0	0	5.56	0	0	0.36
8	0	0	5.61	0	0	0
11	0	0	0	8.66	0	2.44
12	0	0	4.89	0	0	2.55
14	52.18	0	28.78	55	0	3.29
15	0	7.75	0	0	0	5.22
17	0	0	0	0	0	4.45
18	0	0	0	0	0	4.85
22	0	0	0	0	0	0.12
24	0	0	3.06	0	0	0
27	0	0	2.78	0	0	0.55
31	0	33.06	0	0	0	0.41
32	0	0	0	0	0	0
Total	**52.18**	**40.81**	**50.68**	**63.66**	**0**	**26.32**

is executed considering the new variable for the worst 192 hours, and the feasibility of its result is validated running the multi-period AC OPF for 8760 h.

Table 2.4 presents DG and BSS's total capacity and location, considering that the grid provides energy in the most critical hours. Thus, the total DERs capacity installed decreases, i.e., 37.4%, when the system is connected to the grid regarding the previous case. The total capacity of DG drop-down 31.5% is explained by the absence of PV panels, which is replaced by a little increase of WT capacity. The batteries' hosting capacity also decreases 48.07%, from 50.68 MW to 26.32 MW. Moreover, the grid's energy is only 5.6% over the evaluated period (8760 h), and the renewable system supplies the remaining 94.4%. In other words, if the renewable system provides only 94.4% of the total energy and not the 100%, the CapEx decrease by 22.81%.

Fig. 2.7 presents the energy provided by the DERs and the grid by months, where the grid mostly participates in January, February, July, and August, with a 7.5 % on average. Thus, out of a total of 9.22 GW/yr, 8.38 GW/yr (94.4%) are provided by WT and Lead-acid battery. Furthermore, the battery's role follows the same pattern as the off-grid case, where its more significant operation is in January, February, and July.

Finally, Table 2.5 shows a comparison between the autonomous system and the

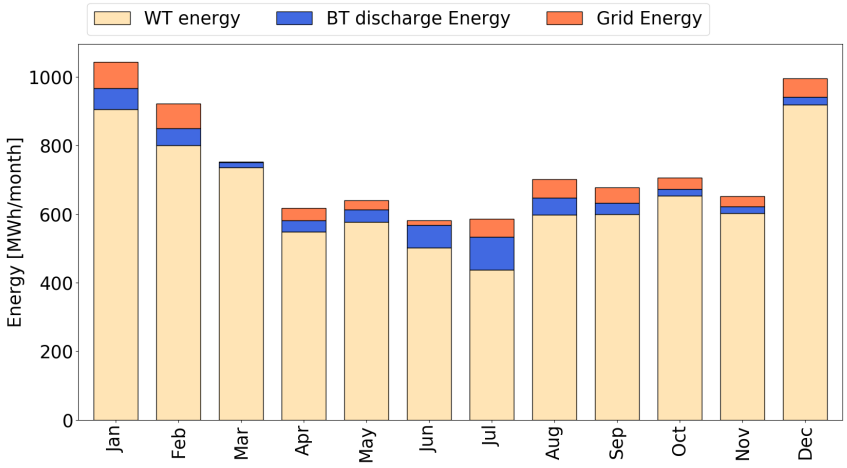

Figure 2.7: Energy seasonality for grid-connected case. Battery charge has been discounted from the energy generated by the WT

Table 2.5: Economic indicator for the cases of studies

Indicator	Off-grid	Connected	Decrease
CAPEX [k€]	123,962.91	95,689.66	22.81%
OPEX [k€]	52,484.57	27,364.13	47.86%
Energy supplied	100%	94.40%	5.60%
DG [MW]	92.99	63.66	31.54%
BSS [MWh]	50.68	26.32	48.07%

system connected to the grid, highlighting the most relevant indicators, where the CapEx and OpEx are actualized for a time horizon of 20 years and considering a discount rate of 6.5%.

2.7 Chapter conclusions

This chapter has proposed a model able to provide a feasible solution to the problem associated with the optimal location and sizing of different DG and BSS into a DN, over 8760 h and considering technical constraints, through linearization and the application of a modified GA to reduce the computational burden of the original problem.

The model has been tested considering an off-grid system, fully supplied by renewables, and a grid-connected system. Under the specificities of the adopted case studies, a network connected to the grid becomes much more efficient in terms of CapEx than an off-grid one because the latter requires a more significant investment

to achieve supply the 100% of the electricity load. In this way, the results support that a small grid power share in the hours with low generation significantly affects the CapEx reduction. The main factor contributing to this reduction can be attributed to the battery capacity, which decreases from 50.68 MW to 26.32 MW and the absence of PV panels. Under the formulation proposed, the most crucial factor in deciding which type of storage devices are installed is the CapEx more than the efficiency. i.e., a greater percentage of efficiency does not justify a high investment in batteries.

Chapter 3

On the optimal sizing and location of DERs: A two-stage stochastic approach including EVs and DR

3.1 Introduction

The optimal DERs location and sizing presented in the previous chapter from a deterministic perspective is addressed in this chapter by a stochastic programming approach, considering a low-voltage DN with high penetration of plug-in electric vehicles (PEV) and users with demand response. The stochastic formulation presented in this chapter includes i) economic variables related to the capital cost of the DERs capacity installed with their respective operational costs and ii) operational technical constraints based on the AC power flow equations. The formulation estimates the DG capacity in terms of apparent power, i.e., the capacity found by the model relates the active and reactive power injected from DG to the DN simultaneously. The linearization and the algorithm presented in the previous chapter solve the MINLP, and the backward algorithm is applied to reduce the number of scenarios. The model is tested in the IEEE 69-bus system under 18 different scenarios of 24 hours to measure the DERs capacity installed variability. Finally, the results showed that i) the set of scenarios selected are decisive for the optimal capacity installed affecting the investment and the grid dependence, ii) the PEVs affect the total DERs capacity installed and the operation costs, and iii) the reactive power provided by the DERs might supply the total reactive power demand.

Therefore, the chapter is outlined as follows. A literature review is presented in Section 3.2. Then, Section 3.3 describes the two-stage stochastic model for the DERs' optimal sizing and allocation. The methodology used to linearize and solve de model

is explained in Section 3.4, together with scenario creation and the assumption to address the reactive power. Section 3.5 presents six cases studies where the model is tested and compared. Section 3.6 explains the limitation of the formulation proposed in this chapter. Finally, Section 3.7 presents the conclusions.

3.2 Literature review

Researchers have extensively addressed the optimal sizing and/or placement of DG and/or BSS into DN. For example, The model proposed by the authors in [46] uses the second-order cone programming to address the power flow equation non-convexity and find the optimal placement and sizing of DGs. The exact optimal problem is driven by [47]; however, the authors propose a robust model using the information gap decision theory technique. Work in [16] uses K-means clustering for the location and sizing of PV generation, and the authors in [17] uses an ant-lion optimization algorithm to solve the optimal allocation and sizing of DGs based on a loss sensitive factor. In [48], a comprehensive review and critical discussion of the state-of-the-art analytical techniques for optimal DG integration in power DN is presented.

On the other hand, BSS's optimal sizing and location are studied in [14] through a multi-objective optimization problem minimizing the power losses and the capital cost and using an elitist non-dominated sorting genetic algorithm-II to solve the model. In [49], the BSS sizing and siting problem is settled through a combination of a stochastic and robust optimization problem. The authors in [50], based on the PV location and penetration, the optimal battery placement and sizing problem is solved to manage voltage issues through the impedance matrix. In [15] the conservation voltage reduction is used to find the optimal BSS sizing and placement in a DN with high RES penetration. The work done by [19] proposes a multi-objective optimization problem to find the optimal sizing and allocation for DG and BSS, which is solved using the particle swarm algorithm and the modified non-sorting dominated genetic algorithm. Likewise, the authors in [29] addresses the simultaneous integration of DERs and include the optimum allocation of section switches for clustering the ADN into several MGs.

The previous formulations and approaches have been applied to address the sizing and siting of the DERs under a deterministic framework, mostly and without considered the DR or the EVs as variables. However, the transport sector electrification and the DR by the end-users are two new components gaining momentum in the new researches related to the DN planning for an efficient transition because their proper

implementation might improve network reliability [51]. The DR is defined by [52] as planned changes in electrical energy consumption patterns by end-use customers to improve the timing or/and the amount of their energy consumption in response to variable electrical energy prices overtime or incentive payments. Thus, the DR can support the stochasticity associated with the DGs through peak shavings, hosting capacity enhancement, and generation cost reduction [53]. On the other hand, EVs present a viable opportunity to introduce much higher shares of renewables into the overall power generation mix and create significant additional electricity demand [54].

In this regard, a comprehensive long-term distribution planning framework is developed by [55] to obtain the optimal sizing and siting of DG, substations, capacitors, feeders considering smart PEV charging demand, and DR under a deterministic perspective. The work done by [56] proposes a bilevel multi-stage optimization model for the distribution expansion planning (DEP) problem considering PEV. The authors in [56] use Bender decomposition to solve a two-stage DEP considering PEV and using the Monte Carlo simulation to model the uncertainty associated with the PEV. However, the formulation is not based on the OPF and does not include the angle and the reactive power. In our previous work [57], DG and BSS's optimal placement and sizing are addressed under a deterministic model based on the OPF equations but without considering DR and EVs. Besides in [57], the reactive power DG capacity is obtained separately from the active power overestimating the apparent power.

The previous literature highlights the significant impact and role of the DGs and BSS (DERs), EVs and DR in DN planning. The proper integration of these elements means efficient network operation, resiliency increasing, network stability, and reducing capital and operational cost. Thus their optimal integration is a field that is still in development due to the high complexity that involves the inclusion of these technologies and their stochastic behaviour into an optimization model, which include the network technical constraints. However, a lack of stochastic programming models is observed since most are deterministic models, which consider the stochasticity through different scenarios but not under a stochastic programming framework. Besides, the models available in the literature have not included the DERs apparent power capacity, their location, the DR effects, the EVs implication, and the reactive power compensation in the voltage stability simultaneously into a single two-stage stochastic model.

3.3 Mathematical Formulation

This section presents a two-stage stochastic mixed-integer non-linear problem (TSS-MINLP) for the sizing and location of DERs into low-voltage DN, considering network technical constraints, DG, storage devices, PEV, and DR. Thus, the objective function is formulated as follows:

$$Minimize \;\; F = B_I + B_C + DG_I + DG_C - EV + Gr. \tag{3.1}$$

Where:

$$B_I = \sum_{l\in\Psi}\sum_{i\in\mathcal{B}} y_i^l I_l^{bt} + \gamma_{l,i}^b Cb_l, \tag{3.2}$$

$$B_C = \sum_{l\in\Psi}\sum_{i\in\mathcal{B}}\sum_{t\in\mathcal{T}}\sum_{s\in\mathcal{S}} OMB_i^l(ds_{i,t,s}^l)\Delta t, \tag{3.3}$$

$$DG_I = \sum_{k\in\Omega}\sum_{i\in\mathcal{B}} x_i^k I_k^{gn} + \gamma_{k,i}^a Cp_k, \tag{3.4}$$

$$DG_C = \sum_{k\in\Omega}\sum_{i\in\mathcal{B}}\sum_{t\in\mathcal{T}}\sum_{s\in\mathcal{S}} OMG_i^k(pg_{i,t,s}^k + qg_{i,t,s}^k), \tag{3.5}$$

$$Gr = \sum_{i\in\mathcal{B}}\sum_{t\in\mathcal{T}}\sum_{s\in\mathcal{S}} \lambda_{t,s}(gp_{i,t,s} + gq_{i,t,s}), \tag{3.6}$$

$$EV = \sum_{i\in\mathcal{B}}\sum_{t\in\mathcal{T}}\sum_{s\in\mathcal{S}} (ds_{i,t,s}^{ev}\Delta t\varphi^{ev} H_t E_i^{ev}). \tag{3.7}$$

Similarly to the formulation presented in the previous chapter, Eq. (3.2) represents the battery's capital cost (B_I) through i) a binary variable (y_i^l) for the storage location and ii) a continuous variable ($\gamma_{l,i}^b$) for the battery capacity. This capital cost structure has been considered to avoid the non-linearity of multiply the location and the capacity variables. The cost associated with the battery installation includes the power electronics and is independent of the installed storage capacity. The battery's operational cost (B_C) is considered in Eq. (3.3) through the energy discharged to measure the battery use and degradation. The DG follows a similar cost structure. The capital cost (DG_I) in Eq. (3.4) is composed of a binary variable (x_i^k) when the resource is installed and a continuous variable ($\gamma_{k,i}^a$) for the apparent power capacity. Likewise, the operational costs of DG and the grid's power (Gr) are considered in Eq. (3.5) and (3.6), respectively, through the active and reactive power.

Eq. (3.7) represents the energy provided by EVs, where the power discharged is multiplied by the discharge efficiency, and two binary parameters which indicate i) if the EV is connected to the grid and ii) if the bus possesses an EV. Thus, the Eq. (3.1) minimizes the DERs capital and operational cost, the active and reactive power from

the external grid, and promote the energy provided by the EVs when they are plugged into the network. The first stage variables correspond to the DERs location and capacity, and the second stage variables are associated with the remaining variables that depend on the power provided by the DERs.

The formulation uses the power flow equations, for both lines and nodes, as a base to consider the technical constraints. Therefore; $\forall i \in \mathcal{B}, \forall t \in \mathcal{T}, \forall s \in \mathcal{S}$

$$v_{i,t,s}^2 G_i + v_{i,t,s} \sum_{(i,j)\in\mathcal{L}} v_{j,t,s}[G_{i,j}cos(\Delta\theta_{t,s}^{i,j}) + B_{i,j}sin(\Delta\theta_{t,s}^{i,j})] = \sum_{k\in\Omega} pg_{i,t,s}^k + \sum_{l\in\Psi}(ds_{i,t,s}^l - ch_{i,t,s}^l) - pl_{i,t,s} + gp_{i,t,s} + (ds_{i,t,s}^{ev} - ch_{i,t,s}^{ev}). \quad (3.8)$$

$$- v_{i,t,s}^2 B_i + v_{i,t,s} \sum_{(i,j)\in\mathcal{L}} v_{j,t,s}[G_{i,j}sin(\Delta\theta_{t,s}^{i,j}) - B_{i,j}cos(\Delta\theta_{t,s}^{i,j})] = \sum_{k\in\Omega} qg_{i,t,s}^k - QL_{i,t} + gq_{i,t,s}, \quad (3.9)$$

Therefore; $\forall (i,j) \in \mathcal{L}, \forall t \in \mathcal{T}, \forall s \in \mathcal{S}$,

$$v_{i,t,s}v_{j,t}[G_{i,j}cos(\Delta\theta_{t,s}^{i,j}) + B_{i,j}sin(\Delta\theta_{t,s}^{i,j})] - G_{i,j}v_{i,t,s}^2 = p_{t,s}^{i,j}, \quad (3.10)$$

$$v_{i,t,s}v_{j,t,s}[G_{i,j}sin(\Delta\theta_{t,s}^{i,j}) - B_{i,j}cos(\Delta\theta_{t,s}^{i,j})] + v_{i,t,s}^2(B_{i,j} - Bs_{i,j}) = q_{t,s}^{i,j}. \quad (3.11)$$

The right-hand side of Eq. (3.8) considers form left to right, the active power from de DG units, the discharge or charge from/to the batteries, the electricity demand, the power supplied by the external grid, and the EV discharge or charge. The left-hand side remains without variation. Unlike active power, the right-hand side of Eq. (3.9) considers the reactive power demand as a parameter known ($QL_{i,t}$) where the reactive power is supplied by the DGs units ($qg_{i,t,s}^k$) or the external grid ($gq_{i,t,s}$). Eqs. (3.10) and (3.11) related to the lines power flow are not explained because they do not present any change from the original AC OPF formulation.

The active and reactive power injected from the DG units is bounded by the following constraints. Therefore; $\forall i \in \mathcal{B}, \forall k \in \Omega, \forall s \in \mathcal{S}$,

$$0 \leq pg_{i,t,s}^k \leq \gamma_{k,i}^p PG_{k,t,s}^{max}, \quad (3.12)$$

$$\gamma_{k,i}^p \leq x_i^k U_k^g, \quad (3.13)$$

$$-\Gamma_{k,t,s}\gamma_{k,i}^s \leq qg_{i,t,s}^k \leq \gamma_{k,i}^s \Gamma_{k,t,s}. \quad (3.14)$$

Eq. (3.12) bound the power injected by the DG units by multiplicating the active power capacity and the maximum power available to generate at a certain period.

This maximum power corresponds to the DERs power generation normalized curve, regarding its maximum value (see section 3.4.1 for an example). Likewise, Eq. (3.13) limits the active power capacity under a maximum capacity allowed multiplied by whether the DG unit is installed. Eq. (3.14) is deduced through the relation between the active and reactive power injected into the grid and the apparent power capacity installed (properly addressed in 3.4.5). Thus, Γ is the percentage of available reactive power that can be absorbed or injected into the grid, multiplied by the apparent power capacity installed.

Eqs. (3.15) and (3.16) correspond to the voltage and line capacities, respectively. Therefore; $\forall i \in \mathcal{B}, \forall t \in \mathcal{T}, \forall s \in \mathcal{S}$,

$$V^{min} \leq v_{i,t,s} \leq V^{max}, \tag{3.15}$$

$$\sqrt{p^2_{i,j,t,s} + q^2_{i,j,t,s}} \leq S^{max}_{i,j}. \tag{3.16}$$

The set of Eqs. (3.17)-(3.22) that represent the battery behaviour have been taken from the previous chapter, where every variable and equation are explained. Therefore; $\forall i \in \mathcal{B}, \forall t \in \mathcal{T}, \forall l \in \Psi, \forall s \in \mathcal{S}$,

$$soc^l_{i,t+1,s} = soc^l_{i,t,s} + [\varphi^l ch^l_{i,t,s} - \frac{1}{\varphi^l} ds^l_{i,t,s}]\Delta t, \tag{3.17}$$

$$(\gamma^b_{l,i}) SOC^{min}_l \leq soc^l_{i,t,s} \leq SOC^{max}_l (\gamma^b_{l,i}), \tag{3.18}$$

$$\gamma^b_{l,i} \leq y^l_i U^b_l, \tag{3.19}$$

$$ch^l_{i,t,s} \leq w^l_{i,t,s} M^l, \tag{3.20}$$

$$ds^l_{i,t,s} \leq M^l(1 - w^l_{i,t,s}) - M^l(1 - y^l_i), \tag{3.21}$$

$$w^l_{i,t,s} \leq y^l_i. \tag{3.22}$$

Based on the battery formulation, the Eqs. (3.23)-(3.27) model the EV behaviour. Thus; $\forall i \in \mathcal{B}, \forall t \in \mathcal{T}, \forall s \in \mathcal{S}$,

$$soc^{ev}_{i,t+1,s} = soc^{ev}_{i,t,s} + [\varphi^{ev} ch^{ev}_{i,t,s} - \frac{1}{\varphi^{ev}} ds^{ev}_{i,t,s}]\Delta t H_t E^{ev}_i - \frac{Dc^{ev}_t}{\varphi^{ev}} \Delta t (1 - H_t) E^{ev}_i, \tag{3.23}$$

$$\psi^{ev} \underline{SOC}^{ev}_t \leq soc^{ev}_{i,t,s} \leq \overline{SOC}^{ev}_t \psi^{ev}, \tag{3.24}$$

$$ch^{ev}_{i,t,s} \leq w^{ev}_{i,t,s} M^{ev}, \tag{3.25}$$

$$ds^{ev}_{i,t,s} \leq M^{ev}(1 - w^{ev}_{i,t,s}) - M^{ev}(1 - E^{ev}_i), \tag{3.26}$$

$$w^{ev}_{i,t,s} \leq E^{ev}_i. \tag{3.27}$$

Eq. (3.23) includes additional two known binary vectors, which indicate whether the bus possesses an EV connection (E^{ev}_i) and the EV plug-in profile (H_t), respectively. Thus, when the EV is not connected to the grid ($H_t = 0$), its state of charge

decreases constantly in Dc_t^{ev} kWh. Otherwise, it works as a standard battery. Eq. (3.24) indicates the EV operational limits, where the EV storage capacity is multiplied by the minimum and maximum operational range allowed. However, unlike Eq. (3.18), the SOC parameters in Eq. (3.24) possess a sub-index t, which indicate that the minimum and maximum are vectors with length $\mathcal{T}$, allowing to manage the minimums state of charge for the proper EV operation. For example, by default, for the 24 hours, we set the minimum SOC at 10% for every t, except at 8 am, where the minimum is set at 70% to ensure that the EV is at least 70% charged. In other words, the EV could charge or discharge when it is connected, but at 8 am, it must be 70% charged as a minimum. The logical constraints (3.25)-(3.27) are similar to the battery behaviour.

The flexible demand is modeled through the constraints (3.28) and (3.29). Therefore; $\forall i \in \mathcal{B}, \forall t \in \mathcal{T}, \forall s \in \mathcal{S}$,

$$pl_{i,t,s} = Pf_{i,t,s} + \sum_{d \in \mathcal{D}} \tau_{i,t,s}^{d} Pv_i^d. \tag{3.28}$$

Therefore; $\forall i \in \mathcal{B}, \forall d \in \mathcal{D}, \forall s \in \mathcal{S}$,

$$\sum_{t \in \mathcal{T}} \tau_{i,t,s}^{d} = Fl_i^d. \tag{3.29}$$

The total electricity load in Eq. (3.28) is composed of unmanageable demand ($PL_{i,t}$) and flexible demand (Pfd^d), which could be activated at any time t depend on the generation and consumption level, in order to minimize the energy purchased to the grid. Thus, the binary variable $\tau_{i,t}^d$ is 1 when the flexible load is activated and zero otherwise, allowing different types of flexible loads activated in the same period t, such as air conditioner, wash, and dish machine. Eq (3.29) indicates the total numbers of hours that a type of demand must be activated at a certain time horizon.

Finally, Eq. (3.30) and Eq. (3.31) limit the total capacity installed on the DN.

$$\sum_{i \in \mathcal{B}} \sum_{k \in \Omega} \gamma_{k,i}^{p} \leq U_k^G, \tag{3.30}$$

$$\sum_{i \in \mathcal{B}} \sum_{l \in \Psi} \gamma_{l,i}^{b} \leq U_k^B. \tag{3.31}$$

3.4 Methodology

This section explains i) how the weather resources are managed to create the scenarios, ii) the network, the EV, and the flexible demand parameters, iii) the backward

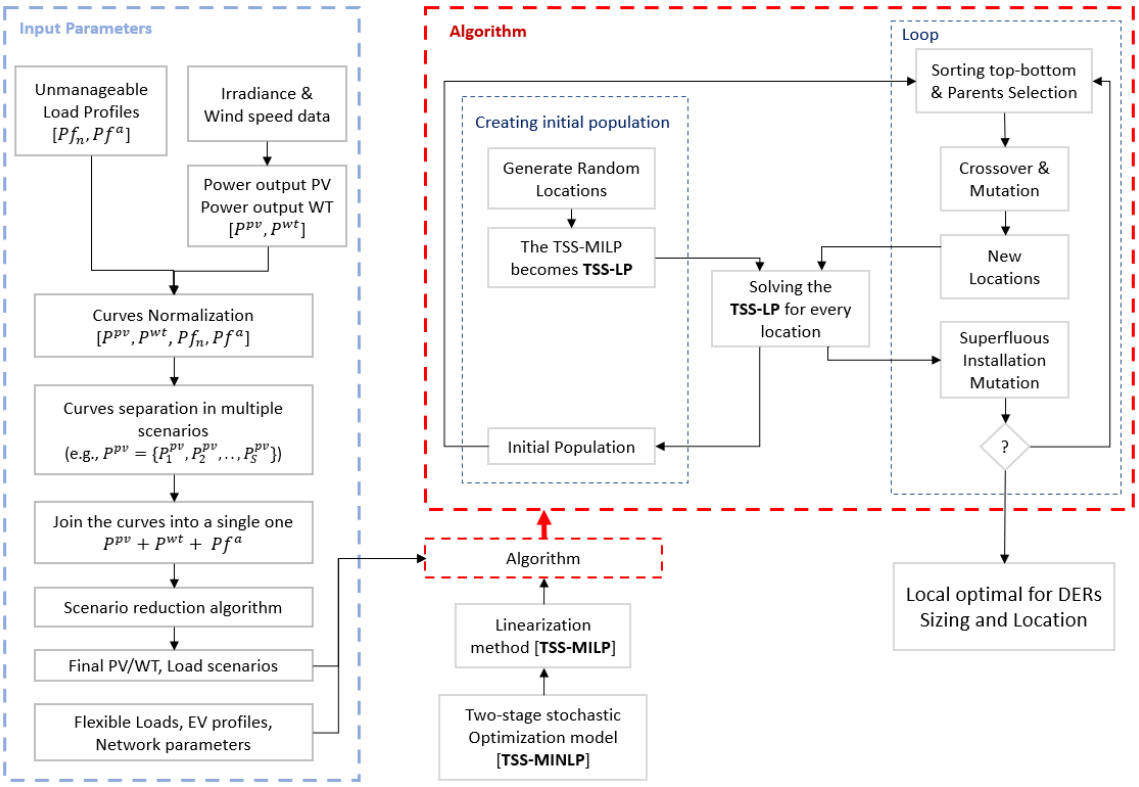

Figure 3.1: Methodology scheme

algorithm to reduce the number of scenarios, iv) the linearization applied to the TSS-MINLP, v) the algorithm to solve the TSS-MILP, and vi) how the reactive power is addressed in the formulation proposed.

3.4.1 DER units and loads modelling

The model considers PV and WT systems like DGs units. The solar irradiation, the environment temperature, and the wind speed are the primary input parameters to generate the power available. The PV power output is generated using [58] and the WT power output following the model [59]. Due to the model find the optimal DER capacity, the power output curves obtained through the models [58, 59] are normalized regarding their respective maximum values. Therefore, for a specific PV and WT technology, the output power is normalized to obtain two vectors, with values between zero and one, representing the PG_t^{max} parameter described in the model. For example, if the final capacity PV installed is 10 kW, and PG_{11}^{max} is 0.3 at 11 am, then the maximum power injected into the DN could be 3 kW.

The unmanageable load profiles follow the same normalizing process. Thus, every profile is normalized concerning its maximum value, and an additional normalized

curve is generated with the aggregated load profiles.

Therefore, the available power for PV and WT systems is represented through two normalized curves named P^{pv} and P^{wt}, which contains their respective PG^{max} for every time slot. Likewise, the load profiles, corresponding to the unmanageable electricity demand, are normalized, naming every normalized load profile Pf_m, where m belongs to the load profiles set M. Lastly, an aggregated normalized curve that includes the total system load Pf^a is generated. Thus, the curves with length N (historical data length) are expressed as follows:

$$\begin{aligned} P^{pv} &= \{PG^{max}_{1,1}, PG^{max}_{2,1}, ..., PG^{max}_{N,1}\} && for \quad k = 1 \\ P^{wt} &= \{PG^{max}_{1,2}, PG^{max}_{2,2}, ..., PG^{max}_{N,2}\} && for \quad k = 2 \\ Pf_m &= \{Pf_1, Pf_2, ..., Pf_M\} && m \in M \\ Pf^a &= \{Pf^a_1, Pf^a_2, ..., Pf^a_N\} \end{aligned}$$

Where,

$$\begin{aligned} Pf_1 &= \{Pf_{1,1}, Pf_{1,2}, ..., Pf_{1,N}\} \\ Pf_2 &= \{Pf_{2,1}, Pf_{2,2}, ..., Pf_{2,N}\} \\ &\vdots \\ Pf_M &= \{Pf_{M,1}, Pf_{M,2}, ..., Pf_{M,N}\} \end{aligned}$$

3.4.2 Scenarios creation

To create multiple scenarios from the historical data, we define a scenario time horizon, and then, the historical data is divided by the time horizon. Thus, every scenario $s \in \mathbb{S}$ possesses a time horizon $\mathcal{T}$ such that $\mathcal{T} = \{t, t + \Delta t, \ldots, \mathcal{T}\}$, where t is the time slot of the previous curves. For example, if the original curves possess one hour of time slot over one year of data, and if the time horizon is set up in 24 hours, every curve would contain 365 scenarios of 24 hours. Therefore, the scenarios for solar power ($k = 1$) are express as following:

$$P^{pv} = \{P^{pv}_1, P^{pv}_2, ..., P^{pv}_S\}$$

where,

$$\begin{aligned} P^{pv}_1 &= \{PG^{max}_{1,1}, PG^{max}_{2,1}, ..., PG^{max}_{T,1}\} && for \quad k = 1 \\ P^{pv}_2 &= \{PG^{max}_{T+1,1}, PG^{max}_{T+2,1}, ..., PG^{max}_{2T,1}\} && for \quad k = 1 \\ &\vdots \\ P^{pv}_S &= \{PG^{max}_{ST+1,1}, PG^{max}_{ST+2,1}, ..., PG^{max}_{N,1}\} && for \quad k = 1 \end{aligned}$$

Nevertheless, considering a high number of scenarios in the model proposed implies high computational efforts [60]. Therefore, to address this issue, a reduction scenario method is used to remove similar scenarios and maintain a small number representing the essential features of the uncertainty. The well known backward algorithm [61] is used in this chapter to reduce the number of scenarios since its accuracy has been proven in many two-stage mixed-integer stochastic programming problems [62].

However, to appropriately applied this algorithm, the three curves (P^{pv}, P^{wt}, Pf^{a}) must be merged into a single one to maintain the temporal relationship between them. The reason to not consider the curves independently is that the algorithm could choose different scenarios for every curve so that the scenario $s \in P_t^{pv}$ would not be related to the scenario choose for P^{wt} or Pf^{a}. The criteria to join the curves have been the difference between the Pf_t^a and the sum of P_t^{pv} and P_t^{wt}. In order to avoid negative values, the difference is set up in zero in cases when the DERs produce more than the load; thus, when a time slot is close to zero means that there are sufficient weather conditions to meet the load, otherwise, a value close to one indicates that the load is much greater than the resources available, and therefore, the capacity that should be installed would be higher. Note that the united curve is used only to select the scenarios through the algorithm; once that the algorithm finds the scenarios, the mathematical model uses the selected scenarios corresponding to P^{pv}, P^{wt}, and Pf_n.

3.4.3 Linearization method

The non-linear and non-convex formulation in section 3.3 requires a linearization method or a convex relaxation method due to the high computation burden of the model in a multiperiod and stochastic context. In the literature, the linearization and relaxation techniques have been applied widely to address the optimal power flow constraints without losing the reactive and angle variables on the process.

Thus, summarizing the literature review done in the previous chapter, the authors in [30] use the QP approach with SOCP to solve a multiperiod AC OPF. A comparison between the QC relaxation with SDP and SOCP is made by [31]. A different techniques overview applied to power system planning, including the interior point method, Newton method, QP, and a hybrid version of linear programming, and integer programming, is presented in [32, 33]. An improving successive linear programming is done by [11] to reduce the number of iterations. This chapter applied the linearization method proposed by [10], transforming the Eqs. (3.8), (3.9), (3.10), (3.11), and (3.16) in linear constraints. Its full explanation is described and tested in the previous chapter.

3.4.4 Algorithm description

The linear model version (TSS-MILP) still has the binary variables problem related to the DERs location. The algorithm developed in the previous chapter ([57]) has been used to address the location variables, transforming the TSS-MILP obtained from the previous step into an TSS-LP. The algorithm uses the logic behind the GA to randomly generate the binary variables and solve the TSS-LP iteratively.

In general terms, the algorithm possesses the same stages as a GA. The initial population creation consists of generating the DERs location and the battery charge/discharge decision randomly. Then, for every set of random location, the TSS-MILP, now an TSS-LP, is solved, and the objective function result is saved as a reference or fitness function (FF) value. Once the initial population is created, start the loop stage where every individual (set of random location) is top-bottom sorted, according to its objective function result, forming couples to proceed with the crossover process, which implies crossing the locations to obtain two new locations, which in turn may undergo some mutation during the process. Then, for every new location, the TSS-LP is solved, and the loop starts again.

An extra stage is proposed in [57], which consists in accelerate the convergence process through a new mutation that changes the location slot with zero capacity instaled. This situation is a possible solution because the location is random, and the capacity is obtained by solving a capacity optimization problem (the TSS-LP).

The complete algorithm description, its convergence and its accuracy have been carefully presented in [57]. Besides, a process summary is represented schematically in Fig. 3.1

3.4.5 Reactive power capacity

The mathematical formulation presented in section 3.3 obtains the optimal apparent power capacity installed to face the load considering the weather conditions and the capital costs associated. The DERs capability to provide reactive power through the power electronic has been a research area over the last years [63]. Many works have studied reactive power compensation from PV and WT systems [64, 65] to manage the voltage stability, the line losses, and the option to provide reactive power AS in a day-ahead market [66]. However, when the apparent capacity is considered, it implies associating the active and the reactive power injected into the node follows the equation presented below. Therefore, $\forall i \in \mathcal{B}, \forall k \in \Omega, \forall s \in \mathcal{S}, \forall t \in \mathcal{T}$,

$$\left(pg^{k}_{i,t,s}\right)^2 + \left(qg^{k}_{i,t,s}\right)^2 \leq \left(\gamma^{s}_{k,i}\right)^2 . \tag{3.32}$$

Nevertheless, unlike Eq. (3.16), the DERs apparent power capacity is a variable and not a parameter as the line apparent power, which belongs to network parameters. Therefore, the linearization proposed by [10] cannot be applied over Eq. (3.30). To handle this non-linearity, we assume a particular power factor (PF); thus, the active power capacity is expressed in terms of the apparent power (Eq. (3.33)), and Eq. (3.32) is rewritten as follow:

$$\gamma^p_{k,i} = PF\gamma^s_{k,i}, \tag{3.33}$$

$$\left(qg^k_{i,t,s}\right)^2 \leq \left(\frac{\gamma^p_{k,i}}{PF}\right)^2 - \left(pg^k_{i,t,s}\right)^2 \tag{3.34}$$

To express the right-hand side of Eq. (3.34) in linear terms, we assume that the power injected into the node is equal to the maximum power available. i.e., $pg^k_{i,t,s} = \gamma^p_{k,i} PG^{max}_{k,t,s}$ in Eq. (3.12). Thus, the reactive power injected into the node is bounded under the following expression:

$$\begin{aligned}
qg^k_{i,t,s} &\leq \sqrt{\left(\frac{\gamma^p_{k,i}}{PF}\right)^2 - \left(\gamma^p_{k,i} PG^{max}_{k,t,s}\right)^2} \\
qg^k_{i,t,s} &\leq \sqrt{\left(\gamma^p_{k,i}\right)^2 \left(\frac{1 - (PG^{max}_{k,t,s} PF)^2}{PF^2}\right)} \\
qg^k_{i,t,s} &\leq \frac{\gamma^p_{k,i}}{PF}\sqrt{1 - (PG^{max}_{k,t,s} PF)^2} \\
qg^k_{i,t,s} &\leq \gamma^s_{k,i}\Gamma_{k,t,s}
\end{aligned}$$

Gamma represents the maximum reactive power available to be supplied; thus, Eq. (3.14) is deduced from Eq. (3.34) considering a PF and assuming that the DERs power injected is equal to the maximum available power in a particular time slot. This assumption allows linearizing the reactive power provided by the DERs, considering the active power injected. However, if the OPF finds a $pg^k < \gamma^p PG^{max}$, then the reactive power margin would be undervalued. This event could happen under peak generation curtailment, but with the storage devices presence and maximizing the DG use, these particular events decrease [67], so that the reactive power undervaluation occurs under very particular circumstances, and therefore, is an acceptable cost to linearize the Eq. (3.34). Note that the assumption is exclusively to find the Γ parameter; the active power pg continues to be a decision variable.

3.4.6 Cost modelling

The objective function considers the trade-off between the capital and operational cost with the energy bought from the grid, which means that these values must be on

the same temporal scale to make them comparable. Therefore, the linear depreciation for the capital cost is considered in the proper scale (e.g., if the temporal scale is 24 hours, the annual linear depreciation is divided by 365). Likewise, the operational cost, usually measured in kWh/yr., is also modified to the kWh/T, where T is the scenario temporal scale.

3.5 Case study and computational results

In this section, the stochastic model is tested for different case studies, always considering the same test system, where each case study possesses three scenarios of 24 h. Then, the classic OPF for a whole year, considering a time slot of one hour, is used to test the capacity/location results from every case, to analyze the trade-off between the power energy share from the renewable system and the power provided by the main grid.

3.5.1 Network and data parameters

The mathematical formulation is tested in the IEEE 69 bus system [68], which contains 68 lines and 47 loads. The peak loads for active and reactive power have been modified to be consistent with the load profiles used, which correspond to residential and commercial USA demands in a low-voltage DN [69]. However, the loads' modifications have been done respecting the original active and reactive power load proportion. Thus, the profiles include 35 and 12 residential and commercial loads, as shown in Table 3.1. Historical temperature, irradiation, and wind speed data from Barcelona [70] have been used to obtain the output power for PV panels and WT.

The maximum generation capacity to install in every node is 20% greater than its peak load, and for nodes without a load, the maximum capacity has been set at 100 kW. Likewise, the total capacity installed for DG and BSS on the DN has been established at 3 MW and 1.5 MW, respectively. For a whole year, the hourly energy price was taken from [45], and the capital and operational cost for the DG types and BSS types from [34, 42, 43, 44].

The DN considers 30 EVs, and every one of them follows the same connection pattern: connected between 7 pm to 8 am and disconnected between 9 am to 6 pm. The EV works like a battery in plugged hours such that at the disconnect hour, its state of charge must be greater than 70%. Every EV possesses a capacity of 24 kWh, a charge/discharge rated power of 3 kW, and a constants discharge rate of 1.3 kW when it is disconnected. It has been considered 12 buses with DR, which takes values

Table 3.1: Peak load of active [kW] and reactive [kVAr] power by bus and profile

Bus	**PL**	**QL**	**Profile**	Bus	**PL**	**QL**	**Profile**
6	2.6	2.2	Residential	48	6.6	4.7	Residential
7	4	3	Residential	51	5.1	3.5	Residential
8	5	3.6	Residential	52	3.6	2.7	Residential
9	4.3	3.1	Residential	53	4.4	3.5	Residential
10	5.6	3.8	Residential	54	6.6	4.8	Residential
13	5.3	3.3	Residential	55	6	4.3	Residential
14	5.3	3.7	Residential	62	6.4	4.6	Residential
16	5.7	3.8	Residential	65	5.9	4.2	Residential
17	6	3.5	Residential	66	6	4.3	Residential
18	6	3.5	Residential	67	6	4.3	Residential
20	1	0.6	Residential	68	6.2	4.4	Residential
22	5	3.5	Residential	69	6.2	4.4	Residential
24	5.6	4	Residential	21	22.8	16.2	FastFood
26	6.1	4.3	Residential	45	26.1	17.5	FastFood
27	6.1	4.3	Residential	61	829.3	592	Hospital
33	5.6	4	Residential	50	320.6	228.8	Hotel
34	4.8	7	Residential	12	29	20.8	Restaurant
35	6	4	Residential	59	33.3	24	Restaurant
36	5.2	3.7	Residential	64	113.5	81	School
37	5.2	3.7	Residential	28	8.7	6.2	Small Office
39	4.8	3.4	Residential	29	8.7	6.2	Small Office
40	5.3	3.8	Residential	11	32.2	23.1	StripMall
41	1.2	1	Residential	49	256.5	183	SuperMarket
43	6	4.3	Residential	46	32.7	21.9	WareHouse

between 2.5 and 7.5 kW, and it can be activated once per day, excepted in bus 12 and 59, which can be activated twice (see Eq. 3.29). Fig. 3.2 shows the DN layout indicating the type of load (residential or commercial) for every bus, the buses with an EV, and which buses have access to DR.

The algorithm and the optimization model have been programmed in Pyomo Python using CPLEX as the main solver, taking around 7 hours to run the algorithm and 12 hours to run the classic OPF for the annual data. In addition, the deterministic model has been validated in the previous chapter, comparing the results using the algorithm and the optimization model with the work in [41]; therefore, as the power flow constraints do not include a drastic change, the authors have extended the deterministic validation to the stochastic version presented in this chapter.

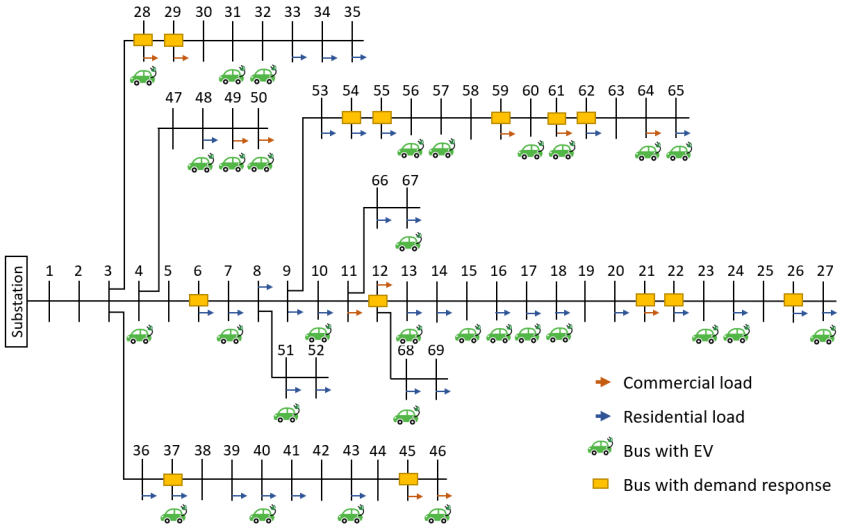

Figure 3.2: Modified IEEE 69-bus distribution network

3.5.2 Case studies

To provide a sensibility perspective about the capacity and location obtained through the model proposed, six different cases have been considered, such that everyone possesses a set of three different non-consecutive scenarios of 24 h. Note that the network and the parameters defined previously are fixed for every case study. Two methods have been used to set the scenarios for the six case studies. The first method is used only to create the first case, which for the first scenario selects the day with the best wind speed and solar irradiation simultaneously, the second scenario with the best solar conditions, and the third scenarios with the best wind speed condition. Then, the backward algorithm obtained the other 15 scenarios belonging to the remaining five cases.

Fig 3.4 shows the scenarios for every case study. Thus, *Case 1* presents the best weather conditions of the remaining cases of studies. In fact, in scenario 1 and 3, the wind resource is higher than the electricity demand at almost every hour, and the scenario 2 possess the best solar irradiation. *Case 2* and *Case 4* possess scenarios with low wind conditions compared with the other cases where at least one scenario possesses suitable wind resources. *Case 6* is the only one with the maximum wind resource for many consecutive hours and the minimum in the next two scenarios. In addition, it possesses the lowest average energy price compared with the remaining cases. *Case 5* is the second case with a lower energy price average, unlike *Case 3*, which possess the highest energy price.

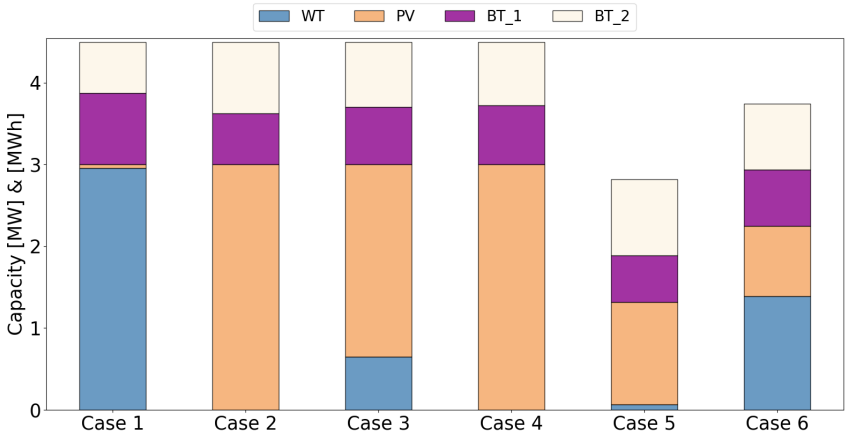

Figure 3.3: Total capacity installed of WT, PV, lead-acid battery (BT 1), and Li-ion battery (BT 2) for every case study.

3.5.3 Computational results

The DERs' location and their respective capacities are presented in detail in Table 3.3 and 3.4. Note that the model installs DERs in many buses because the peak load bounds the maximum installed capacity; therefore, the following analysis is focused on the global DERs capacities for every case study rather than the capacity of each bus. Fig 3.3 presents the total DG and BSS capacity installed for every case study. As is expected, the optimal sizing found by the algorithm depends on the scenario set selected. Therefore, for scenarios with high solar irradiation or wind speed, the capacity associated with PV or WT is higher, as appropriate. In the four first cases, the model installs a different proportion of DG, but the total installed corresponds to the maximum defined, 3MW. However, in Case 5 and 6, the total DG capacity is below this maximum, reaching 1.3 MW and 2.2 MW, respectively. This result occurs because the energy price belonging to these scenarios is lower than the others, impacting the generation capacity assigned. On the other hand, the storage devices sizing always reach their maximum allowed, set at 1.5 MW for all network, changing only the proportion of the type of BSS, prevailing the lead-acid battery in five of the six cases of studies.

According to the methodology presented in the previous section, the location and capacity obtained are used to run the classic OPF to study the energy share provided by the DERs and the main grid. The goal here is to analyze which case or set of scenarios presents a less main grid share when the whole year is considered. Table 3.2 shows these results as follows:

Table 3.2: Power provided by DERs, Load composition, Reactive power, Days from the year, DERs numbers installed, CapEx and OpEx.

		Case 1	Case 2	Case 3	Case 4	Case 5	Case 6
a)	WT	53.2%	0.0%	23.9%	0.0%	8.0%	27.4%
	PV	15.5%	46.7%	46.7%	47.7%	45.8%	45.3%
	Grid	28.3%	51.1%	26.7%	50.0%	44.0%	24.4%
	BT	2.8%	2.0%	2.5%	2.2%	2.0%	2.6%
b)	EV	1.2%	1.2%	1.2%	1.2%	1.2%	1.2%
	Flex Load	0.2%	0.2%	0.2%	0.2%	0.2%	0.2%
	PL	98.7%	98.6%	98.6%	98.6%	98.6%	98.6%
	Total Load	100%	100%	100%	100%	100%	100%
c)	QG DERs	100%	100%	100%	100%	100%	100%
	QG Grid	0%	0%	0%	0%	0%	0%
d)	Days/Sc 1	352	241	96	191	229	318
	Days/Sc 2	2	249	108	243	253	349
	Days/Sc 3	319	314	152	245	312	364
e)	WT units	40	0	10	0	1	7
	PV units	3	44	36	39	18	24
	BT units	54	58	56	50	63	58
f)	Op. Cost [k€]	0.206	0.404	0.193	0.397	0.339	0.175
	CapEx [k€]	3,850	3,008	3,186	2,989	1,521	2,734

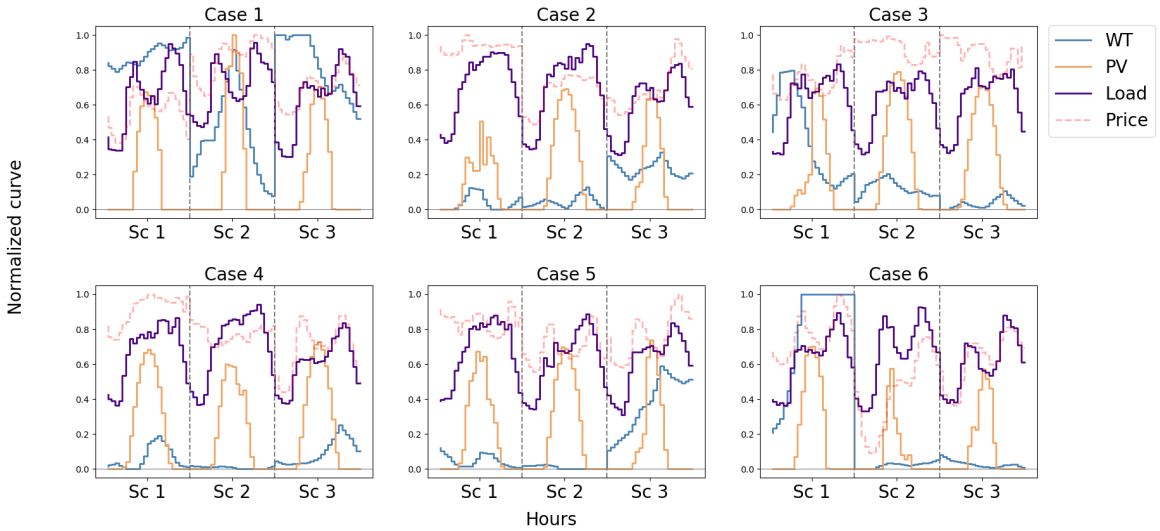

Figure 3.4: Normalized curves of Wind Turbine (WT), Photovoltaic system (PV), Aggregate Load (Load), and Energy Price for every scenario belonging to every case study

a *Power provided by DERs*: the cases study 1, 3, and 6 have the lower primary grid participation and possess a significant WT power installed regarding the other cases where the PV systems are predominant. However, when the PV and WT capacity assigned are similar, the grid's energy is the lowest, which occurs in the sixth case study. In contrast, when the installed capacity is dominated by PV systems, the power provided by the grid is higher. The battery percentage indicates the net energy (the difference between the injected and absorbed energy for the whole year) provided by both types of BSS, which remain stable at around 2.2%.

b *Load composition*: the total system electricity demand comprises a fixed load, a lower percentage of flexible demand, and the energy required to charge the EV. The behaviour of the flexible demand and the EV operation is appropriately addressed in the following subsection.

c *Reactive power*: 100% of the reactive power is provided by the DG units for the whole year, suggesting the great DG potential to offer AS based on reactive power.

d *Days from the year*: indicates the day selected from the annual historical data for every case study. Thus, the first case study comprises three different scenarios, which correspond to day 352, 2, and 9 of the year.

e *DERs numbers installed*: shows the numbers of buses with a DG and or BSS system installed, where almost 80% of the nodes have storage devices installed. The high BSS assignment is explained because i) the power consumption at every node bounds the capacity allowed to install (spreading the total capacity available across the network in several buses), and ii) the storage devices allows increase the DGs efficiency and reduce their capacity installed [67].

f *CapEx and OpEx*: The OpEx indicated in Table 3.2 considered the energy provided by the system and the grid for the whole year. Specifically, the active and reactive power purchased to the grid, the power discharged from the battery, and the power supplied by the DGs. The CapEx includes the batteries' power electronic and its capacity cost, plus the DG placement with their apparent power capacity. The operational costs are strictly related to the percentage informed top of the table since the higher the power provided by the main grid, the bigger the global system cost. On the other hand, the investment

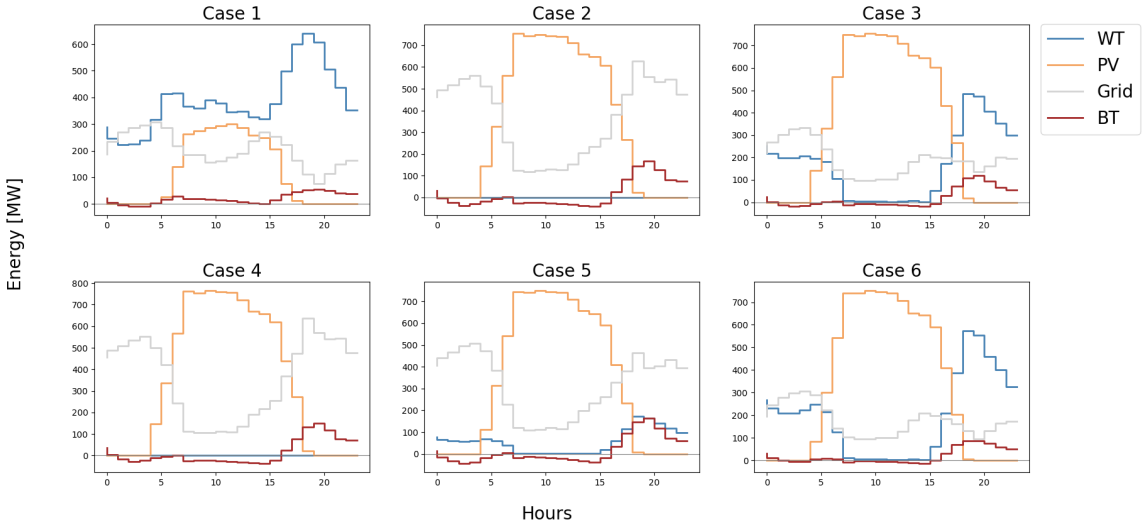

Figure 3.5: Annual aggregate energy in a 24-hour view

is explained mainly by the DGs capacity installed. Thus, the higher the WT capacity, the higher is the total investment.

Fig 3.5 and 3.6 show the energy provided by the DERs and the main grid from an hourly and monthly perspective. The 24 hours view makes it easy to observe when the main grid provides the energy or when the storage devices present a relevant role. Specifically, with high PV power output, the mid hours are when the energy provided by the grid is lower. Likewise, the batteries usually charge in the first 2/3 of the day, and at night, they start discharging, which coincide with a higher energy price. Fig 3.5 suggests that when there is no WT installed, which is the second, fourth, and five case study, the main grid covers the hours without renewable generation, which is totally expected. However, in cases with WT presence, the grid energy decrease and increase the DERs autonomy. On the other hand, Fig 3.6 shows the monthly perspective, which provides the renewable resources seasonality view. Likewise, the battery role, unlike to be lower, the months with higher participation is when there is high power output from the DG.

3.5.4 Flexible demand and electric vehicles

Fig. 3.7 presents the aggregated charge or discharge of the EV by hours. The results show that the EVs discharge during the first and last hours of the day and the hours previous disconnecting. Specifically, contrasting the pricing curve in Fig 3.4 with Fig 3.7 for the first third and in the last hours of the day, the EV discharge occurs when

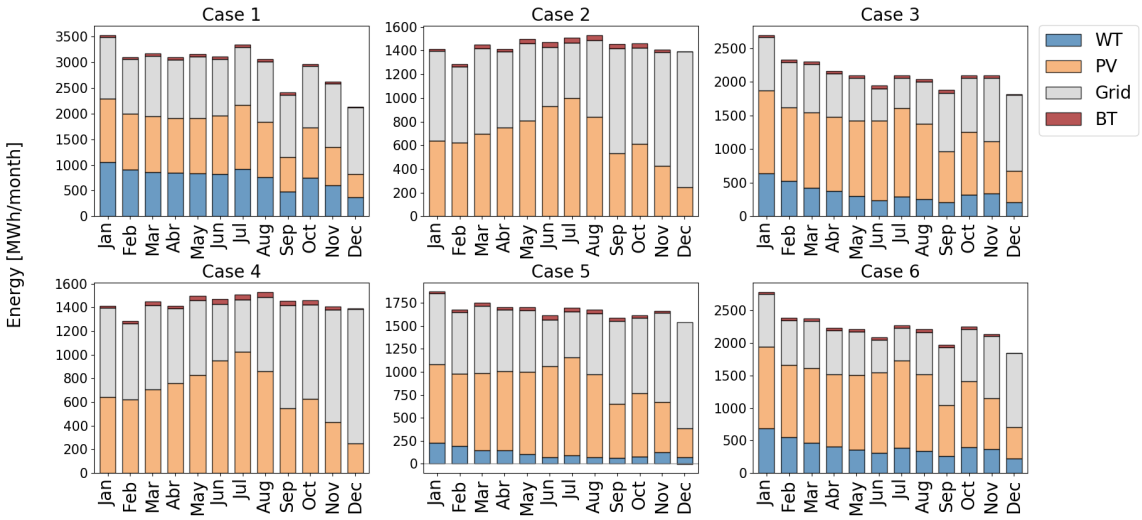

Figure 3.6: Annual aggregate energy in a monthly view

the previous hours to the charging process hours are more expensive. i.e., considering that the EV charge between 2-5 am if the energy price between 0-1 am is expensive than the 2-5 am, then the EV discharge, otherwise, save the EV SOC, as shows the Case 1 and Case 2 in Fig 3.7. In addition, Fig 3.7 shows the EV SOC in the right axis to justified the discharging at the disconnecting previous hours. Thus, when the SOC is greater than 70%, the EV discharge. In case study 3, the EV SOC reaches only 70%, in contrast with other scenarios, due to the energy price is the highest of the cases study, which implies a low charge and discharge cycle.

Nevertheless, what happens if the EV is not able to inject power into the grid? Might this consideration impact the optimal DERs capacity installed? An extra case, taking the modelling of the EV like a load, was tested to answer these questions. Under this case, the EV does not provide power to the grid, the DERs capacity installed decrease because the objective function in (3.1) promote the power from the EV; thus, when the EVs deliver power into the DN, the SOC reach their maximum in some hours to deliver energy in hours when is required. However, when the EV cannot provide energy, the SOC reaches only the minimum SOC required to operate correctly. On the other hand, unlike the CapEx increase when the EVs discharge energy into the DN, the operation cost decreased 4.57% due to the energy provided by the vehicle generate incomes in hours when the energy price is high. Therefore, a trade-off occurs between the DERs capacity installed and the OpEx when the EVs can discharge energy, increasing the investment but decreasing the operational cost.

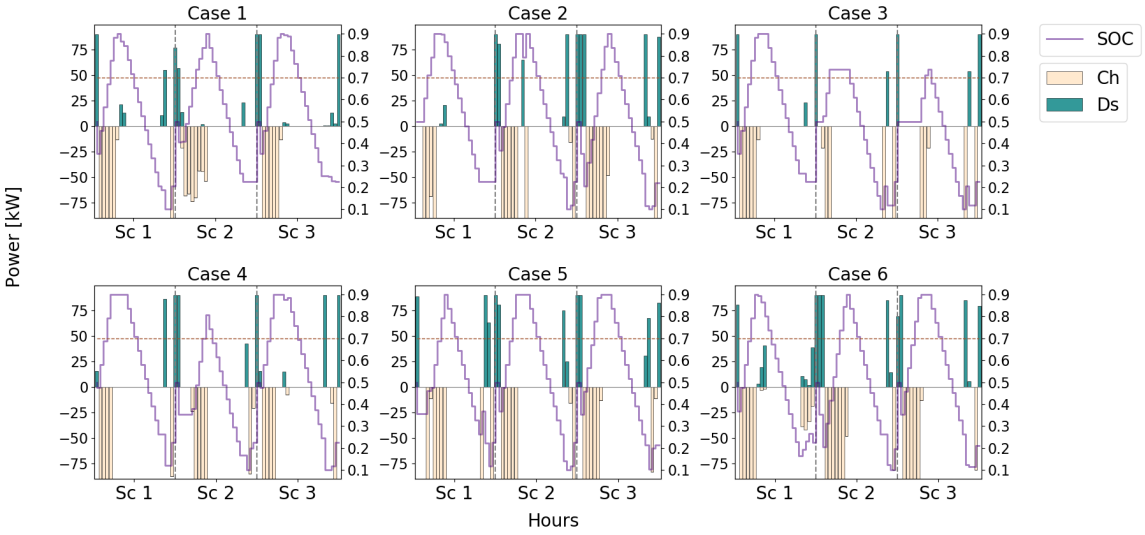

Figure 3.7: Aggregate charge (Ch) and discharge (Ds) by hour of the electric vehicles compared with their aggregated state of charge (SOC).

Finally, Fig 3.8 shows the aggregated flexible demand and when occurs its activation (through the binary variable $\tau^{d}_{i,t,s}$). Thus, comparing Fig 3.4 with Fig 3.8, the criteria followed by the buses to activate their demand response are when the fixed electricity demand is low, when the energy price is low, or when the power generation from the DGs is high.

3.6 Discussion and model limitations

The previous section tested the two-stage stochastic model under 18 different scenarios of 24 hours, grouped into six case studies. The results show that the set of scenarios chosen is critical in the optimal sizing obtained from the model. The backward algorithm used to reduce the numbers of scenarios seems not to be proper to find the optimal set that provides the most representative scenarios of the historical data. In this regards, Case 2 represents the most three statistically different scenarios from the 365; however, when the capacity obtained for this case study is applied for the whole data set, the energy generated by the DERs system is lower than the Case 6. Therefore, to find the optimal global capacity for the whole dataset, a new algorithm is required that find the most representative scenarios in terms of the weather condition, the energy price, and the electricity load.

Despite requiring a previous algorithm to find the proper set of scenarios, the stochastic model proposed includes all the main components to consider for decision-

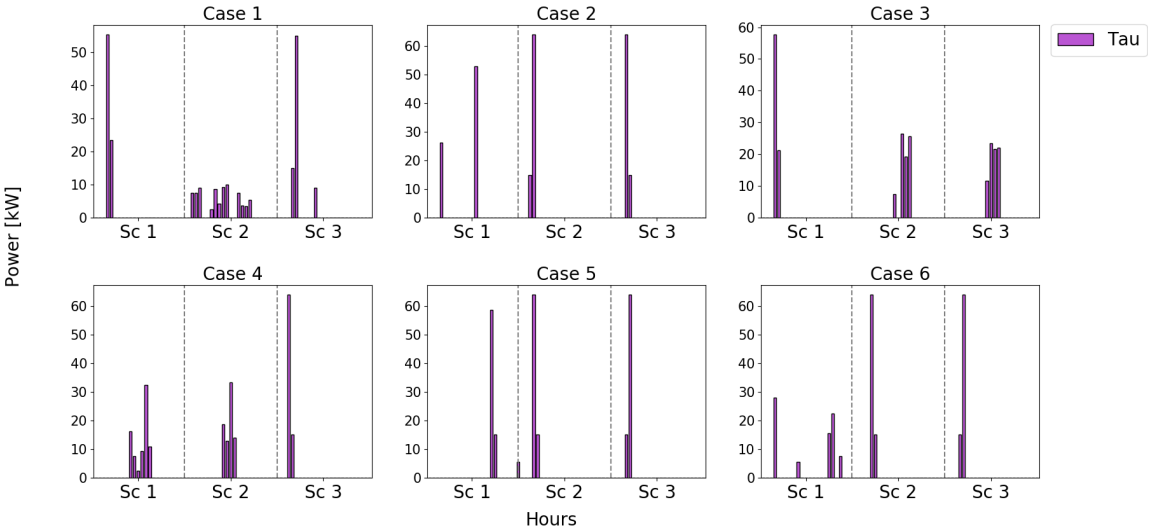

Figure 3.8: Flexible demand uses by hour for every scenario and case study

maker regarding the DERs penetration needed for a proper DN operation. The elements included are different DG types, more than one battery type, PEVs, and DR. In addition, the model finds the optimal sizing for the apparent power, which means that it relates the active and the reactive power together, and it does not overestimate their capacity by calculating them separately. Nevertheless, the model possesses some limitations, which are comment as follows:

The mathematical formulation requires a high computational burden, due to takes around seven hours to solve a case study with three scenarios of 24 hours. However, the model might consider five scenarios of 24 hours or two scenarios of 48 hours, extending its execution time to around 20 hours.

The EVs have been modelled considering only one connecting profile, representing the most probable case [71], which simplifies the model complexity. New profiles could be added to the formulation; however, this profile variety could significantly affect the algorithm execution time. In addition, the EV battery degradation has not been considered in the objective function as a penalization due to what the model seeks is to study the effects of the PEV behaviour on the final DERs capacity installed.

The power supplied by the main grid is modelled in the consumption point and not from the slack bus, underestimating the energy flow between DN lines. This assumption does not mean a problem when the system is oversized, i.e., the DN is not congested even in the peak generation and load hours. However, if the line congestion is a quality parameter to measure by the DSO, then the main grid power must be modelled from the slack bus.

Table 3.3: Optimal location and sizing of PV and WT for every case study

	PV Bus Location	PV Capacity [kW]	WT Bus Location	WT Capacity [kW]
Case 1	49; 52	16.23; 20.55	4; 5; 6; 7; 8; 9; 10; 11; 12; 13; 15; 16; 17; 18; 21; 22; 23; 26; 32; 33; 42; 44; 45; 47; 49; 50; 51; 52; 54; 55; 56; 57; 58; 59; 61; 62; 64; 65; 66; 69	34.65; 100; 3; 5; 6; 5; 7; 39; 35; 6; 100; 7; 7; 7; 27; 6; 51.76; 7; 33.03; 7; 33.37; 100; 31; 83.41; 308; 385; 6; 4; 8; 7; 100; 100; 100; 40; 995; 8; 136; 7; 7; 7
Case 2	3; 4; 5; 6; 8; 9; 10; 12; 13; 14; 18; 19; 25; 31; 32; 34; 35; 36; 37; 38; 40; 41; 42; 43; 44; 45; 46; 49; 50; 51; 52; 53; 54; 55; 56; 57; 60; 61; 63; 64; 65; 67; 68; 69	100; 100; 100; 3; 6; 5; 7; 35; 6; 3.82; 5.01; 82.65; 41.08; 48.4; 37.07; 6; 7; 6; 6; 13.59; 6; 1; 18.75; 5.4; 9.32; 26.47; 32.44; 308; 385; 6; 4; 5; 8; 7; 100	-	-
Case 3	5; 7; 8; 11; 12; 15; 18; 19; 23; 24; 27; 29; 31; 32; 33; 34; 36; 39; 40; 41; 42; 44; 45; 49; 50; 52; 56; 57; 58; 59; 61; 62; 63; 64; 67; 68	100; 5; 6; 34.47; 31.69; 22.29; 2.17; 17.45; 63.98; 7; 7; 3.59; 29.46; 25.53; 4.69; 4.84; 6; 6; 6; 1; 40.7; 25.1; 30.52; 208.05; 223.1; 4; 34.6; 12.27; 100; 40; 995; 8; 100; 136; 5.81; 7	3; 6; 24; 57; 60; 61; 62; 63; 64; 65	69.38; 3; 0.68; 26.01; 55.32; 299.26; 6.75; 44.57; 136; 4.71
Case 4	4; 5; 6; 7; 8; 9; 10; 11; 12; 13; 14; 15; 23; 26; 27; 31; 35; 45; 46; 47; 49; 50; 51; 53; 54; 55; 56; 57; 58; 60; 61; 62; 63; 64; 65; 66; 67; 68; 69	94.38; 100; 3; 5; 6; 5; 7; 39; 35; 6; 6; 58.41; 85.84; 7; 7; 68.49; 7; 26.63; 34.48; 74.11; 278.09; 346.57; 6; 5; 8; 7; 100; 100; 100; 100; 995; 8; 100; 136; 7; 7; 7; 7; 7	-	-
Case 5	2; 4; 9; 11; 12; 15; 18; 21; 25; 45; 50; 60; 61; 64; 65; 66; 68; 69	13.74; 21.21; 0.78; 25.3; 17.04; 9.35; 5.8; 18.15; 17.37; 31; 277.03; 60.23; 630.08; 98.92; 7; 5.14; 7; 7	49	308
Case 6	2; 11; 13; 14; 15; 17; 20; 22; 24; 26; 27; 34; 35; 36; 38; 44; 45; 56; 59; 61; 63; 64; 65; 67	100; 28.46; 6; 6; 32.04; 7; 1; 6; 7; 7; 7; 6; 7; 6; 11.39; 23.28; 31; 4.27; 23.13; 445.4; 2.31; 81.11; 4.78; 7	12; 49; 50; 60; 61; 62; 68	8.41; 308; 385; 8.94; 661.51; 8; 7

The DR has been represented through a binary variable to model different electronic devices with flexible hour operation, like wash machine, air-conditioning, and dishwasher. Notwithstanding, the flexibility can be modelled through a continuous variable that represents the energy that could be reduced by the user when he/she estimate convenience, where the energy-reduced must be penalized through an op-

Table 3.4: Optimal location and sizing of BT for every case study

	BT Bus Location	BT Capacity [kWh]
Case 1	2; 3; 4; 5; 6; 7; 8; 10; 12; 13; 14; 15; 16; 17; 19; 20; 23; 24; 25; 26; 29; 31; 33; 34; 35; 36; 37; 38; 39; 40; 41; 42; 43; 44; 45; 46; 47; 48; 49; 51; 53; 54; 55; 57; 58; 59; 60; 61; 62; 63; 64; 65; 66; 68	100; 91.91; 50; 9.41; 2; 3; 3; 4; 18; 6; 3; 50; 4; 4; 46.31; 2; 50; 4; 29.41; 4; 5; 50; 4; 3; 4; 3; 6; 50; 6; 6; 1; 68.6; 4; 50; 32; 20; 50; 4; 98.64; 3; 6; 4; 4; 50; 50; 40; 100; 35.71; 4; 100; 68; 4; 8; 4
Case 2	2; 3; 4; 5; 6; 7; 8; 9; 11; 12; 13; 14; 16; 18; 19; 21; 22; 23; 24; 25; 26; 27; 28; 29; 30; 31; 32; 33; 34; 35; 36; 37; 38; 39; 40; 41; 42; 43; 44; 45; 46; 47; 48; 49; 50; 52; 54; 55; 56; 58; 60; 62; 63; 64; 66; 67; 68; 69	50; 50; 50; 79.41; 4; 6; 3; 3; 20; 18; 6; 3; 4; 8; 79.41; 12.5; 6; 90.46; 4; 79.41; 4; 8; 10; 10; 50; 50; 92.5; 8; 3; 8; 3; 6; 44.12; 6; 3; 1; 100; 4; 14.71; 32; 20; 42.28; 4; 35.71; 123.64; 2; 8; 4; 44.12; 27.21; 69.12; 4; 29.41; 25; 8; 4; 8; 8
Case 3	3; 4; 5; 6; 8; 12; 13; 14; 15; 16; 17; 18; 19; 20; 22; 23; 24; 25; 26; 27; 30; 31; 32; 33; 34; 35; 36; 37; 38; 39; 40; 41; 42; 44; 45; 46; 47; 48; 49; 50; 51; 55; 56; 57; 58; 59; 60; 61; 62; 63; 64; 65; 66; 67; 68; 69	25; 35.71; 71.25; 2; 3; 36; 3; 6; 77.62; 4; 4; 8; 35.71; 1; 6; 54.41; 4; 50; 4; 4; 50; 79.41; 79.41; 8; 3; 8; 3; 6; 65.12; 6; 3; 1; 50; 85.71; 14.71; 40; 25; 4; 58.82; 35.71; 6; 4; 21.25; 29.41; 67.54; 40; 65.12; 62.92; 4; 50; 65.12; 8; 4; 4; 4; 4
Case 4	3; 5; 6; 7; 8; 9; 13; 14; 15; 16; 17; 18; 19; 20; 23; 24; 25; 26; 27; 28; 29; 30; 31; 32; 33; 34; 35; 37; 39; 40; 41; 42; 44; 45; 48; 49; 50; 51; 53; 55; 57; 58; 59; 61; 62; 63; 64; 65; 67; 68	50; 100; 2; 3; 3; 3; 3; 3; 50; 4; 4; 4; 50; 1; 94.12; 4; 79.41; 8; 8; 5; 5; 100; 95.74; 100; 8; 6; 8; 6; 3; 6; 1; 94.12; 29.41; 32; 8; 132.14; 66.99; 6; 6; 8; 100; 50; 14.71; 29.41; 4; 50; 31.96; 4; 8; 8
Case 5	3; 5; 7; 8; 9; 10; 12; 13; 14; 15; 16; 17; 19; 23; 25; 26; 28; 29; 30; 31; 32; 33; 34; 35; 36; 37; 39; 42; 44; 45; 46; 47; 48; 50; 52; 53; 54; 55; 56; 58; 59; 60; 63; 65; 66; 67; 68; 69	71.25; 50; 6; 6; 6; 8; 18; 6; 6; 39.71; 4; 8; 39.71; 50.42; 75.13; 4; 5; 10; 50.42; 35.71; 72.25; 4; 6; 4; 6; 6; 6; 62.92; 79.41; 16; 40; 65.12; 8; 96.43; 4; 6; 4; 8; 50; 35.71; 40; 64.71; 64.71; 8; 8; 8; 8; 8
Case 6	2; 3; 5; 6; 9; 10; 11; 12; 13; 15; 16; 18; 19; 20; 21; 22; 23; 24; 25; 26; 27; 28; 29; 30; 31; 33; 34; 35; 36; 37; 38; 39; 40; 41; 42; 43; 44; 45; 46; 47; 48; 50; 52; 53; 54; 56; 57; 58; 59; 60; 61; 62; 64; 65; 66; 67; 68; 69	44.12; 98.21; 70.17; 2; 3; 8; 17.86; 36; 3; 92.33; 8; 4; 30.36; 1; 14; 3; 92.33; 4; 44.12; 4; 8; 10; 5; 48.21; 91.91; 4; 3; 4; 3; 3; 26.25; 6; 6; 1; 46.93; 4; 44.12; 16; 20; 85; 8; 52.5; 2; 6; 8; 44.12; 17.5; 67.5; 40; 79.41; 61.98; 8; 66.07; 4; 8; 4; 4; 4

portunity cost in the objective function.

The model finds the CapEx associated with the DGs and BSSs regarding their capacity and installation costs. Besides, the operational costs related to the power injected and the battery degradation (minimized in the objective function) is exclusively for the time horizon that belongs to every scenario. To obtain a reference value for the annual operational cost, the classic OPF is executed for the annual historical data using the location and the capacity obtained by the algorithm (see section 3.5). However, economic indicator like the net present value (NPV), the payback, and the internal return rate (IRR) are not considered. Still, they might be obtained separately using the investment and the operational cost delivered from the model.

ASs related to reactive power might be considered in future papers because the

reactive power provided by the DERs is enough to supply the reactive power demand.

3.7 Chapter conclusions

This chapter addresses the optimal placement and sizing of different DG and BSS into a low-voltage DN, considering PEVs and DR under a two-stage programming problem framework. The first stage variables are related DERs capital cost in terms of location and capacity installed, and the second stage variables are associated with the power provided by the DERs, PEVs, and de energy managed through the DR. A linearization and an algorithm based on the GA have been used to address the non-linear constraints and the binary variables. The model has been tested in a modified IEEE 69 bus system under 18 scenarios to observe the DERs capacity installed variability. Finally, the results have been used to run a classic OPF to study the power provided by DERs concerning the utility grid.

The results have shown that the set of scenarios chosen to test the model are decisive in the DERs capacity proportion installed, presenting a CapEx variation between 3,850 k€ and 1,520 k€, and a year main grid dependence range between 51.1% and 24.4%. On the other hand, the EVs presence suggests a reducing operational cost (4.57%) related to the energy provided by the main grid due to their capacity to inject energy in hours with a high price; however, a high EVs penetration might increase DERs capacity installation. Besides, the DG capability to provide reactive power indicates that it might be possible to supply a high percentage of the reactive power load from renewable resources and provide ASs to the utility grid. Therefore, the model proposed provides the DSOs with a powerful and versatile tool to analyze different planning scenarios for a DN considering economic and technical constraints.

Chapter 4

A virtual microgrids scheduling model

4.1 Introduction

Resilience concept has become increasingly used in the literature related to the DN with high penetration levels of DERs, in order to provide greater autonomy and flexibility to face unexpected power generation situations [72]. In this context, MGs play a relevant role in the transition process to smart grids because they offer an electrical structure that allows improving the monitoring and management control of the renewable resources on a small scale [73, 74]. However, following the definition of MGs given by the U.S Department of Energy [75] an electrical boundary fixed might not be exploiting all the flexibility providing by a MG.

This chapter presents a method based on an optimization mathematical model for the scheduling operation of a DN. The contribution of the proposed method lies in the fact that it permits to configure and operate the DN as a set of VMs with high penetration level of DG and BSS. The topology of such VMs are modulated in time in response of grid failures, thus minimizing load curtailment, maximizing local renewable resource and storage utilization as well. The formulation provides the load reduced by bus to balance the system at every hour, the global probability to present energy not supplied (ENS), and for every bus, a flexibility load response range is considered to avoid its total load curtailment for small load reductions. The model has been constructed considering a linear version of the AC OPF constraints extended for multiperiod, and it has been tested in a modified version of the IEEE 33-bus radial distribution system considering four different scenarios of 72 hours, where the global energy curtailment has been 27.9% without demand-side response (DSR) and 10.4%

considering a 30% of flexibility load response. Every scenario execution takes less than a minute which makes it proper for distribution system operational planning.

Thus, this chapter is organized as follows. Section 4.2 presents the literature review. Then, Section 4.3 describes the problematic where the mathematical model is situated, and the methodology follows to validate the model under different scenarios. Section 4.4 presents the mathematical model with the nonlinear constraints already linearized. Section 4.5, the model proposed, is tested in a case of study. And finally, the results are discussed in section 4.6.

4.2 Literature review

The concept of virtual VM with dynamic boundaries has begun to sound as an alternative way to increase the resilience of conventional DN [76, 77] based on the IEEE Standard 1547.4 [78], which establish that the reliability and operation of DNs can be improved by dividing the DN into multiple "isolated systems". Still exist discussion about a common definition of VMs with dynamic limits, however, there are some common characteristics; the work in [79] proposes that a VM are developed from a centralized DN, possess the same features of an MG but with a flexible structure based on virtual boundaries. The work done by [80] considers a dynamic MG as an MG with flexible boundaries that expand or shrink to keep the balance between power generation and power consumption all the time. The work in [81] considers the paradigm of dynamic MG as a mechanism to partition continuously a DN based on the balance between generation and electricity demand.

The key factor of the previous definitions is the capability of the DN to find the best partition such that minimizes the load curtailment and balances the power system under failure or unbalanced scenarios produced by the stochastic behavior of the DG. Likewise, this responsiveness is based on the autonomy level of the ADN, i.e., the installed capacity of DG and batteries, thus, as higher is the installed capacity, higher would be the autonomy. However, meet 100% of the electricity load only with DERs requires a high investment, which could make unprofitable the implementation of these technologies in a DN and/or bring voltage issues [82]. Therefore, in most cases, a trade-off between the energy provided by DERs and the utility grid occurs, where the grid helps the DERs fill the energy gap in the critical hours, decreasing the installed capacity needed of the renewable resources [34]. Thus, the necessity of partition the ADN into VMs under failures of the utility grid gains momentum, because, under failure scenarios, the gap cover by the grid, when the DERs do not

meet the load, will produce an unbalanced system, unless the ADN faces this issue dividing itself into virtual "island systems".

Some clustering techniques [83, 84] and methodologies have been applied to find an optimal partition that allows to the network adopt this dynamic structure. GA has been used in [85] to partition a DN in order to minimize the energy exchange between MGs. The work developed in [79] proposes a hierarchical bottom-to-top algorithm based on community detection [86] using an Electrical Coupling Strength as modularity index, which is defined as a composite weighted factor for the analysis of the electrical connection, to size the partition quality. In [87] a greedy and particle swarm optimization algorithm based on community detection is used to find sub-communities through an index based on the voltage sensitivity matrix and the active/reactive power. The electrical distance is used in [88, 89] to partition a DN into sub-systems. The greedy algorithm is used to find the best partition and the particle swarm optimization to manage the voltage control for each MGs. A control system based on Kruskal's algorithm from graph theory is presented in [5] to synchronize and separate DN into multiple island systems to keep the system balanced. In [90] a bi-level optimization problem is presented to transform an active DN in multiple MGs using spectral graph theory to define the maximum numbers of sub-networks through a MINLP, and a second lower-level problem to measure the reliability of the MGs formed by the upper-level. An optimal scheduling model is presented in [91] to tackle dynamic MG reconfiguration, where a linear version of the AC OPF is proposed and uses the bender decomposition method to decompose and coordinate the grid-connected system and isolated operation through a master problem and subproblem, respectively.

The previous literature set out that the techniques used until now for partition and dynamic MG reconfiguration are based on spectral graph theory and hierarchical and community detection algorithms mostly. Nevertheless, to our best knowledge, there is not a single mathematical optimization model which provides the DN dynamic reconfiguration scheduling, based on DSR and load curtailment, such that it prevents widespread blackouts as a result of low power generation or network failures, for DN with high penetration of DG and BSS. In order to extend the literature, the proposed model tackle this issue.

4.3 Problem definition and methodology

Currently, the distribution and transmission systems are supported by different control mechanisms to face the deviation between electricity production and the load [92, 93]. This work, typically managed by the transmission system operator (TSO), keeps the energy balancing through three types control reserves which differ by the temporal space in which they are applied. Therefore, why to partition a DN to face unexpected events if there are mechanisms of control to tackle these kinds of issues? Because what is looking for in the resilience concept associated to the DN with high penetration levels of DERs is dispense with these control mechanisms and be able to self-adapted to a failure of high impact on the grid [94]. Therefore, the ADN must be able to size the energy amount that is not possible to meet due to the absence of the utility grid and identify the load points which could be applied a load curtailment in order to minimize the energy losses.

The DSR concept is related to the amount of energy which the ADN could shave to avoid an unbalanced system under the absence of the utility grid [95]. i.e. if the ADN possess the flexibility to reduce a percentage of its energy load, the global curtailment will be lower than the case of an ADN where there is no chance to reduce the load more than to zero to avoid an unbalanced system. However, the flexibility degree of the DSR must be known by the ADN previously such that the model can decide when and how much load reduce.

Under this context, the model proposed in this chapter seek to create VMs based on load curtailment and/or DSR to balance the system under the absence of the grid and low power generation.

The methodology follows in this chapter consists of two stages: A first step focuses on the strategic decisions related to the capacity and location that should have the DG and BSS into the DN. And a second step which tackles the capability of the DN to face unexpected failures through the self-partition into VMs.

The placement and sizing have been addressed separately in the previous chapters, where a novel algorithm is presented which allows finding an optimal solution of the capacity and location for different types of DGs and BSSs considering a time horizon longer than 24 hours and basing its formulation in an AC OPF to include the technical constraints of the network, which is represented in the upper level of Figure 4.1. The lower level corresponds to seek the optimal topology of the DN in case that the power energy is insufficient to meet the electricity load. Therefore, follows Figure 4.1, the optimal model for the VMs topology scheduling (VMTS) is executed for scenarios of

72 hours, and every hour going to have two possible results regarding the system: The first one, where the capacity installed, weather conditions and the electricity load are balanced, which means that the DN does not needs to be partitioned into VMs. However, if in the second case, the electricity load is not satisfied by the power generation of the DGs, the model going to find the amount of energy load that must be reduced at each bus to balance the system, where every load point possesses a range of load that can be reduced. If the load curtailment exceeds this range, the load in that point is reduced to zero and the bus is isolated becoming in a bound of VM. Thus, for each hour where these conditions appear, the model provides the scheduling of the topology that must follow the DN to balance the system all the time, sacrificing, of course, a load curtailment that is minimizing on the Objective function but avoiding an outage.

In order to make sure that the topologies found by the mathematical model be feasible for the classic AC OPF problem, the loads associated with the isolated nodes are replaced by zeros and the buses with a reduced load within its range of flexibility are modified. The DN with the new set of loads is executed in a multi-period AC OPF. Thus, the feasible solutions of the VMTS model are also feasible for the classic AC OPF problem.

4.4 Optimal model for scheduling virtual microgrids topology

The formulation explained in this chapter is a modified version of the model presented in the previous chapter, which use as the main structure an AC OPF extended to multi-period and a linearization done by [10]. However, unlike of [34] which finds the optimal place and location of DERs into a DN, the following model is focused on finding the scheduling of a dynamic topology of an ADN to face lower generation scenarios or failure on the utility grid, through the minimization of the load curtailment in order to find the weakest nodes, and identify eventual flexibilities. The model is explained in two subsections; the first one corresponds to the base structure to find the proper topology of the ADN to face unbalances issues without taking into account a flexible demand response, and a second section, where the power consumption is not a parameter anymore but a variable, in order to include flexibility on demand.

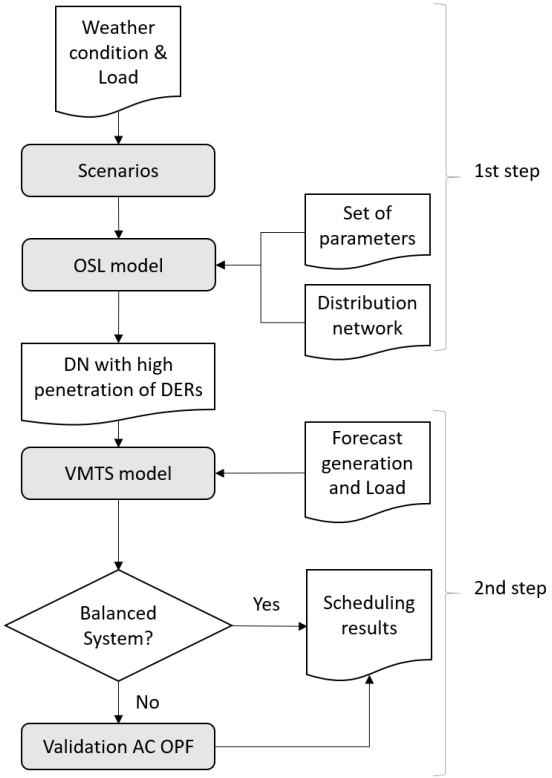

Figure 4.1: Methodology structure for self-adaptive distribution networks

4.4.1 Model without flexible demand

The virtual microgrids topology scheduling (VMTS) model is described as follows:

$$Min\ F = \Upsilon \sum_{i \in \mathcal{B}} \sum_{t \in \mathcal{T}} \delta^{p}_{i,t} + \delta^{q}_{i,t} + \sum_{(i,j) \in \mathcal{L}} \sum_{t \in \mathcal{T}} \mid p^{i,j}_{t} \mid + \mid q^{i,j}_{t} \mid . \tag{4.1}$$

The objective function in Eq. (4.1). minimize the active ($\delta^{p}_{i,t}$) and reactive ($\delta^{q}_{i,t}$) power not-supplied by the DERs, represented by the left side of the equation, and the active ($p^{i,j}_{t}$) and reactive ($q^{i,j}_{t}$) power flow between the nodes, corresponding to the right side. This structure allows us to promote the fulfillment of the electricity load (left side) since the positive variables $\delta^{p}_{i,t}$ and $\delta^{q}_{i,t}$ are penalized (Υ) when their values are greater than zero, if and only if, the power generation and the energy storage is not enough to meet the load. In addition, when it is not a chance to meet the power consumption, the objective function prioritizes the loads with or closer to a DG or BSS, through the minimization of the flow variables ($p^{i,j}_{t}$) and ($q^{i,j}_{t}$). In order to penalize the flow between nodes, the absolute value for the active and reactive power flow between nodes is considered, which can take negative and positive values

depending on the flow direction, and because an absolute value require a simple change of variable to become linear.

The formulation constraints are as follows: Eq. (4.2) and (4.3) correspond to active and reactive nodal power flow equations, therefore; $\forall i \in \mathcal{B}, \forall t \in \mathcal{T}$,

$$vs_{i,t}[G_i + \sum_{(i,j)\in\mathcal{L}} G_{i,j}] + \sum_{(i,j)\in\mathcal{L}} p_t^{i,j} = \sum_{k\in\Omega} pg_{i,t}^k + \lambda_{i,t}^p - PL_{i,t} + \sum_{l\in\Psi}(ds_{i,t}^l - ch_{i,t}^l), \quad (4.2)$$

$$- vs_{i,t}[B_i + \sum_{(i,j)\in\mathcal{L}} (B_{i,j} - Bs_{i,j})] + \sum_{(i,j)\in\mathcal{L}} q_t^{i,j} = \sum_{k\in\Omega} qg_{i,t}^k + \lambda_{i,t}^q - QL_{i,t}. \quad (4.3)$$

Both equations, and the remaining constraints, have already been linearized using the methodology presented in [10], holding the left side of these equations like the classic AC OPF. However, on the right side, we consider; the active power injected by the distributed resource ($pg_{i,t}^k$); a virtual active power ($\lambda_{i,t}^p$), which represents the power remained to meet the load in case of low generation; the active power demanded by the node ($PL_{i,t}$), wherein this formulation is a parameter; and the power absorbed ($ch_{i,t}^l$) or injected ($ds_{i,t}^l$) from the battery to the grid. The same structure follows Eq. (4.3).

The set of constraints from (4.4) to (4.7) correspond to the linear version of the active and reactive power flow equation which have been widely explained in section 2.4 , therefore; $\forall (i,j) \in \mathcal{L}, \forall t \in \mathcal{T}$,

$$G_{i,j}\left[\frac{vs_{i,t} - vs_{j,t}}{2}\right] - B_{i,j}(\Delta\theta_t^{i,j}) + LP_{i,j} = p_t^{i,j}, \quad (4.4)$$

$$- B_{i,j}\left[\frac{vs_{i,t} - vs_{j,t}}{2}\right] - G_{i,j}(\Delta\theta_t^{i,j}) + LQ_{i,j} = q_t^{i,j}, \quad (4.5)$$

$$LP_{i,j} = G_{i,j}[\Delta\widehat{\theta}_t^{i,j}]m_{i,j} + G_{i,j}\left[\frac{\widehat{V}_{i,t} - \widehat{V}_{j,t}}{\widehat{V}_{i,t} + \widehat{V}_{j,t}}\right] - \frac{G_{i,j}}{2}[(\Delta\widehat{\theta}_t^{i,j})^2 + (\Delta\widehat{V}_{i,j,t})^2], \quad (4.6)$$

$$LQ_{i,j} = -B_{i,j}[\Delta\widehat{\theta}_t^{i,j}]m_{i,j} - B_{i,j}\left[\frac{\widehat{V}_{i,t} - \widehat{V}_{j,t}}{\widehat{V}_{i,t} + \widehat{V}_{j,t}}\right] + \frac{B_{i,j}}{2}[(\Delta\widehat{\theta}_t^{i,j})^2 + (\Delta\widehat{V}_{i,j,t})^2]. \quad (4.7)$$

Power load and virtual power are explained in constraints (4.8)-(4.11), therefore; $\forall i \in \mathcal{B}, \forall t \in \mathcal{T}$,

$$PL_{i,t} = \gamma_{i,t}^p + \delta_{i,t}^p, \quad (4.8)$$

$$\lambda_{i,t}^p \leq \delta_{i,t}^p, \quad (4.9)$$

$$QL_{i,t} = \gamma_{i,t}^q + \delta_{i,t}^q, \quad (4.10)$$

$$\lambda_{i,t}^q \leq \delta_{i,t}^q. \quad (4.11)$$

Eq. (4.8) represents the total power load which depends on the power supplied ($\gamma^p_{i,t}$) and not-supplied ($\delta^p_{i,t}$) in every node i, thus, the total load is composed by this two type of variable, where the power not-supplied is penalized in the objective function, to ensure that $\delta^p_{i,t}$ is as small as possible. Eq. (4.9) the power not-delivered ($\delta^p_{i,t}$), bound the virtual power $\lambda^p_{i,t}$ which represents the remaining power that it is needed to meet the total power load (see Eq. (4.2). Therefore, if the power generation is insufficient to provide the power required, the virtual power ($\lambda^p_{i,t}$) is going to fulfill this gap, being penalized in the objective function, if and only if, this gap is equal or lower than the power not-supplied ($\delta^p_{i,t}$) in the node i. Constraints (4.10) and (4.11) describe the same logic but for reactive power load.

Active and reactive power limits together with the voltage security constraints are considered in Eqs. (4.12) - (4.14), therefore; $\forall i \in \mathcal{B}, \forall k \in \Omega$,

$$(V_i^{min})^2 \leq vs_{i,t} \leq (V_i^{max})^2, \tag{4.12}$$

$$U_l^g PG_{k,t}^{min} \leq pg_{i,t}^k \leq U_l^g PG_{k,t}^{max}, \tag{4.13}$$

$$U_l^q QG_{k,t}^{min} \leq qg_{i,t}^k \leq U_l^q QG_{k,t}^{max}. \tag{4.14}$$

Eq. (4.12) makes sure that the voltage in each node and at every period is within the limits allowed. The parameters are squared due to the change of variable needed to linearize the original power flow equation. Constraints (4.13) establish the limits for the power injected by the DG in the node through two different parameters; U_l^g corresponds to the total power capacity installed and $PG_{k,t}^{max}$ is the power generated by the DG in a certain period, which is a normalized power generation curve. Therefore, Eq. (4.13) establishes the maximum power that can be injected in Eq. (4.2) at every hour, where $PG_{k,t}^{max}$ follow the behavior of a PV/WT power generation, and it allows to include the stochastic behavior of the DG into the OPF constraints.

The sets of constraints (4.15) - (4.18) represent linear version of the apparent power limit, therefore; $\forall (i,j) \in \mathcal{L}, \forall t \in \mathcal{T}, \forall r \in \mathcal{R}$,

$$A_{i,j}^r p_t^{i,j} + B_{i,j}^r q_t^{i,j} + C_{i,j}^r \geq 0, \tag{4.15}$$

$$-A_{i,j}^r p_t^{i,j} + B_{i,j}^r q_t^{i,j} + C_{i,j}^r \geq 0, \tag{4.16}$$

Where:

$$A_{i,j}^r = -S_{i,j}^{max} cos(\beta_{i,j}^r) \; ; \; B_{i,j}^r = -S_{i,j}^{max} sin(\beta_{i,j}^r), \tag{4.17}$$

$$C_{i,j}^r = (S_{i,j}^{max})^2 \; ; \; \beta_{i,j}^r = \alpha + (r-1)\frac{\pi - 2\alpha}{\mathbb{R} - 1}. \tag{4.18}$$

Eq. (4.15) and (4.16) emerge as a set of constraints which represent a polygon formed by $r \in \mathcal{R}$ lines that define a feasible region approximation of the original apparent power limit, which is a circle. Thus, the bigger the set $\mathcal{R}$, the closer will be the polygon to the circle.

The battery modeling is expressed following the below equations. However, their full explanation has been addressed in section 2.3. Therefore; $\forall i \in \mathcal{B}, \forall t \in \mathcal{T}, \forall l \in \Psi$,

$$soc^l_{i,t+1} = soc^l_{i,t} + [\varphi^l ch^l_{i,t} - \frac{1}{\varphi^l} ds^l_{i,t}]\Delta t, \tag{4.19}$$

$$U^b_l SOC^{min}_l \leq soc^l_{i,t} \leq SOC^{max}_l U^b_l, \tag{4.20}$$

$$ch^l_{i,t}\Delta t \leq w^l_{i,t} M^l, \tag{4.21}$$

$$ds^l_{i,t}\Delta t \leq M^l(1 - w^l_{i,t}) - M^l(1 - Y^l_i), \tag{4.22}$$

$$w^l_{i,t} \leq Y^l_i. \tag{4.23}$$

4.4.2 Model with flexible demand

In this section the equations (4.1), (4.2), (4.8) are rewritten in order to include the DSR into the model explained previously, and a new constrain is added to bound the flexibility degree of the energy demand.

$$Min\ G = \Upsilon \sum_{i\in\mathcal{B}} \sum_{t\in\mathcal{T}} \delta^p_{i,t} + \delta^q_{i,t} + \sum_{(i,j)\in\mathcal{L}} \sum_{t\in\mathcal{T}} \mid p^t_{i,j} \mid + \mid q^t_{i,j} \mid + \sum_{i\in\mathcal{B}} \sum_{t\in\mathcal{T}} \mu_{i,t}. \tag{4.24}$$

Eq. (4.24) is the new objective function which, unlike (4.1), the amount of power consumption reduced ($\mu_{i,t}$) is minimized together with the energy flow and the active/reactive power not supplied, in order to balance the system. However, this new variable $\mu_{i,t}$ must be lower or equal than the demand response of every load. Therefore; $\forall i \in \mathcal{B}, \forall t \in \mathcal{T}$

$$\mu_{i,t} \leq \Omega_{i,t} PL_{i,t}. \tag{4.25}$$

$\Omega_{i,t}$ in Eq. (4.25) represents the percentage of demand response of every load at every time. In addition, $\mu_{i,t}$ must be integrated in Eqs. (4.2) and (4.8) to keep the balance in the power flow equations, where the parameter $PL_{i,t}$ passes to be an initial power consumption where the flexibility response is subtracted. Thus; $\forall i \in \mathcal{B}, \forall t \in \mathcal{T}$

$$vs_{i,t}[G_i + \sum_{(i,j)\in\mathcal{L}} G_{i,j}] + \sum_{(i,j)\in\mathcal{L}} p^{i,j}_t = \sum_{k\in\Omega} pg^k_{i,t} + \lambda^p_{i,t} - PL_{i,t} + \mu_{i,t} + \sum_{l\in\Psi} (ds^l_{i,t} - ch^l_{i,t}) \tag{4.26}$$

$$PL_{i,t} - \mu_{i,t} = \gamma^p_{i,t} + \delta^p_{i,t}. \tag{4.27}$$

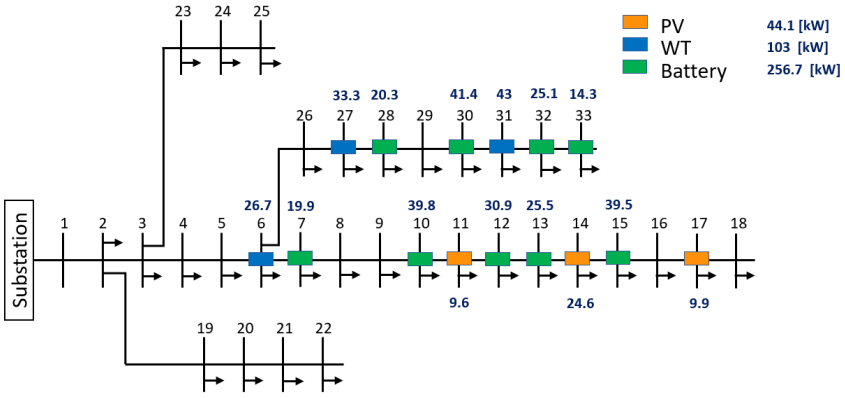

Figure 4.2: Capacity and location for DERs in the PG&E 33-bus radial distribution network.

4.5 Case study

In this section the two versions of the mathematical model are applied under different scenarios, considering the PG&E 33-bus radial DN [40]. The sizing and location of the DERs have been obtained using the algorithm presented in 2.5, considering a connected-grid system because an autonomous network, i.e. the energy, is provided 100% by DERs, it is not a proper case of study to observe the capability of the ADN to form sub-systems when the grid failures. Therefore, using [34], the location and sizing have been set as shown in Figure 4.2

In order to test the mathematical optimization model, four different 72-hour scenarios corresponding for each season of the year are taken into account to study the different topologies formed by the ADN when the system is disconnected from the utility grid and the weather conditions are not capable to supply the 100% of the power consumption. The weather resources are taken from historical data; [39] for the wind speed and [38] for the temperature and irradiation. The mathematical model has been programmed in Python using CPLEX as the main solver.

The available resources compared with the energy demand, for the periods of study are presented in Figure 4.3. Every curve has been normalized to respect the magnitude and visualize under what hour or period, there are more power capability than others. For example, the fourth period possesses a high-level wind resource, which means that the wind turbine will be able to produce energy at its maximum capacity. On the other hand, there are many consecutive hours that show a very low power capability for PV panels and wind turbines, which will force load curtailment and the partitioning of the ADN into sub-systems. The DSR parameter is sets in

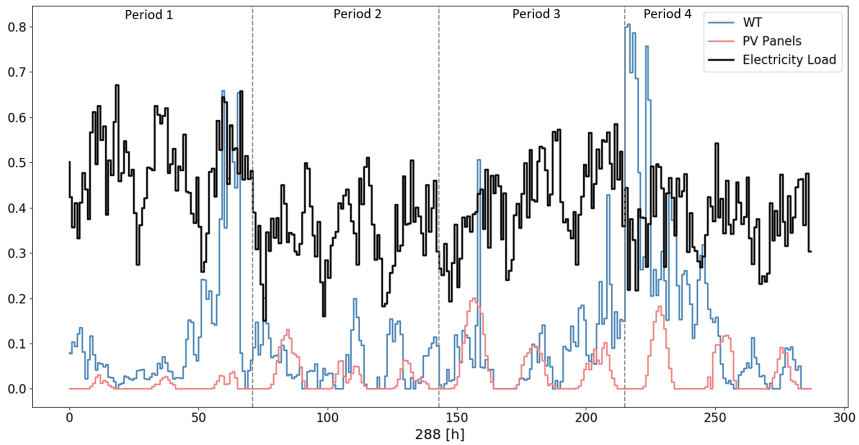

Figure 4.3: The four consecutive scenarios of 72 hours. The vertical axis is the percentage of the total capacity that can be used by the WT/PV or the percentage of the energy demand for every hour.

30% for every load at every time.

Remark that the goal of the case of study is; (1) to size the DSR effect on the DN topology scheduling, and (2) to show the *type* of data provided by the model and how this information can be useful in terms of operational planning for DSO. It is important to mention this factor because the results depend exclusively on the DERs capacity, electricity demand, season, geographic location, weather conditions, and the DSR considered.

4.5.1 Model performance

The mathematical formulation, explained in section 4.4, has been compared with its MINLP version to observe the huge time differences between non-linear and linear version. Thus, Table 4.1 shows the times execution for both model, and their respective OF. When the model is not multi-period, both formulations reach to the same OF, however, when the model is extended to multi-period, the computation burden for the MINLP increase faster than the MILP to the point that at hour 12 the time for the MINLP is around 5.5 hours, which is much longer than the alternative version that take only 3.79 seconds, keeping an error close to the 7%. Due to the exponential time execution increase for the MINLP version, the Table 4.1 has been completed until hour 12 and not beyond. Nevertheless, the MILP running time for 72h is close to a minute, that puts it within the operational range of DSO.

Table 4.1: Performance of the MINLP and MILP

	1h	6h	12h	24h	72h
MINLP [s]	1.79	25.86	20038.7	–	–
OF [kWh/pr.]	0.1	0.65	1.32	–	–
Status	ok	ok	ok	–	–
MILP [s]	0.15	0.26	0.892	4.12	58.38
OF [kWh/pr.]	0.1	0.69	1.41	3.79	534496.43
Status	ok	ok	ok	ok	ok
OF error	0%	6.2%	6.8%	–	–

In order to improve the understanding of the data obtained from the model, the results are grouped as follows:

- *Model operation* explains how the model meets the energy load through the available resources and show the role of the storage devices.
- *Weakest points* identify the nodes with a high probability of ENS. This probability considers any percentage of non-compliance from the total load for a certain bus at every hour.
- *Flexibility Market* presents the amount of ENS for every node at every hour and compares the total ENS when DSR is considered and when it is not.
- *Dynamic topologies* shows the topology scheduling that must follow the ADN to pass from an unbalanced system to a balanced system, with lower load compliance than the original.

4.5.2 Mathematical model operation

Figure 4.4 and Figure 4.5 are presented to show how the model proposed to operate to meet the energy demand with the available resources (Figure 4.4) and observe the impact of the storage devices (Figure 4.5) for a certain scenario without considering DSR. Thus, the *fourth period* has been considered where at the first hours it is possible to meet the energy load with the DERs, due to existing high wind resources and irradiation. Furthermore, the SOC of the batteries increases during the first half of the scenario, achieving its maximum, to face the second half where the weather conditions are not the best. From the 40th hour on, the batteries are discharged (see Figure 4.5) and start to appear the first nodes with low energy not supplied by the system because the discharge rate of the battery does not allow to fulfill the gap between load and generation. Finally, at the end of the period, there is not

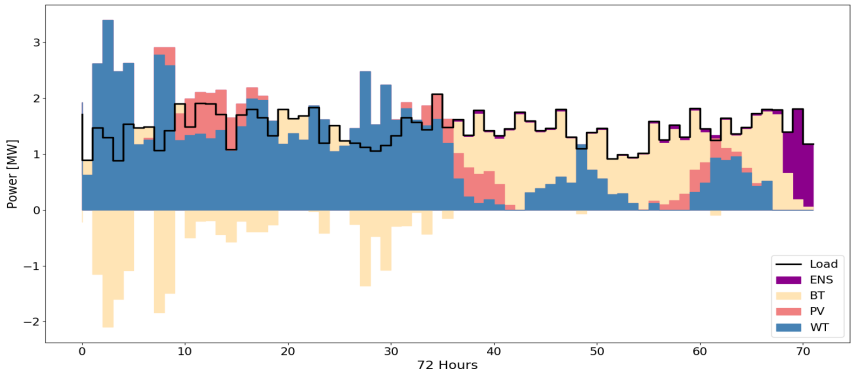

Figure 4.4: Scenario 4: electricity demand fulfillment behavior

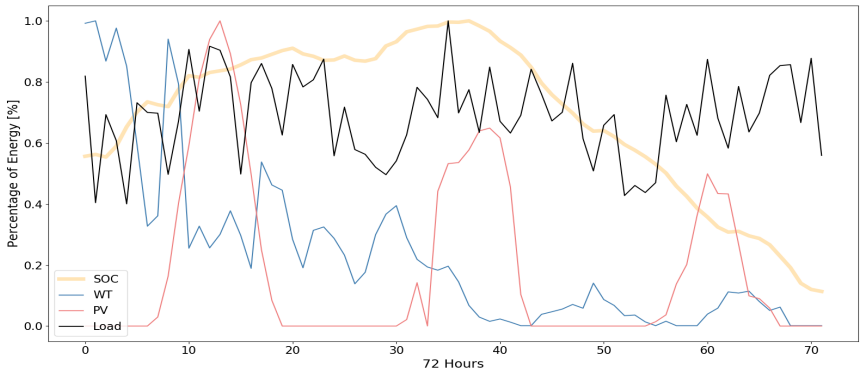

Figure 4.5: Scenario 4: SOC of batteries vs. load, and wind/irradiation resources available

enough energy stored in the batteries to meet the energy demand. To improve the visualization of Figure 4.4. the energy provided by the DERs has been overlapped to observe the share of the energy demand that is satisfied by each resource, and for Figure 4.5, the curves have been normalized, taking as reference the maximum value of each curve.

In global terms, for the 288 hours considered, composed of 4 scenarios of 72 h, the total energy demanded by the system is 434.17 MWh/pr. of which 56.3% is provided by WT, 8.2% by PV panels, 13.4% the storage systems, and 4.6% of energy losses. The ENS when the DSR is not taken into account is 27.9%, however, when a 30% of DSR is considered, i.e. every load point can reduce its energy load at a maximum of 30%, otherwise, the load is reduced to zero, the ENS drop-down 62.7%, from 27.9% to 10.4%. Therefore, for the installed capacity and for the considered scenarios, the system could provide 73.3% of the energy as maximum, and the remaining energy load would be reduced or traded through an eventual energy flexibility market.

4.5.3 Weakest nodes

The weak nodes of the ADN have been represented in Table 4.2 through the probability of every bus to not meet the total electricity load in a period of 72h. i.e. for a scenario of 72h, if in every hour of this scenario, a certain bus does not supply the entire energy demand, its probability of default is 100%. The first column indicates the buses, where bus 1, has not been considered because does not has a load at any time. The following 4 columns indicate the different scenarios of 72 hours considered, and the column *Total* shows the probability of every bus for ENS considering a 288 h period. The remaining columns possesses the same meaning, but considering the DSR version model, and the last column **(A)** indicates if the bus possesses or is next to a DERs. Thus, in Table 4.2 the buses with a DG or BSS installed have a lower probability of default when the weather conditions are not proper to generate enough power to meet demand with the capacity installed, and the support of the utility grid is not guaranteed. Specifically, the buses with WT installed are the ones which have the lowest probability of default followed by the nodes with PV panels and the nodes with a storage system. Moreover, as the objective function (4.1) and (4.24) minimize the energy flow through the lines when there is non-compliance, the nodes which are furthermost of the buses with a DERs system, are the points with the highest probability to present load curtailment, as is the case of the upper section of the DN test system {23, 24, 25} and the lower section {19, 20, 21, 22}.

4.5.4 Energy for flexibility market

Unlike Table 4.2 which shows the probability of default, Table 4.3 presents the *amount of energy* that is not possible to fully supply the system, for every bus, and for every scenario. For example, in the fourth scenario, the second bus, in Table 4.3; it would be required to generate an extra 0.11 MWh to meet the electricity load on the weather conditions considered, and not produce a load curtailment for the second bus, in order to avoid an unbalanced system. Therefore, this extra energy for each node and for every hour could be used by the DSO to be traded in an eventual energy flexibility market. On the other hand, for the same previous example, when the DSR is considered into the formulation, occurs that the extra 0.11 MWh can be reduced (because it is within the flexibility range response) and therefore a total load shaved is not needed. In addition, the right part of Table 4.3 shows a clear decrement of ENS due to the DSR effect, where is visualized easily in the fourth scenario, which does not present load reduced. The proportion of ENS for every node, follow the

Table 4.2: Probability that a bus has energy not-supplied

	Without DSR (%)					With DSR (%)					
Bus	**Sc 1**	**Sc 2**	**Sc 3**	**Sc 4**	**Total**	**Sc 1**	**Sc 2**	**Sc 3**	**Sc 4**	**Total**	**(A)**
1	0	0	0	0	0	0	0	0	0	0	No
2	65.3	52.8	37.5	4.2	39.9	11.1	5.6	1.4	0	4.5	No
3	65.3	6.9	5.6	4.2	20.5	11.1	5.6	1.4	0	4.5	No
4	45.8	5.6	2.8	4.2	14.6	9.7	5.6	1.4	0	4.2	No
5	25	4.2	0	4.2	8.3	5.6	4.2	1.4	0	2.8	Yes
6	8.3	2.8	0	4.2	3.8	0	2.8	0	0	0.7	Yes
7	8.3	5.6	1.4	4.2	4.9	9.7	5.6	1.4	0	4.2	Yes
8	65.3	6.9	2.8	4.2	19.8	11.1	5.6	0	0	4.2	Yes
9	48.6	6.9	1.4	2.8	14.9	11.1	5.6	0	0	4.2	Yes
10	11.1	6.9	1.4	2.8	5.6	11.1	4.2	0	0	3.8	Yes
11	20.8	11.1	2.8	2.8	9.4	8.3	5.6	0	0	3.5	Yes
12	12.5	13.9	5.6	2.8	8.7	12.5	5.6	0	0	4.5	Yes
13	13.9	13.9	2.8	2.8	8.3	12.5	2.8	0	0	3.8	Yes
14	43.1	9.7	5.6	2.8	15.3	9.7	2.8	2.8	0	3.8	Yes
15	15.3	13.9	5.6	1.4	9	13.9	5.6	2.8	0	5.6	Yes
16	48.6	13.9	6.9	2.8	18.1	13.9	9.7	2.8	0	6.6	Yes
17	70.8	13.9	5.6	2.8	23.3	12.5	5.6	2.8	0	5.2	Yes
18	70.8	30.6	9.7	2.8	28.5	61.1	11.1	2.8	0	18.8	Yes
19	66.7	66.7	50	4.2	46.9	51.4	5.6	1.4	0	14.6	No
20	68.1	90.3	72.2	4.2	58.7	63.9	6.9	1.4	0	18.1	No
21	69.4	100	79.2	15.3	66	65.3	54.2	2.8	0	30.6	No
22	69.4	100	79.2	47.2	74	65.3	62.5	2.8	0	32.6	No
23	65.3	58.3	43.1	4.2	42.7	26.4	5.6	1.4	0	8.3	No
24	68.1	76.4	59.7	4.2	52.1	58.3	6.9	1.4	0	16.7	No
25	68.1	100	79.2	4.2	62.8	65.3	6.9	2.8	0	18.8	No
26	4.2	2.8	0	4.2	2.8	0	1.4	0	0	0.3	Yes
27	0	0	0	4.2	1	0	0	0	0	0	Yes
28	5.6	4.2	0	2.8	3.1	4.2	2.8	1.4	0	2.1	Yes
29	6.9	4.2	0	2.8	3.5	8.3	4.2	1.4	0	3.5	Yes
30	5.6	4.2	0	2.8	3.1	6.9	2.8	0	0	2.4	Yes
31	0	1.4	0	2.8	1	0	0	0	0	0	Yes
32	6.9	4.2	1.4	2.8	3.8	8.3	1.4	0	0	2.4	Yes
33	8.3	4.2	1.4	1.4	3.8	9.7	4.2	1.4	0	3.8	Yes

same pattern of Table 4.2, because, for the nodes with power generation or storage devices, the amount of extra energy needed to fulfill the electricity load is lower than the buses without DERs.

4.5.5 Dynamic topology

The dynamic topology offered by the model is by all means the variable associated with the ENS ($\delta^p_{i,t}$), which takes values greater than zero when the DERs cannot provide sufficient energy to meet the demand. These values are recorded for every period at each bus. Table 4.4 shows simplified results of these values, where the values greater than the maximum DSR flexibility have been replaced by one, and when these values are within the range allowed by the DSR or the load is satisfied, the values are zero for the sake of clarity. Specifically, Table 4.4 represents the results for the time comprised between period 40h to 48h corresponding to the second scenario. This scenario has been selected because presents many buses with load curtailment which is the case at hour 46. Taking as reference the results in Table 4.4, the hour 46 has been depicted in Figure 4.6 to observe how the VMs, represented by binary numbers in the previous table, take form in the ADN. The red points indicate the nodes where the load has been decreased to zero, and the dashed red lines to visualize the isolated system which is bounded by the red points. For those nodes where the load has been suppressed but there are power generation, the energy injected in these red points is used to meet the demand in the closest points of the ADN which the load is not zero. On the other hand, when the DSR is included in the formulation, the load curtailment is reduced, as shown on the right side of Table 4.4, leaving only the buses 21 and 22 without energy supplied and formed the VM represented in Figure 4.7.

4.6 Chapter conclusions

This chapter has presented an optimization model to find the topology that must follow an ADN to self-balancing under unexpected grid failures, identifying the load reduction required to balance again the system, and isolate the loads, with a curtailment greater than its capacity response, which become the limits of the VMs formed. Every new topology has been validated using the classic AC OPF model, to make sure that the feasible solution of the model proposed is also a feasible solution for the model used by the DSO.

The model has been tested under four scenarios of 72 hours to consider the seasonality of renewable resources, and the location and sizing of the DERs have been

Table 4.3: Energy not-supplied and its percentage of non-compliance

B	Without DSR								With DSR								(A)
	ENS				ENS in %				ENS				ENS in %				
	S1	S2	S3	S4	S1	S2	S3	S4	S1	S2	S3	S4	S1	S2	S3	S4	
1	0	0	0	0	0	0	0	0	0	0	0	0	0	0	0	0	No
2	2.3	1.4	1.1	0.1	66	54	36	4	0.3	0.1	0	0	8	4	1	0	No
3	2.1	0.2	0.1	0.1	66	8	5	4	0.3	0.1	0	0	8	4	1	0	No
4	1.8	0.2	0.1	0.1	43	6	3	4	0.3	0.1	0	0	7	4	1	0	No
5	0.3	0.1	0	0.1	16	4	0	4	0.1	0	0	0	3	2	1	0	Yes
6	0.1	0	0	0.1	5	2	0	4	0	0	0	0	0	1	0	0	Yes
7	0.5	0.2	0	0.2	8	5	0	4	0.3	0.2	0	0	5	3	0	0	Yes
8	4.6	0.3	0.1	0.2	66	6	2	3	0.6	0.2	0	0	8	4	0	0	Yes
9	1	0.1	0	0.1	49	8	2	3	0.2	0.1	0	0	8	4	0	0	Yes
10	0.2	0.1	0	0.1	10	8	2	3	0.2	0.1	0	0	7	3	0	0	Yes
11	0.3	0.1	0	0	17	9	2	3	0.1	0	0	0	6	2	0	0	Yes
12	0.3	0.2	0.1	0.1	12	15	5	3	0.2	0.1	0	0	8	4	0	0	Yes
13	0.3	0.2	0	0.1	13	13	2	3	0.2	0	0	0	9	1	0	0	Yes
14	1.5	0.2	0.2	0	35	7	4	1	0.2	0	0	0	6	0	1	0	Yes
15	0.3	0.2	0.1	0	14	14	5	1	0.2	0.1	0	0	8	4	1	0	Yes
16	1	0.2	0.1	0.1	46	15	6	3	0.2	0.1	0	0	10	7	2	0	Yes
17	1.2	0.1	0.1	0.1	58	9	5	3	0.2	0.1	0	0	7	4	2	0	Yes
18	2.2	0.7	0.2	0.1	71	29	8	3	1.4	0.2	0.1	0	43	8	2	0	Yes
19	2.1	1.5	1.2	0.1	67	67	46	4	1.2	0.1	0	0	38	4	1	0	No
20	2.2	2.1	1.9	0.1	68	92	69	4	1.4	0.1	0	0	45	5	1	0	No
21	2.2	2.3	2.1	0.4	69	100	77	15	1.5	0.9	0.1	0	46	38	2	0	No
22	2.2	2.3	2.1	1.1	69	100	77	47	1.5	1	0.1	0	46	45	2	0	No
23	2.1	1.3	1.1	0.1	66	59	40	4	0.5	0.1	0	0	17	4	1	0	No
24	9.9	7.9	6.6	0.5	67	75	53	4	6.1	0.5	0.1	0	42	5	1	0	No
25	10	10.5	9.4	0.5	68	99	75	4	6.7	0.6	0.2	0	46	5	2	0	No
26	0	0	0	0.1	1	2	0	4	0	0	0	0	0	1	0	0	Yes
27	0	0	0	0.1	0	0	0	4	0	0	0	0	0	0	0	0	Yes
28	0.1	0.1	0	0.1	4	3	0	3	0	0	0	0	2	2	1	0	Yes
29	0.3	0.1	0	0.1	7	4	0	3	0.2	0.1	0	0	4	3	1	0	Yes
30	0.4	0.1	0	0.2	5	3	0	3	0.3	0	0	0	4	1	0	0	Yes
31	0	0	0	0.1	0	0	0	3	0	0	0	0	0	0	0	0	Yes
32	0.4	0.1	0	0.1	5	2	0	2	0.2	0.1	0	0	2	1	0	0	Yes
33	0.2	0.1	0	0	8	4	2	1	0.1	0.1	0	0	6	3	0	0	Yes

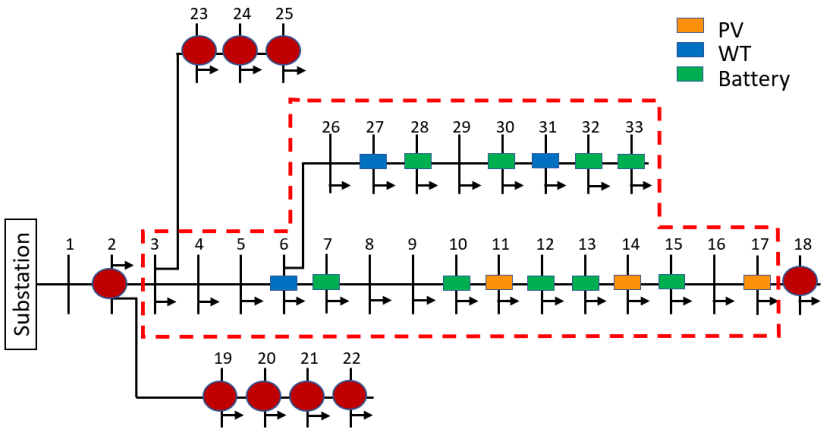

Figure 4.6: PG&E 33-bus radial DN partitioning for the second scenario at 46h. Red balls indicate the loads reduced to zero, without considering DSR into the model

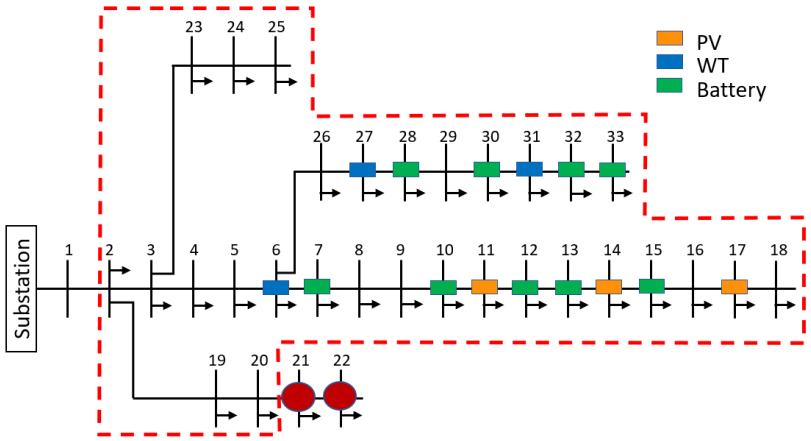

Figure 4.7: PG&E 33-bus radial DN partitioning for the second scenario at 46h. Considering DSR into the model

taken into account as parameters known. Thus, the nodes which have presented a high probability of ENS and a high load curtailment, have been further away from the DG and BSS. This result is explained because the objective function minimizes the flow between the nodes so that the model prioritizes the loads closer to a DG or BSS. In addition, when DSR is included in the load parameters, the global load curtailment is reduced by 62.7%, i.e. from 27.9% when the DSR is not included in the mathematical model, to a 10.4% when the loads are capable of self-modified in order to avoid an unbalanced system.

Table 4.4: DN topology under the third scenario

	Scenario 2 without DSR									**Scenario 2 with DSR**								
Bus	**40**	**41**	**42**	**43**	**44**	**45**	**46**	**47**	**48**	**40**	**41**	**42**	**43**	**44**	**45**	**46**	**47**	**48**
1	0	0	0	0	0	0	**0**	0	0	0	0	0	0	0	0	**0**	0	0
2	0	0	0	0	1	1	**1**	1	1	0	0	0	0	0	0	**0**	0	0
3	0	0	0	0	0	0	**0**	0	0	0	0	0	0	0	0	**0**	0	0
4	0	0	0	0	0	0	**0**	0	0	0	0	0	0	0	0	**0**	0	0
5	0	0	0	0	0	0	**0**	0	0	0	0	0	0	0	0	**0**	0	0
6	0	0	0	0	0	0	**0**	0	0	0	0	0	0	0	0	**0**	0	0
7	0	0	0	0	0	0	**0**	0	0	0	0	0	0	0	0	**0**	0	0
8	0	0	0	0	0	0	**0**	0	0	0	0	0	0	0	0	**0**	0	0
9	0	0	0	0	0	0	**0**	0	0	0	0	0	0	0	0	**0**	0	0
10	0	0	0	0	0	0	**0**	0	0	0	0	0	0	0	0	**0**	0	0
11	0	0	0	0	0	0	**0**	0	0	0	0	0	0	0	0	**0**	0	0
12	0	0	0	0	0	0	**0**	0	0	0	0	0	0	0	0	**0**	0	0
13	0	0	0	0	0	0	**0**	0	0	0	0	0	0	0	0	**0**	0	0
14	0	0	0	0	0	0	**0**	0	0	0	0	0	0	0	0	**0**	0	0
15	0	0	0	0	0	0	**0**	0	0	0	0	0	0	0	0	**0**	0	0
16	0	0	0	0	0	0	**0**	0	0	0	0	0	0	0	0	**0**	0	0
17	0	0	0	0	0	0	**0**	0	0	0	0	0	0	0	0	**0**	0	0
18	0	0	1	0	0	0	**1**	0	0	0	0	0	0	0	0	**0**	0	0
19	0	0	0	0	1	1	**1**	1	1	0	0	0	0	0	0	**0**	0	0
20	1	1	1	1	1	1	**1**	1	1	0	0	0	0	0	0	**0**	0	0
21	1	1	1	1	1	1	**1**	1	1	0	0	0	0	1	1	**1**	1	1
22	1	1	1	1	1	1	**1**	1	1	0	0	0	0	1	1	**1**	1	1
23	0	0	0	0	1	1	**1**	1	1	0	0	0	0	0	0	**0**	0	0
24	1	0	1	1	1	1	**1**	1	1	0	0	0	0	0	0	**0**	0	0
25	1	1	1	1	1	1	**1**	1	1	0	0	0	0	0	0	**0**	0	0
26	0	0	0	0	0	0	**0**	0	0	0	0	0	0	0	0	**0**	0	0
27	0	0	0	0	0	0	**0**	0	0	0	0	0	0	0	0	**0**	0	0
28	0	0	0	0	0	0	**0**	0	0	0	0	0	0	0	0	**0**	0	0
29	0	0	0	0	0	0	**0**	0	0	0	0	0	0	0	0	**0**	0	0
30	0	0	0	0	0	0	**0**	0	0	0	0	0	0	0	0	**0**	0	0
31	0	0	0	0	0	0	**0**	0	0	0	0	0	0	0	0	**0**	0	0
32	0	0	0	0	0	0	**0**	0	0	0	0	0	0	0	0	**0**	0	0
33	0	0	0	0	0	0	**0**	0	0	0	0	0	0	0	0	**0**	0	0

Chapter 5

A Benders decomposition approach for solving a P2P energy trading problem under uncertainty

5.1 Introduction

The constant decrease in the prices of DG is allowing residential users to opt for small-scale self-generation and BSS, providing them greater autonomy and control over electricity consumption. This new paradigm of more active, aware, and empowered users has prompted a rethinking of the residential DN to face future ECs with high penetration of DERs and eventual ECs operating under a TE scheme [6]. P2P energy trading is one of the potential emerging alternative schemes to model this paradigm and increase the efficiency in an EC with high DERs penetration and users willing to sell their energy surplus to other community users in an eventual LEM [7]. Thus, many research papers have addressed the challenge of modeling these new consumer-centric TE schemes over the last years to study their benefits and proper operation.

In consequence, this chapter presents a new two-stage stochastic programming model to address a scheduling day-ahead problem of an energy community operating under a P2P energy trading scheme. The formulation proposed i) considers the network technical constraints, ii) prevents the energy buying and selling by a user simultaneously, and iii) allows the prosumers to act as buyers or sellers depending on their load consumption and self-generation. In order to reduce the shared information by consumers/prosumers that trade energy in the LEM, the proposed model is decomposed into a master problem (MP) that manages the network technical limitation and subproblems (SPs) that handled the LEM. With this purpose, the Benders decomposition approach is implemented using the recently introduced Strengthened

Benders cuts to address the binary variables related to the market and battery operation present in the SPs. The model and the algorithm are tested in the 69-bus radial distribution system, considering from 3 to 39 agents trading energy to measure the model scalability and the algorithm convergence showing that the proposed methodology reduces the LEM's shared information without increasing the energy community cost.

Thus, the chapter structure is summarized as follows. Section 5.2 presents the literature review. Section 5.3 defines the market design and presents the two-stage programming formulation considering a centralized market to explain the market operation through the variables and equations. Section 5.4 explains the privacy-preserving decision-making mechanism for end-users through the Bender decomposition application. The case study and the computational results are presented in Section 5.5. The conclusions and further researches are discussed in Section 5.6.

5.2 Literature review

Different techniques have been applied in the P2P energy trading field to promote user energy sharing, establish the local market pricing, and manage users' private information. We refer the reader to [96] and [97] for a recent and comprehensive review of related academic papers, classification and techniques, and industrial applications in P2P energy trading.

In what follows, we review more recent works on P2P trading and group them into deterministic and two-stage stochastic approaches to highlight the differences between the methods.

5.2.0.1 Deterministic approaches

Centralized markets have been addressed, for example, in [98], where the coordinator has complete control over the community batteries and seeks to minimize grid operation costs. However, network technical constraints, such as the balance equations in nodes and lines, including the reactive power effect and the voltage limit operation, are not considered in that work, which might lead to infeasible or impractical solutions for real cases. Additionally, centralized markets usually entail that the coordinator has access to users' private information, which restricts users' autonomy and privacy.

Decentralized markets are an alternative to keep users' autonomy and privacy. Those markets have been addressed, for example, in [99, 100, 101, 102, 103]. The

work in [99] proposes a deterministic TE framework for trading energy between prosumers with BSS and DG and seeks to maximize the community surplus. In the same research direction, a decentralized P2P energy trading model is presented in [100], which uses the primal-dual gradient method to manage the trading scheme. This deterministic model includes technical constraints through the Power Transfer Distribution Factor (PTDF); however, the BSS and DG are not modeled explicitly, rather only the energy shortage or surplus is considered an input parameter. On its part, a dual decomposition method is proposed in [101] to coordinate the interaction between multi-regional prosumers under a P2P energy trading scheme maximizing the social welfare and including the voltage levels and the reactive power; however, batteries are not considered in the formulation, and the model is tested in a small network. Those issues are addressed in [102] and [103]. In [102] a decentralized model for a collaborative operation of MGs with the utility grid is investigated, considering technical constraints and restricting batteries to either charge or discharge at each slot time, and propose a Benders decomposition method to manage users' private information.

On the other hand, in [103], an optimization algorithm based on the Alternating Direction Method of Multipliers (ADMM) is proposed to address day-ahead operational planning of a grid-connected local energy community preserving the users' private information. The model in [103] is decomposed into two stages such that the first stage minimizes the cost of buying energy to the utility grid, and the second stage minimizes the internal losses considering the line resistance and the voltage level.

Community-based energy markets have also been addressed from other disciplines. A game-theoretic approach under a cooperative structure is investigated in [104, 105, 106, 107] and the non-cooperative structures in [108, 109, 110] to model the P2P energy market. They generally focus on studying users' incentives to trade energy between them. The main results show that the TE framework provides efficiency in the DERs use and increases community welfare. Likewise, a Continuous Double-Auction (CDA) mechanism is widely used in the literature to establish the LEM price for the bids and asks (see, e.g., [97, 111, 112, 113]). However, to the best of our knowledge, under a P2P energy trading scheme, no work considers the voltage levels and the reactive power in the formulation, which are critical factors to maintain the network balanced (see, e.g., [114, 115, 116, 96, 117]).

The previous literature focuses on modeling trading energy markets between prosumers and consumers under a wide range of different assumptions and constraints

and developing efficient algorithms to find reasonable quality solutions for the resulting models, providing valuable knowledge about these new markets. However, they do not consider the inherent uncertainties related to energy generation and consumption, which might impact the network efficiency and the community's social welfare.

5.2.0.2 Stochastic approaches

Contrary to deterministic approaches, stochastic models are recently gaining attention from scholars. Centralized markets under uncertainty have been investigated in [118, 119, 120, 121, 122, 123, 124]. Thus, an initial work is presented by [118] to address the uncertainty in energy trading markets through a hybrid stochastic/robust optimization model. The same approach is presented by [119] and [120] but using the General Nash Bargaining framework to decompose the original model into operational and bargaining problem. Authors in [121] use a stochastic approach to deal with the price uncertainty in the P2P energy market and avoid arbitrage by the users with the real-time market through a bi-level model based on a non-cooperative leader-follower game. Then, a two-stage robust optimization (RO) model is formulated by [122] to deal with uncertainties in a day-ahead and real-time spot market, maximizing the microgrids' profit and using the Benders decomposition approach for solving the resulting two-stage stochastic problem. Similarly, the RO approach is used by authors in [123] to manage the uncertainty marginal price in a P2P energy trading using the column-and-constraint generation (CCG) to decompose the robust model into subproblems. Likewise, the Markov decision process is used in [124] to solve a stochastic leader-fellow P2P energy trading model under a game theory approach that considers social attributes.

On the other hand, decentralized markets with stochastic parameters have been studied in [125, 126, 127, 128, 129, 130, 131]. Specifically, authors of [125] propose a model to address the P2P energy traded, preserving the users' information and covering the day-ahead and intraday market. A two-stage stochastic programming model is presented to manage the day-ahead market, such that the first stage variable includes the energy that the user is willing to trade in the real-time market, and in the second stage, the batteries operation is decided. The two-stage stochastic problem is decomposed into a set of stochastic subproblems, one for each user, and then solved through an ADMM algorithm. In [126] and [127] a distributionally robust co-optimization (DRO) model for the P2P energy trading and network operation of interconnected microgrids is presented. The energy requirement of each MG is managed in the first stage, and the strategy price is determined using an ADMM

algorithm in the second stage. A similar strategy is proposed by [128] for users in a small-scale system using the RO approach and the ADMM to manage the privacy. In the same research line, [129] proposes a nested market clearing algorithm and a DRO approach to clear the market and manage the prosumers' behavior, respectively, where the ADMM is implemented to solve the DRO and preserve user privacy.

However, few articles have explored alternative methods of the well-known ADMM to decompose the stochastic models and manage user privacy under a non-centralized energy trading scheme. Authors in [130] propose a stochastic cartel nonlinear model which is decomposed using a surrogate Lagrangian relaxation method, and the work presented by [131] provides an enhanced Benders decomposition to manage the energy transaction in smart buildings. These two recently introduced methods extend the research line related to decomposition algorithms applied to manage decentralized energy trading schemes under uncertainty.

The previous literature summarized deterministic and stochastic approaches to address P2P energy trading under different market schemes, where decomposition methods play a relevant role in modeling the users' interaction and managing their private information. However, most articles do not restrict BESS to simultaneously avoid the charging and discharging process because most do not include the network limitations. This unrealistic assumption generally simplifies the decomposition method application sacrificing the model accuracy. On the other hand, a common assumption in the above works is that all users possess a storage system to allow a flexible response to the load and generation forecast when a day-ahead and intraday market are considered. However, this assumption reflects another unrealistic situation because a community market is expected to be composed of consumers and prosumers, where prosumers have self-generation and/or a storage system and not necessarily both. Likewise, some reviewed articles define a fixed set of sellers (prosumers) and buyers (consumers) to implement game theory approaches. However, it is expected that in an energy trading framework, users with DERs can sell or buy energy in the LEM depending on their consumption and not always belongs to the sellers' group.

In addition, the formulations available in the literature rarely are tested under a significant number of agents, and only in few models consider the voltage stability and the reactive power, which prevents proving the models' scalability and their real application. Even the models that include these variables ([103],[125] and [126]) solve the resulting optimization model through the ADMM. However, the use of binary

variables might complicate the convergence of this algorithm even by solving augmented dual Lagrangian problems. Likewise, the enhanced Benders decomposition algorithm proposed by [131], which is the closest to what is presented in this chapter, defines a fixed group of sellers and buyers to compete under the game theory approach and assumes that all the sellers have a storage system.

5.3 Problem definition

5.3.1 Market design

The authors in [96] and [97] establish three groups to categorize P2P energy trading models based on the interaction between the market players. Thus, in a centralized design, a coordinator decides the energy exchanged among users in the most cost-effective way, maximizing the community's social welfare. However, the customers play a passive role under this design, while the coordinator has full access to the users' assets and information (e.g., [132, 133, 134]). On the contrary, in a decentralized market design, the users have complete control over their devices, and they decide when to sell or buy; however, the total community efficiency is affected because the individual profit is prioritized over the community welfare (e.g., [135, 136, 137]). The distributed market design is the third group, and it is between the two above, where a coordinator provides accurate information about pricing and the community requirement, and the user decides when to sell/buy, generating better coordination between peers than decentralized design, improving the efficiency of the market (e.g., [138, 139]).

Based on the definitions presented in [96] and [97], this chapter covers the P2P energy trading scheme under a centralized and distributed market design. Thus, the community manager (CM) is defined as a coordinator between the agents, the DSO, and the retailer in order to set the hourly energy imported (resp. exported) from (resp. to) the grid by the energy community in the day-ahead market. Specifically, the CM coordinates the energy traded in the LEM, considering the technical network constraints and identifying the energy surplus feed-in to the external grid or the energy bought to the retailer to maintain the system balanced at every time interval, as shown Fig. 5.1. Besides, the commodities traded in the local market include only the active power and not the reactive power; therefore, the CM also coordinates the reactive power required from the external grid to supply the reactive demand considering the voltage levels and the line capacities to avoid eventual network congestions produced by the energy exchanged between agents.

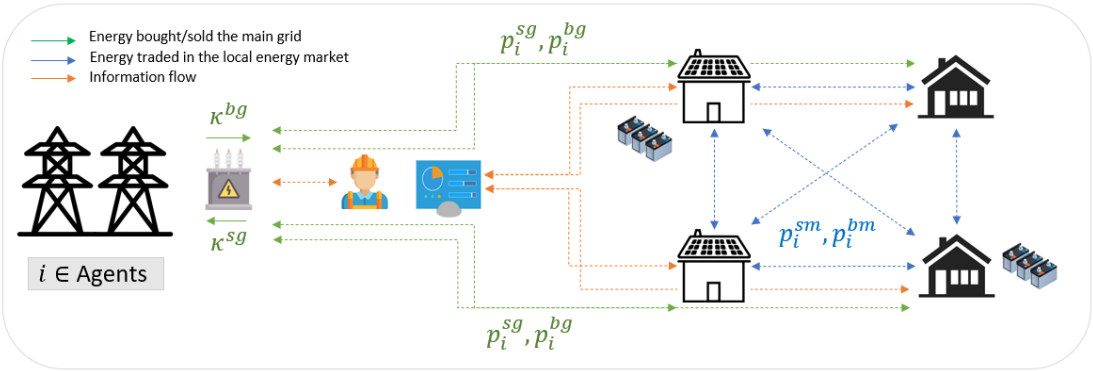

Figure 5.1: P2P energy trading schematic diagram modeled

The substation connected to the slack bus is the energy exchange point between the external grid and the users. When the energy self-generated by the community is not enough to supply the total load, the retailer provides the remaining power at the same price for every agent. The users or agents considered in this chapter might have a rooftop PV system or a storage device. Likewise, an agent with at least one of these technologies is a prosumer, which can trade energy between their neighbor and/or sell the energy surplus to the grid. On the contrary, a consumer is considered a user who only demands electricity. Finally, the prices used in this chapter correspond to i) the energy brought from the grid, which is a known parameter, ii) the feed-in tariff, which usually represents a fraction of the energy bought from the grid, and iii) the price of the energy traded in the local market, which is variable and in this case is estimated through the Lagrange multipliers (used in [140, 141]) associated to the active and reactive power nodal constraints to identify the marginal cost to maintain the network balance.

5.3.2 Two-stage stochastic approach

The literature review showed that most P2P energy trading formulations are modeled from a deterministic approach, i.e., load consumption and PV generation are assumed to be known beforehand. However, these parameters are unknown under a day-ahead market context, and their wrong forecast could bring extra costs to the agents and the retailer. Therefore, in this chapter it is assumed that the exact value of these parameters is unknown. However, some information on their possible value is available through the probability distribution function, representing the uncertainty of a finite set of discrete scenarios S, obtained by sampling from the continuous distributions of

the random parameters. Thus, a scenario $s \in S$ corresponds to a possible realization of the energy prices, PV generation, and load consumption.

Under the previous uncertainty context, the two-stage stochastic programming approach appears as a suitable alternative for addressing the load/generation uncertainty and improving decisions regarding the hourly energy planning that the community will demand (resp. deliver) in the day-ahead market. Specifically, the two-stage stochastic approach defines two sets of decisions, which must be made in two different stages of the decision process. The first-stage decisions correspond to the "here-and-now" decisions that have to be made prior to realizing the stochastic parameters. In our P2P energy trading market, these decisions correspond to the lack/surplus energy from/to the grid to keep the system balanced. On the other hand, the second stage decisions correspond to the "wait-and-see" decisions that can be postponed after realizing the stochastic parameters. These decisions can be seen as recourse actions undertaken to adjust the initial planning to the actual realization of energy consumption and PV generation. In this regard, the proposed two-stage stochastic approach aims to find day-ahead scheduling for the energy bought/sold to the grid that minimizes the global community cost. This approach leads to an equivalent deterministic mixed-integer linear program described in the next section.

5.3.3 Centralized model

The approach provided by this chapter allows the CM to coordinate the LEM operation under a distributed market design, i.e., without knowing the users' information related to their consumption or DERs use. Nonetheless, we first introduce a centralized market design as a Mixed-Integer Linear Programming formulation (MILP), which will allow us to better explain the market operation before describing the methodology to provide a more active role for the users and reduce the information shared in the LEM.

Let κ_t^{bg} (resp. κ_t^{sg}) be the energy bought (resp. sold) from the grid at time period t. This variables' definition leads us to the following objective function:

$$minimize \;\; z = \sum_{t \in \mathcal{T}} \sum_{s \in \mathcal{S}} \rho_s (\lambda_{t,s}^{bg} \kappa_t^{bg} - \lambda_{t,s}^{sg} \kappa_t^{sg}). \tag{5.1}$$

The objective function (5.1) minimizes the cost of the external network dependency through the first-stage variables, i.e., the total cost of the power injected and absorbed by the substation. The power provided by the grid (κ^{bg}) corresponds to

the gap that the LEM cannot meet through the energy traded between peers, and the power absorbed (κ^{sg}) corresponds to the power surpluses generated by the DERs that is not stored in the batteries and is not traded in the LEM. Besides, $\rho_s \in [0, 1]$ is of the likelihood of occurrence the scenario $s \in S$ with $\sum_{s \in S} \rho_s = 1$.

The following constraints bound the feasible solutions space through the network technical limitations, batteries behavior, and the LEM rules.

5.3.3.1 Network technical constraints

The formulation proposed in this article uses the OPF equations to include the network limitations. However, due to the high computational burden associated with the original AC-OPF problem applied to a two-stage stochastic programming problem, the following constraints have been already linearized using the approach developed in [142]. This linearization method has been selected because its convergence has been validated and tested in [143, 144, 145, 146], showing an error lower than 1.3% and requiring no additional network information. For other linearization methods, we suggest to the readers review the works in [147, 148, 149, 150]. In this regard, Eqs. (5.2) and (5.3) correspond to the balancing equations in every node for the active and reactive power, respectively. Specifically, the right-hand side of Eq. (5.2), which corresponds to the active power, depends on the type of bus. Thus, if the bus possesses an agent that trades energy in the community market, Eq. (5.2) considers from left to right: the power generated by the rooftop solar PV system (pg); the power injected (ds) and absorbed (ch) by the battery, and the electricity load (PL). On the contrary, if the bus is the substation, Eq. (5.2) considers the power provided (κ^{bg}) and absorbed (κ^{sg}) by the substation. Thus, $\forall t \in \mathcal{T}, \forall s \in \mathcal{S}$:

$$v_{i,t,s}(G_i + \sum_{(i,j)\in\mathcal{L}} G_{i,j}) + \sum_{(i,j)\in\mathcal{L}} p_{t,s}^{i,j}$$

$$= \begin{cases} pg_{i,t,s} + ds_{i,t,s} - ch_{i,t,s} - PL_{i,t,s} & \forall i \in \mathcal{A}, \\ \kappa_t^{bg} - \kappa_t^{sg} & \text{substation}, \\ 0 & \text{otherwise}. \end{cases} \tag{5.2}$$

Likewise, Eq. (5.3) considers the reactive power provided by the substation in every node, assuming that the distributed sources only generate active power. Thus, the reactive power (QL) is considered within the power flow equations affecting the line flow capacity, the voltage levels, and the angles, assuming that the external grid

supplies the entire reactive power demand because the LEM only trades active power. Therefore, $\forall t \in \mathcal{T}, \forall s \in \mathcal{S}$, $\forall i \in \mathcal{B}$:

$$-v_{i,t,s}(B_i + \sum_{(i,j)\in\mathcal{L}} (B_{i,j} - Bs_{i,j})) + \sum_{(i,j)\in\mathcal{L}} q_{t,s}^{i,j} = q\kappa_{i,t,s}^{bg} - QL_{i,t,s}. \tag{5.3}$$

Eqs. (5.4) correspond to the linearized line power flow equations, which do not present variation regarding [142]. Therefore; $\forall (i,j) \in \mathcal{L}, \forall t \in \mathcal{T}, \forall s \in \mathcal{S}$:

$$G_{i,j}\left(\frac{\Delta v_{t,s}^{i,j}}{2}\right) - B_{i,j}(\Delta\theta_{t,s}^{i,j}) + LP_{i,j} = p_{t,s}^{i,j}, \tag{5.4a}$$

$$-B_{i,j}\left(\frac{\Delta v_{t,s}^{i,j}}{2}\right) - G_{i,j}(\Delta\theta_{t,s}^{i,j}) + LQ_{i,j} = q_{t,s}^{i,j}. \tag{5.4b}$$

The parameters LP and LQ represent a loss factor that depends on the angle and the voltage. We refer the reader to [142] for a detailed explanation of the linearization methodology and the parameters introduced to handle the non-linearities and the loss factor.

The power injected by the rooftop PV system into the grid in Eq. (5.5a) must be lower or equal to the installed capacity multiplied by the parameter PG^{max}, representing the PV power normalized curve for every time t. Eq. (5.5b) limits the power provided and absorbed by the substation. Likewise, Eq. (5.5c) fixes the operational voltage ranges, and Eq. (5.5d) establishes the line's capacity. Therefore, $\forall s \in \mathcal{S}$:

$$0 \leq pg_{i,t,s} \leq PG_{t,s}^{max} DG_i \qquad \forall i \in \mathcal{A}, \forall t \in \mathcal{T}, \tag{5.5a}$$

$$0 \leq \kappa_t^{sg},\ \kappa_t^{bg} \leq \kappa^{max} \qquad \forall t \in \mathcal{T}, \tag{5.5b}$$

$$V^{min} \leq v_{i,t,s} \leq V^{max} \qquad \forall i \in \mathcal{B}, \forall t \in \mathcal{T}, \tag{5.5c}$$

$$\sqrt{(p_{t,s}^{i,j})^2 + (q_{t,s}^{i,j})^2} \leq S_{i,j}^{max} \qquad \forall (i,j) \in \mathcal{L}, \forall t \in \mathcal{T}. \tag{5.5d}$$

The quadratic expression in (5.5d) is linearized, converting the circumference into a regular polygon of $\mathcal{R}$ sided (see, e.g.,[151]) as follows:

$$A_{i,j}^r p_{t,s}^{i,j} + B_{i,j}^r q_{t,s}^{i,j} + C_{i,j}^r S_{i,j}^{max} \leq 0 \qquad \mathcal{R} = \{1, 2, ..r\}. \tag{5.6}$$

5.3.3.2 Battery modelling

The following set of constraints models the battery behavior which had been explained in detail in 2.3. Eq. (5.7a) represents the battery SOC for the next period, which depends on the current SOC plus (resp. minus) the energy-charged (resp. discharged) as appropriate. Eq. (5.7b) establishes the operational range of the battery multiplied by its installed capacity. Note that if an agent does not have a battery, its energy storage capacity is zero, forcing the other battery variables to zero. The formulation uses a binary variable to model the charge and discharge battery process because both actions cannot be executed simultaneously. Thus, Eq. (5.7c) represents the charging process, and Eq. (5.7d) the battery discharge. Therefore; $\forall i \in \mathcal{A}, \forall t \in \mathcal{T}, \forall s \in \mathcal{S}$

$$soc_{i,t+1,s} = soc_{i,t,s} + [\varphi^{ch} ch_{i,t,s} - \frac{1}{\varphi^{ds}} ds_{i,t,s}]\Delta t, \tag{5.7a}$$

$$SOC^{min} BT_i \leq soc_{i,t,s} \leq SOC^{max} BT_i, \tag{5.7b}$$

$$ch_{i,t,s} \leq PB(w_{i,t,s}), \tag{5.7c}$$

$$ds_{i,t,s} \leq PB(1 - w_{i,t,s}). \tag{5.7d}$$

5.3.3.3 Local energy market rules

Market constraints seek to identify the energy amount traded in the community market and the energy bought/sold to the grid for every agent. Thus, Eq. (5.8a) represents the relationship between the energy amount demanded and self-generated (left-hand side) and the energy traded in the LEM or bought/sold to the grid (right-hand side). However, to avoid an agent's purchase and sale of energy simultaneously, a binary variable (y) is introduced in Eqs. (5.8b) and (5.8c) to ensure that the energy selling occurs in the LEM only when the agent has an energy surplus (5.8b), or the energy purchasing occurs only when the agents require external energy to meet its electricity demand. (5.8c). i.e., if there is a power surplus, y takes value one and zero otherwise. Therefore; $\forall i \in \mathcal{A}, \forall t \in \mathcal{T}, \forall s \in \mathcal{S}$

$$pg_{i,t,s} + ds_{i,t,s} - ch_{i,t,s} - PL_{i,t,s} - \varepsilon_{i,t,s} = p^{sm}_{i,t,s} + p^{sg}_{i,t,s} + p^{bm}_{i,t,s} + p^{bg}_{i,t,s}, \tag{5.8a}$$

$$p^{sm}_{i,t,s} + p^{sg}_{i,t,s} \leq M y_{i,t,s}, \tag{5.8b}$$

$$p^{bm}_{i,t,s} + p^{bg}_{i,t,s} \geq M(y_{i,t,s} - 1), \tag{5.8c}$$

$$p^{bg}_{i,t,s}, p^{bm}_{i,t,s} \leq 0; \quad p^{sg}_{i,t,s}, p^{sm}_{i,t,s} \geq 0 \tag{5.8d}$$

In addition, to visualize the difference between the energy amount sold/bought to the market/grid, the Eqs. (5.9a) and (5.9b) are defined. Specifically, Eq. (5.9a)

indicates that the total power sold to the grid must be equal to the energy absorbed by the substation, which combined with Eq. (5.8a) provides the energy sold in the LEM and to the grid for every user. In a homologous way, Eq. (5.9b) establish the total power bought within the grid. Therefore; $\forall t \in \mathcal{T}, \forall s \in \mathcal{S}$

$$\sum_{i \in \mathcal{A}} p^{sg}_{i,t,s} = \kappa^{sg}_{t} \tag{5.9a}$$

$$-\sum_{i \in \mathcal{A}} p^{bg}_{i,t,s} = \kappa^{bg}_{t} \tag{5.9b}$$

Note that Eqs. (5.9) match the energy amount provided by the DERs with the energy exported to the grid. This equality is possible because the line losses are represented by ε in Eq. (5.8a). If ε is not defined, in Eq. (5.9a), the power sold by DERs would be greater than the exported to the gird, and in Eq. (5.9b), the power bought by the users would be lower than the total imported due to line losses. However, the ε variable introduction allows separating the line losses and matching the energy traded in the LEM with the energy bought/sold from/to the gird.

Finally, the market balance equation is defined in Eq. (5.10) such that all the energy sold in the LEM is bought.

$$\sum_{i \in \mathcal{A}} p^{sm}_{i,t,s} + \sum_{i \in \mathcal{A}} p^{bm}_{i,t,s} = 0. \tag{5.10}$$

5.4 Decentralized approach

In this section, the previous centralized model is reformulated into a distributed model to decrease the information shared by the users with the CM and increase the role of the prosumer in the LEM through an iterative scheme of supply and demand between users and the CM, considering at every moment the network limitations.

5.4.1 Preliminaries

The following equations must be rewritten to hide the agents' information from the CM when the previous formulation is addressed under a distributed perspective. To this end, we define in Eq. (5.11) the variable Δp (left-hand-side of Eq. 5.8a) to represent the difference between the load consumption and energy self-generated by the agents, modifying Eq.(5.2) as follows:

$$\Delta p_{i,t,s} = pg_{i,t,s} + ds_{i,t,s} - ch_{i,t,s} - PL_{i,t,s} - \varepsilon_{i,t,s}, \tag{5.11}$$

$$v_{i,t,s}(G_i + \sum_{(i,j)\in\mathcal{L}} G_{i,j}) + \sum_{(i,j)\in\mathcal{L}} p_{t,s}^{i,j}$$

$$= \begin{cases} \Delta p_{i,t,s} + \varepsilon_{i,t,s} & \forall i \in \mathcal{A}, \\ \kappa_t^{bg} - \kappa_t^{sg} & \text{substation}, \\ 0 & \text{otherwise}. \end{cases} \tag{5.12}$$

Note that Eq. (5.12) hides the user load consumption, the energy self-generated by the PV systems, and the battery operation, providing to the CM only the information related to whether the users will operate as a generator or a consumer. Besides, as Δp includes the line losses, and Eq. (5.2) does not, the new Eq. (5.12) must add the ε variable to neutralize the Δp and maintain the equality defined in Eq. (5.2). Likewise, the Δp definition modify the equations (5.8) related to the LEM operation, such that Δp in Eq. (5.11) can take a positive value when the agent generates more energy than its electricity load (operate as a small generator) or take negative values in the opposite case, operating as a traditional consumer. Eq. (5.13a) reflects this situation opening up Δp into Δp^+ and Δp^-. Thus, in Eqs. (5.13b) and (5.13c), the power surplus (Δp^+) comprises the power sold to the market plus the power sold to the grid, and the power lack (Δp^-) includes the power bought from the market and the grid, respectively. Besides, to avoid simultaneous selling and to buy action by the agents, the logical constraints (5.13d) and (5.13e) ensure through a binary variable that the agents only sell energy when they have surplus; otherwise, they must buy energy from the market or the grid.

$$\Delta p_{i,t,s} = \Delta p_{i,t,s}^{+} + \Delta p_{i,t,s}^{-}, \tag{5.13a}$$

$$\Delta p_{i,t,s}^{+} = p_{i,t,s}^{sm} + p_{i,t,s}^{sg}, \tag{5.13b}$$

$$\Delta p_{i,t,s}^{-} = p_{i,t,s}^{bm} + p_{i,t,s}^{bg}, \tag{5.13c}$$

$$\Delta p_{i,t,s}^{+} \leq M(y_{i,t,s}), \tag{5.13d}$$

$$\Delta p_{i,t,s}^{-} \geq M(y_{i,t,s} - 1). \tag{5.13e}$$

In addition, the constraint (5.10) related to the total energy traded in the LEM must be rewritten in terms of variables known by the CM. Therefore, using Eqs. (5.9) and (5.13), Eq. (5.10) is rewritten as follows; $\forall t \in \mathcal{T}, \forall s \in \mathcal{S}$:

$$\kappa_t^{sg} - \kappa_t^{bg} - \sum_{i\in\mathcal{A}} \Delta p_{i,t,s} = 0. \tag{5.14}$$

5.4.2 The Benders decomposition approach (BD)

Once the users' information has been hidden through the Δp variable, the bender decomposition approach is applied to separate the centralized model into a Master Problem (MP) related to the information known by the CM and the network constraints and SubProblems (SP), which address the users' information. The iterative methodology used in the BD algorithm allows for increasing the agents' participation in the LEM because they interact individually and continuously with the CM to respect the network constraints and minimize the global community cost as follows:

Users receive a suggestion from the CM regarding the partial information related to p^{bg}, p^{sg}, and Δp, which initially respect the network technical limitation (MP solution). Then, the users individually take the CM suggestion and minimize the power bought from the grid depending on its power generation, battery operation, and load consumption, and return new values for p^{bg}, p^{sg} and Δp (SP solutions), which are taken by the CM and verified if the currents values respect the network technical constraints. If these new values do not respect the network limitations, then the CM suggests a new consumption plan, taking into account the previous information provided by the users. This iterative process occurs until it converges in the optimal solution, which minimizes the cost of energy required from the grid and respects all network technical constraints.

It is worth remarking that the CM partially knows the users' information through the p^{bg}, p^{sg} and Δp. This information is crucial for the CM to manage and keep the network balanced. Nonetheless, this information is only partial because it does not provide the power generated by its DERs, their consumption, or the battery operation, guaranteeing users autonomy and privacy. Thus, the MP and the SPs are defined as follows:

5.4.2.1 Master Problem

Let $\mathcal{Q}_i(\cdot)$ be a recourse function that represent the cost of the agents i given the MP decisions $\Delta p, \varepsilon, p^{bg}, p^{sg}$. Thus, the MP is defined as follows:

$$\min \sum_{i \in \mathcal{A}} \mathcal{Q}_i(\Delta p, \varepsilon, p^{bg}, p^{sg}). \tag{5.15}$$

subject to

- The network technical constraints (5.3), (5.4) and (5.12).
- The voltage and lines capacity (5.5b)-(5.5d), and (5.6).

- The global LEM necessities (5.9).
- The LEM balancing (5.14).

5.4.2.2 Subproblems

Given the MP solution $\Delta p, \varepsilon, p^{bg}, p^{sg}$, we now define a set of SPs, one for each agent. Thus, for each $i \in \mathcal{A}$, we have the following SP:

$$\mathcal{Q}_i(\Delta p, \varepsilon, p^{bg}, p^{sg}) = \min \sum_{t \in \mathcal{T}} \sum_{s \in \mathcal{S}} \lambda^{bg}_{t,s} p^{bg}_{i,t,s} - \lambda^{sg}_{t,s} p^{sg}_{i,t,s}. \tag{5.16}$$

subject to

- The users' consumption and battery operation (5.11), (5.5a), (5.7), and (5.13).

Each SP thus focuses on defining a plan for its own power generation, battery operation, and load consumption based on the power levels from the external grid imposed by the MP.

Note that usually, in a Benders decomposition, integer constraints are included in the MP. However, integer constraints related to batteries operation and LEM rules are the SPs in our case. This poses the following issue, classical Benders cuts rely on the linear relaxation of SPs and, hence, it does not consider the integrality of the decision variables; this might lead to non-implementable solutions. Therefore, we propose to use a recently introduced type of cut, called Strengthened Benders' cuts (see [152] and [153]). These cuts rely on a Lagrangian relaxation of SPs, allowing us to guarantee the feasibility of integer constraints.

5.4.2.3 Strengthened Benders' cuts

This family of cuts is based on the observation that a valid cut can be generated by solving a Lagrangian relaxation, where the corresponding Lagrangian multiplier are fixed to the dual solution of the linear relaxation. Therefore, Benders' cuts can be strengthened by solving a mixed-integer program rather than only a linear program. Thus, in order to generate a Strengthened Benders' cut, we must first reformulate each SP by introducing the following variables: $\Delta\bar{p}_{i,t,s}, \bar{\varepsilon}_{i,t,s}, \bar{p}^{bg}_{i,t,s}, \bar{p}^{sg}_{i,t,s}$ for each $i \in \mathcal{A}, t \in \mathcal{T}, s \in \mathcal{S}$. Thus, for each $i \in \mathcal{A}$, we reformulate the SPs as follows:

$$\mathcal{Q}_i(\Delta p, \varepsilon, p^{bg}, p^{sg}) = \min \sum_{t \in \mathcal{T}} \sum_{s \in \mathcal{S}} (\lambda^{bg}_{t,s} \bar{p}^{bg}_{i,t,s} - \lambda^{sg}_{t,s} \bar{p}^{sg}_{i,t,s}) \tag{5.17a}$$

$\forall t \in \mathcal{T}$, $s \in \mathcal{S}$ subject to

$$\Delta\bar{p}_{i,t,s} = \Delta p_{i,t,s} \tag{5.17b}$$

$$\bar{\varepsilon}_{i,t,s} = \varepsilon_{i,t,s} \tag{5.17c}$$

$$\bar{p}^{bg}_{i,t,s} = p^{bg}_{i,t,s} \tag{5.17d}$$

$$\bar{p}^{sg}_{i,t,s} = p^{sg}_{i,t,s} \tag{5.17e}$$

$$\Delta\bar{p}_{i,t,s} = pg_{i,t,s} + ds_{i,t,s} - ch_{i,t,s} - PL_{i,t,s} - \bar{\varepsilon}_{i,t,s} \tag{5.17f}$$

$$\Delta\bar{p}_{i,t,s} = \Delta p^{+}_{i,t,s} + \Delta p^{-}_{i,t,s} \tag{5.17g}$$

Constraints (5.5a), (5.7), (5.13)

Note that the constraints (5.11) and (5.13b) are rewritten with respect to the redundant variables $\Delta\bar{p}_{i,t,s}$ and $\bar{\varepsilon}_{i,t,s}$ as (5.17f) and (5.17g), respectively. Although variables $\Delta\bar{p}_{i,t,s}, \bar{\varepsilon}_{i,t,s}, \bar{p}^{bg}_{i,t,s}, \bar{p}^{sg}_{i,t,s}$ and constraints (5.17b)-(5.17e) are redundant for the SP_i, they play a key role in the generation of Strengthened Benders' cuts used to approximate the recourse functions.

We refer the reader to [152] and [153] for more detail about these cuts family.

Constraints (5.17b)-(5.17e) are then dualized leading to the following relaxed SPs:

$$\begin{aligned}\underline{\mathcal{Q}}_i(\Delta p, \varepsilon, p^{bg}, p^{sg}) = \min \sum_{t\in\mathcal{T}}\sum_{s\in\mathcal{S}} & \lambda^{bg}_{t,s}\bar{p}^{bg}_{i,t,s} - \lambda^{sg}_{t,s}\bar{p}^{sg}_{i,t,s} \\ & + \pi^{\Delta}_{i,t,s}(\Delta\bar{p}_{i,t,s} - \Delta p_{i,t,s}) + \pi^{\varepsilon}_{i,t,s}(\bar{\varepsilon}_{i,t,s} - \varepsilon_{i,t,s}) \\ & + \pi^{bg}_{i,t,s}(\bar{p}^{bg}_{i,t,s} - p^{bg}_{i,t,s}) + \pi^{sg}_{i,t,s}(\bar{p}^{sg}_{i,t,s} - p^{sg}_{i,t,s}).\end{aligned} \tag{5.18a}$$

$\forall t \in \mathcal{T}, s \in \mathcal{S}$ subject to:

$$\text{Constraints (5.5a), (5.7), (5.13), (5.17f), (5.17g).} \tag{5.18b}$$

Where π^{Δ} , π^{ε}, π^{bg} and π^{sg} are the Lagrange multipliers of the constraints (5.17b), (5.17c), (5.17d) and (5.17e), respectively.

Note that, by relaxing Constraints (5.17b)-(5.17e), the resulting SPs (5.18a)-(5.18b) are always feasible because variables $\Delta\bar{p}_{i,t,s}, \bar{\varepsilon}_{i,t,s}, \bar{p}^{bg}_{i,t,s}, \bar{p}^{sg}_{i,t,s}$ are now free to balance Constraints (5.5a),(5.7), (5.13), (5.17f),(5.17g).

Let $\psi_i(\cdot)$ be the approximation of the recourse function $\mathcal{Q}_i(\cdot)$ available at iteration j of the BD algorithm, which is defined by the set of supporting hyperplanes generated until iteration j. Thus for each $i \in \mathcal{A}$:

$$\psi_i(\Delta p, \varepsilon, p^{bg}, p^{sg}) = \min\{\eta_i : \eta_i \geq \nu_i^k - \sum_{t\in\mathcal{T}}\sum_{s\in\mathcal{S}} \pi_{i,t,s}^{\Delta,k}\Delta p_{i,t,s} - \pi_{i,t,s}^{\varepsilon,k}\varepsilon_{i,t,s} - \pi_{i,t,s}^{bg,k}p_{i,t,s}^{bg} - \pi_{i,t,s}^{sg,k}p_{i,t,s}^{sg} \quad \forall k \in \{1,\ldots,j-1\}\}. \tag{5.19a}$$

Where

$$\nu_i^k = \sum_{t\in\mathcal{T}}\sum_{s\in\mathcal{S}} \lambda_{t,s}^{bg}\bar{p}_{i,t,s}^{bg,k} - \lambda_{t,s}^{sg}\bar{p}_{i,t,s}^{sg,k} + \pi_{i,t,s}^{\Delta,k}(\Delta\bar{p}_{i,t,s}^{k}) + \pi_{i,t,s}^{\varepsilon,k}(\bar{\varepsilon}_{i,t,s}) + \pi_{i,t,s}^{bg,k}\bar{p}_{i,t,s}^{bg,k} + \pi_{i,t,s}^{sg,k}\bar{p}_{i,t,s}^{sg,k}, \tag{5.19b}$$

and $\pi_i^{\Delta,k}, \pi_i^{\varepsilon,k}, \pi_i^{sg,k}, \pi_i^{bg,k}$ are the coefficients of the cut generated at iteration $k < j$ by solving the Lagrangian relaxation (5.18a)-(5.18b). This leads to the following approximate the MP reformulation:

$$\min \sum_{i\in\mathcal{A}} \eta_i. \tag{5.20a}$$

Subject to

$$\text{Constraints } (5.5b) - (5.5d), (5.9), (5.3) - (5.6), (5.12), (5.14). \tag{5.20b}$$

$$\eta_i \geq \nu_i^k - \sum_{t\in\mathcal{T}}\sum_{s\in\mathcal{S}} \pi_{i,t,s}^{\Delta,k}(\Delta p_{i,t,s}) - \pi_{i,t,s}^{\varepsilon,k}(\varepsilon_{i,t,s}) - \pi_{i,t,s}^{bg,k}p_{i,t,s}^{bg} - \pi_{i,t,s}^{sg,k}p_{i,t,s}^{sg} \quad \forall k \in \{1,\ldots,j-1\}\}. \tag{5.20c}$$

Thus, at each iteration of the BD algorithm, the MP is solved with a current approximation of the recourse functions. Its output is a feasible plan for the network, which consists of each agent's power levels from the external grid. Then, the approximation of the recourse functions is further improved by solving the SPs and generating a new linear cut.

5.4.3 Cut strategy

Note that in order to generate a Strengthened Benders' cut, we must solve the SPs (5.18a)-(5.18b) with a fixed dual solution, i.e., $\pi^{\Delta}, \pi^{\varepsilon}, \pi^{sg}, \pi^{bg}$ are fixed. These values can be arbitrarily chosen and then improved through a sub-gradient algorithm. However, it entails solving a series of mixed-integer linear programs for each SP, which might be computationally demanding. An alternative is to solve the linear relaxation

of SPs (5.5a),(5.7), (5.13),(5.17a)-(5.17g) and fixing the variables $\pi^{\Delta}, \pi^{\varepsilon}, \pi^{sg}, \pi^{bg}$ to the dual values of corresponding Constraints (5.17b)-(5.17e), which entails only solving a linear and mixed-integer linear program for each SP. Nonetheless, these SPs might be infeasible because the solution of the MP does not give them enough flexibility to satisfy their energy demand. We, therefore, introduce an auxiliary variable ζ that allows us to balance equation (5.17f) when necessary. For this purpose the variable ζ is penalized in the objective function with a large enough coefficient, i.e., $\bar{M} >> \lambda^{bg}$ and, hence, variables ζ only take a positive value when the demand in constraints (5.17f) cannot be satisfied by the energy production, the stock energy on the battery or the assigned energy from the retailers.

This reformulation and cut strategy have two main advantages. First, it is always feasible and, hence, we can compute an upper bound of the centralized problem by solving it at any iteration of the BD algorithm. Second, we can use a Strengthened Benders' cuts strategy to under-approximate the recourse functions. This approach is computationally advantaged as its only requests to solve the linear relaxation of each SP and the corresponding Lagrangian relaxation at each iteration of the Benders algorithm. Note that this approach differs from one of the Dual Lagrangian SPs are solved through a subgradient algorithm, which entails solving a series of mixed-integer linear programs. As a result, a reduced computational effort is requested to generate Strengthened Benders' cuts.

Note that the convergence of the algorithm is no longer theoretically guaranteed due to the use of Strengthened Benders Cuts rather than the Dual Lagrangian cuts but, as this approximation leads to a significant reduction of the computational effort required at each iteration of the algorithm, it may positively impact the solution quality in practice (see, e.g., [154] and [155]). Nonetheless, the algorithm provide both a valid feasible solution (upper bound) for the problem and a lower bound given by the approximation of the recourse functions in the master problem. Thus, the quality of the solution, with respect to the the optimal solution, can be measure trough the gap between these solutions.

5.4.4 Summary

As a synthesis, the main steps of the proposed BD algorithm applied to the stochastic LEM problem are summarized in Algorithm 1.

Algorithm 1: Benders algorithm

Initialize $LB \leftarrow -\infty, UB \leftarrow +\infty, k \leftarrow 0$
while *no stopping criterion is satisfied* **do**
  Solve the master problem (5.20a)-(5.20c)
  Collect master solutions $\Delta p_{i,t,s}, \varepsilon_{i,t,s}, p^{bg}_{i,t,s}, p^{sg}_{i,t,s}$
  Update the lower bound $LB = \sum_{i \in \mathcal{A}} \tilde{\eta}_i$
  for $i \in \mathcal{A}$ **do**
    Solve the linear relaxation of subproblem (5.5a),(5.7), (5.13),(5.17a)-(5.17g) for agent i, fixing the corresponding master solution.
    Collect the dual values $\pi^{\Delta,k}_i, \pi^{\varepsilon,k}_i, \pi^{bg,k}_{i,t,s}, \pi^{sg,k}_{i,t,s}$ of Constraints (5.17b)-(5.17e).
    Solve the Lagrangian relaxation (5.18a)-(5.18b) with current approximation $\psi_i(\cdot)$ and fixing the corresponding dual values.
    Collect the redundant variables $\bar{p}^{bg}$ and $\bar{p}^{sg}$ and the cut coefficient ν^k_i.
  end
  Update the upper bound $UB = \sum_{i \in \mathcal{A}} \sum_{t \in \mathcal{T}} \sum_{s \in \mathcal{S}} \lambda^{bg}_{t,s} \bar{p}^{bg}_{i,t,s} - \lambda^{sg}_{t,s} \bar{p}^{sg}_{i,t,s}$
  Add the Strengthened Benders' cuts to the master problem.
  $k \leftarrow k + 1$.
end

5.5 Computational results

This section assesses the centralized and distributed approaches in an Low-voltage DN, considering different scenarios and load profiles. The algorithm convergence and its time operation are analyzed and contrasted with the single centralized formulation. Likewise, different agents' numbers participating in the LEM are considered to measure the algorithm scalability. Besides, it is analyzed how the flexibility provided by the batteries allows the community to compromise the total energy bought or sold to the grid in a day-ahead market scheme.

5.5.1 Case study parameters

The 69-bus distribution system containing 68 branches and 40 loads is used to test the mathematical approaches. The peak active and reactive power has been modified to consider only residential profiles to address a small residential community market appropriately. Specifically, the peak loads oscillate between 2-5 [kW], and the reactive power maintains the original proportion concerning the active power. Fig 5.2 shows the test system with the loads distribution identifying the users with PV and storage systems, in which the PV systems capacity is 20% greater than the peak active

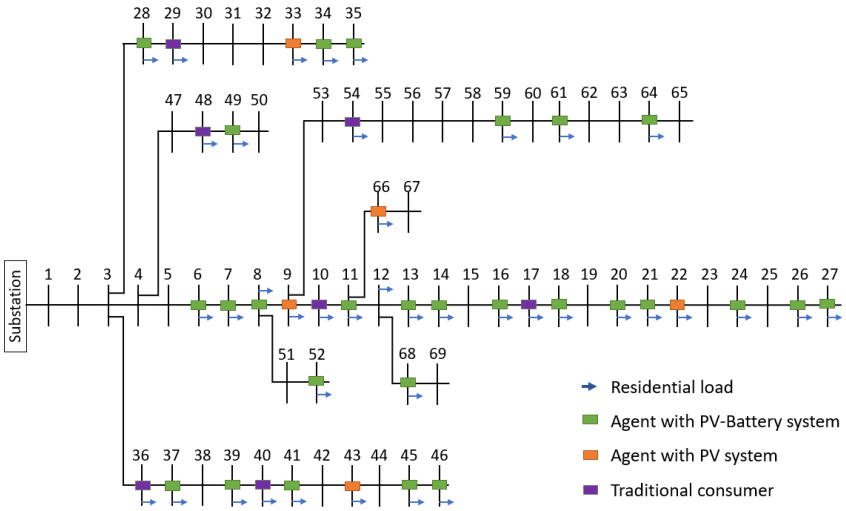

Figure 5.2: Modified IEEE 69-bus distribution network.

load, and for BSS, an 80% greater than the maximum electricity demand. The case study includes 39 agents, of which seven agents are traditional consumers without self-generation, five possess PV systems, and the remaining agents have hybrid PV-battery systems.

The total electricity load reaches up to 139 [kW], the reactive power to 99.2 [kVAr], the total PV power installed to 177 [kW], and the total battery capacity to 309 [kWh] with an efficiency of 85% - 87% in the charging and discharging process (see Table 5.1). Note that the high BSS penetration allows facing the two-stage stochastic problem nature.

The curves shown in Fig 5.3 and Fig 5.4 correspond to three scenarios of 24 hours obtained from annual data with a timeslot of one hour. Specifically, Fig. 5.3 shows the twenty-three different residential load profiles [69] used to highlight the benefits of operating under a P2P energy trading scheme. The first scenario possesses the higher total load with 991.98 [kWh] and peak power of 59.98 [kW], followed by the second scenario with 842.23 [kWh] and peak power of 53.5 [kW], and the third case with 807.51 [kWh], and 505.59 [kW] of peak power.

On the other hand, Fig. 5.4 provides the aggregated load curves considering the thirty-nine agents together with the normalized curve of PV power generation [70] and the energy prices [45]. Likewise, the first scenario considers a total PV generation of 872.08 [kWh], which is the higher generation with a peak power of 177 [kW] at 13 hours, followed by the second scenario with a total generation of 770.48 [kWh] with a peak power of 123 [kW], and the third scenario in 24 hours generates 734 [kWh] with

Table 5.1: Load and DERs parameters

Bus	PL	QL	PV	BT	**Bus**	PL	QL	PV	BT
6	5	4.23	7.5	15	**33**	3	2.14	4.5	0
7	4	2.97	6	12	**34**	3	4.42	4.5	9
8	4	2.88	6	12	**35**	3	2	4.5	9
9	4	2.93	0	0	**36**	2	1.43	0	0
10	3	2.04	4.5	0	**37**	4	2.85	6	12
11	5	3.59	7.5	15	**39**	4	2.83	6	12
12	3	2.15	4.5	9	**40**	5	3.54	7.5	15
13	5	3.13	7.5	15	**41**	2	1.67	3	6
14	5	3.44	7.5	15	**43**	2	1.43	3	0
16	4	2.64	6	12	**45**	4	2.68	6	12
17	3	1.75	0	0	**46**	2	1.34	3	6
18	2	1.17	3	6	**48**	3	2.14	0	0
20	2	1.2	3	6	**49**	2	1.43	3	6
21	5	3.55	7.5	15	**52**	2	1.2	3	6
22	3	2.1	4.5	0	**54**	5	2.9	0	0
24	3	2.14	4.5	9	**59**	3	2.5	4.5	9
26	5	3.57	7.5	15	**61**	4	2.7	6	12
27	3	2.14	4.5	9	**64**	4	3.1	6	12
28	4	2.86	6	12	**66**	4	2.8	6	0
29	4	2.86	0	0	**68**	2	0.8	3	6

a peak power of 99.12 [kW] at 14 hours. Therefore, considering the load consumption and the PV generation described above, the PV systems provide 87.91 % of the total load in the first scenario, followed by the second scenario with 91.48 % and 90.9 % for the third scenario. Thus, the first scenario is the most demanding, followed by the second and the third.

5.5.2 Algorithm convergence and scalability assessment

This section presents the algorithm convergence results and addresses the model scalability. It is worth remarking that the algorithm based on Bender decomposition pretends to reduce the information provided by the agents to the CM rather than reduce the computational time from the centralized model. However, the following assessment measures the cost of reducing the shared information in terms of execution time.

Fig 5.5 shows the algorithm convergence for different amounts of agents participating in the LEM, considering the optimal value from the centralized model as a reference. Besides, every case indicates the algorithm running time, considering 2

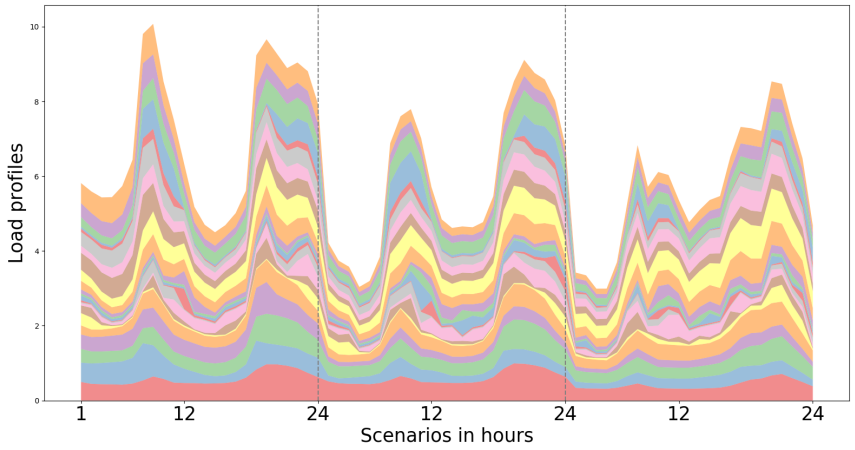

Figure 5.3: Residential load profiles for three different scenarios.

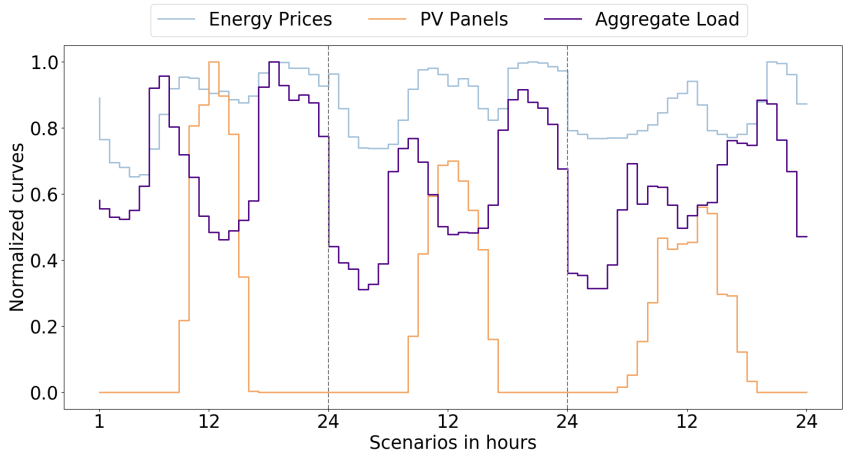

Figure 5.4: Scenarios for the energy prices, the PV power generation, and the aggregated residential loads.

Table 5.2: Average algorithm running times by iteration

Agents number	**3**	**4**	**8**	**16**	**25**	**39**
MP [s]	1.091	1.338	5.265	15.01	38.58	75.29
SP [s]	0.042	0.049	0.098	0.20	0.37	0.67

hours as stop criteria. The execution time for the centralized model is not reported in Fig 5.5, but its time is lower than the algorithm, such that for three agents, the centralized formulation takes 22.8 [s] and 11 [min] for 39 agents. Likewise, considering a maximum running time of two hours, the algorithm converges to the optimal value until 16 agents participate in the LEM. Thus, the algorithm overcomes the maximum running time when the number of agents beats this value.

The average execution time involved at every iteration for the MP and SPs is reported in Table 5.2 to improve the understanding of the significant running time increases when many agents are willing to trade energy in the LEM. Thus, the SPs do not show a significant increase in terms of running time since considering 39 agents, the time required to solve the SPs is, on average lower than one second. However, every MP increases its execution time significantly from 1 [s] to 75 [s] on average when the users' numbers increase. This extra computational burden is explained because the MP includes the technical network constraints and extra constraints added in each iteration of the algorithm due to the Benders cuts.

Therefore, the results show an algorithm based on the Benders cuts that allow reducing the user information shared in LEM, converging to the optimal value given by the centralized model, where the user information is public. In other words, The proposed algorithm reduces information shared between the agents without reducing the community welfare. These results are relevant because the findings reported in [128] for a similar market trading model indicate that the ADMM algorithm is far from the centralized model by 3%. In addition, other alternative mechanisms recently published in the literature like the surrogate Lagrangian relaxation in [130] and an enhanced Benders decomposition in [131] show that these alternative decomposition methods could provide a competitive performance as compared to the one reported by the ADMM under a P2P energy trading framework. In this sense, the convergence results of the algorithm reported in this article are aligned with the recent research.

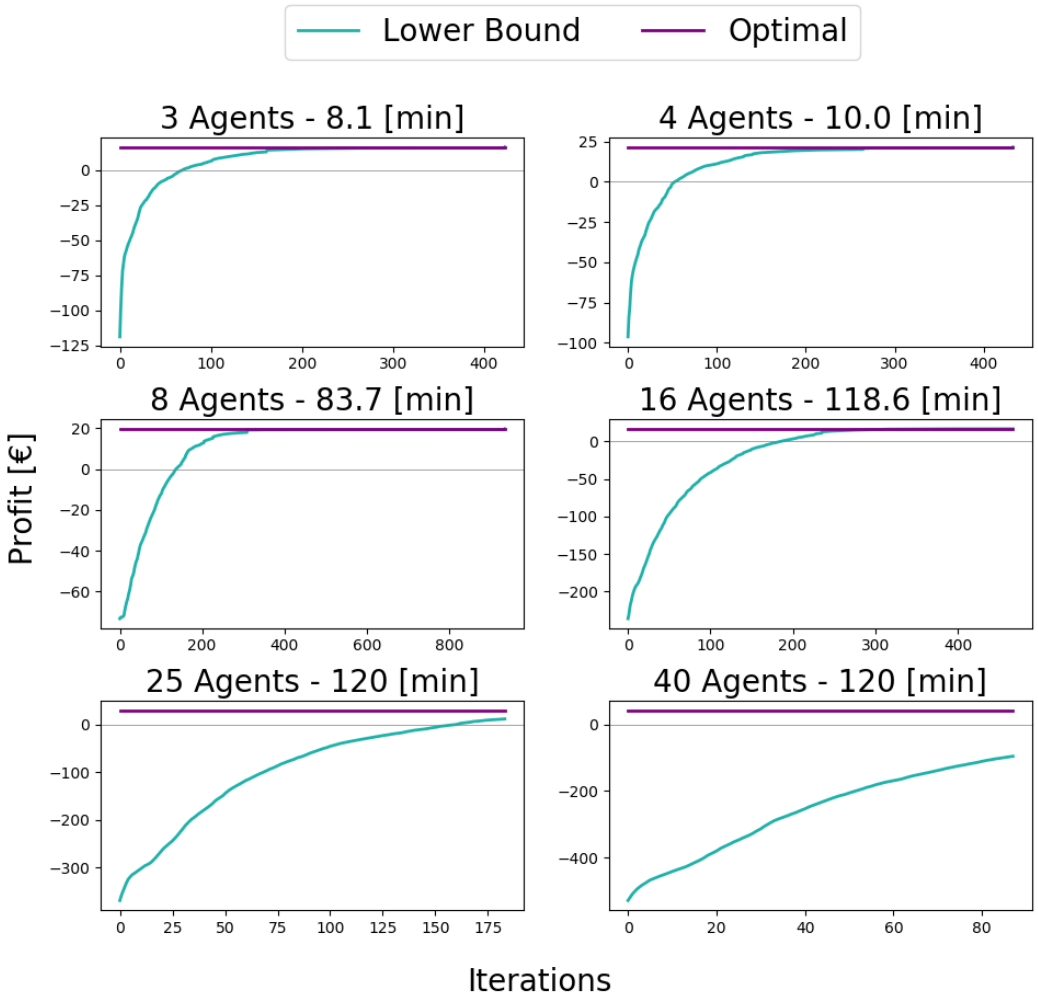

Figure 5.5: Algorithm convergence

5.5.3 Numerical results

This section presents the results considering the scenarios described in the previous section for the thirty-nine agents. Thus, Table 5.3 shows the aggregated results in kWh such that the energy bought and sold to the grid is the same for the three cases due to are the first-stage variables, which are minimized in the objective function. The second-stage variables corresponding to the battery behavior and the energy traded in the LEM show a lower battery and energy traded share in the first scenario than the others because the first one is the most demanding. The remaining two scenarios have higher battery participation and more energy traded in the LEM because the batteries must absorb or inject the surpluses energy committed to buying/selling to the grid in the first stage, which is also traded in the market.

Table 5.3: Global energy share for the three different scenarios

	Variable	Scn 1	Scn 2	Scn 3
Electricity Load	PL	991.981	842.233	807.511
PV generation	pg	872.11	770.22	733.28
BT discharge	ds	338.35	539.56	518.54
BT charge	ch	274.68	523.88	499.51
Energy bought to the grid	κ^{bg}	431.73	431.73	431.73
Energy sold to the grid	κ^{sg}	375.52	375.52	375.52
Energy traded in the LEM	p^{bm}	331.2	427.2	341.2

5.5.4 Model assessment under different assumptions

Four cases have been considered to visualize the P2P energy trading operation effects on the traditional scheme without trading. Specifically, case (A) corresponds to the DN operating under a P2P energy trading scheme. Case (B) is the same DN, but without energy trading, i.e., the prosumers sell their energy surplus to the primary grid, and the traditional consumer must buy all their demand to the external grid. Case (C) is similar to Case (A), but the battery can charge or discharge simultaneously through linear variables. Case (D) is based on (A), but there are no binary variables in this case, which means that the agents can sell/buy energy in the LEM or to the grid without first meeting their own consumption, and the battery can charge/discharge simultaneously. Thus, cases (C) and (D) aim to observe the distortion produced over the energy traded in the LEM when the binary variables are not included in the formulation, while the main goal between cases (A) and (B) is to quantify the improvements produces of operating under a P2P energy trading scheme.

Fig. 5.6 summarizes the results for the four cases for the three scenarios. Case (D) provides the most prominent results with energy traded in the LEM around 87% and 13% of the energy provided by the grid and a small energy share corresponding to self-consumption for the first and second scenarios. The absence of binary variables explains this irregular share compared with the other cases because there is no control to distinguish the energy to satisfy the load consumption and the energy traded in the LEM. After all, the agents are not restricted to meeting their electricity demand first to sell the energy surplus. Case (C), on the contrary of case (D), the energy traded in the LEM is on average 29% lower than case (A). This reduction is because the batteries take values between [0,1], decreasing the power injected/absorbed by

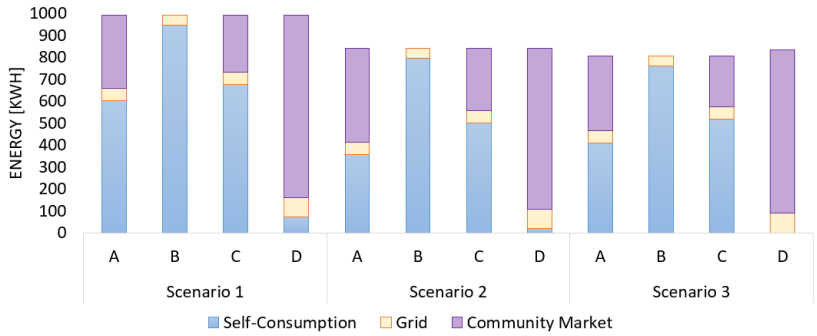

Figure 5.6: Energy share for a case (A) under a P2P energy trading scheme, (B) without Energy trading, (C) considering energy trading but linear batteries, and (D) Energy trading such as batteries and the market trading are linear variables.

the storage devices in this quantity and reducing their energy sharing from the total. Therefore, the improper use of the binary variables can significantly affect the energy amount traded in the local market, undervaluing or overestimating its real operation.

The results for case (B) do not directly impact the main grid dependence due to the high DERs penetration on the case study, but it does affect the community welfare. The community benefits of operating under a P2P energy trading scheme are discussed in detail later; however, it is worth stressing that the energy required from the grid decreased 21.2% regarding case (A), explained mainly with more energy bought in the cheapest hours and more energy trading in the highest hours compared with case (B).

5.5.5 Local energy market and batteries behavior

Fig. 5.7 provides a more detailed battery and market behavior by hours and scenarios. Specifically, the left-hand side shows every scenario's hourly aggregated charging and discharging battery process. As mentioned previously, the first scenario is the most demanding; therefore, the battery uses only in hours with high PV generation and high electricity prices. However, in the second and third scenarios, the batteries must provide the required flexibility to face the remaining energy bought to the grid because, in these scenarios, the load is lower than in the first case.

The right-hand side of Fig. 5.7 shows the hourly energy share from the grid, local market, and self-consumption. The positive grid values correspond to the power provided by the external grid, and the negative values, to the power sold to the grid. Likewise, the self-consumption concept includes the power generated by the PV systems and the power provided by the BSS. Thus, when the self-consumption takes

Figure 5.7: Hourly market and battery behaviour

negative values, it indicates more power charging the batteries than the generated by the PV systems.

For the three scenarios, the highest self-consumption corresponds to the hours with high PV generation, coinciding with the highest power sold to the grid. Besides, the LEM tends to occur during PV generation and the last day hours when the batteries start discharging because the electricity price is higher than the first hours.

5.5.6 Local energy market pricing

Fig. 5.8 shows the LEM pricing for the third scenario obtained from the dual variables corresponding to the nodal balance equations (5.2). Thus, when agents do not have enough self-generation, the LEM price is almost equal to the energy from the grid. On the contrary, when the users have a high energy surplus, the LEM price equals the Feed-in tariff (FIT) option. However, when few agents have the energy capacity to trade in the LEM, the internal price is intermediate between the FIT and the grid price. Similar behavior occurs in the first and the second scenario.

5.5.7 Agents profits

The results of cases A (with energy trading) and B (without energy trading, only energy selling to the grid) have been contrasted to compare the agents' profits. The upper row of Fig. 5.9 shows the profit/cost value for every agent considering the three scenarios, where the orange line corresponds to case A, and the blue line represents

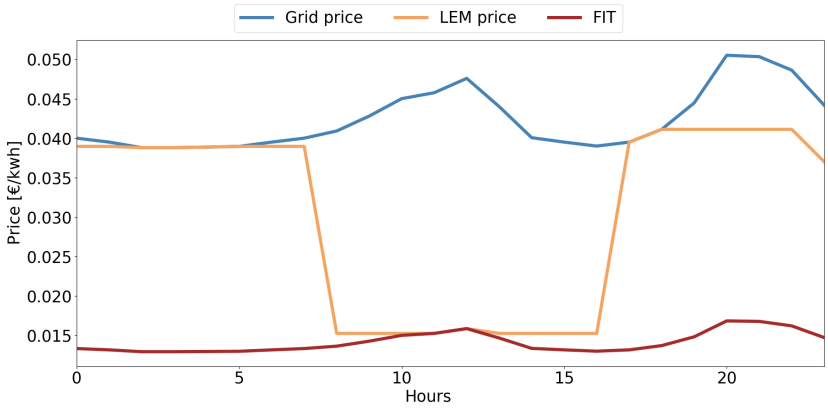

Figure 5.8: Local energy market pricing compared with the FIT and the grid price, corresponding to the third scenario

Case B. On the other hand, the lower row shows the net profit for every agent, which is the difference between the orange with the blue line.

The community welfare shows a slight increase when the agents are capable of trading energy. Specifically, in the first scenario, the benefits increase 17.7%, in the second scenario 18.2%, and 18.6% if the third scenario happens. However, some agents have a higher cost (negative values in Fig.5.9) when they trade energy than when they sell their surplus to the grid. This situation is explained because the model minimizes the total energy bought from the grid and does not maximize the individual profit. Specifically, since the market is modeled under a two-stage stochastic framework, some users with high battery capacity must use their storage to buy (absorb) the extra energy committed in the first stage variables, generating a minimal extra cost (see second row Fig. 5.9).

It is worth noting that the individual profit analysis described above corresponds to a daily operational comparison between operating under a P2P energy trading scheme and not. i.e., the study is not an economic assessment of the long-term profitability of the P2P energy trading scheme. That economic assessment requires a separate researcher, and hence it is out of the scope of the bender decomposition algorithm proposed in this thesis.

5.5.8 Future research and discussion

The previous section leaves implicitly introduced the question related to how to reduce the execution time related to the MPs and accelerate the algorithm convergence times. This issue has not been included within this thesis scope because its study

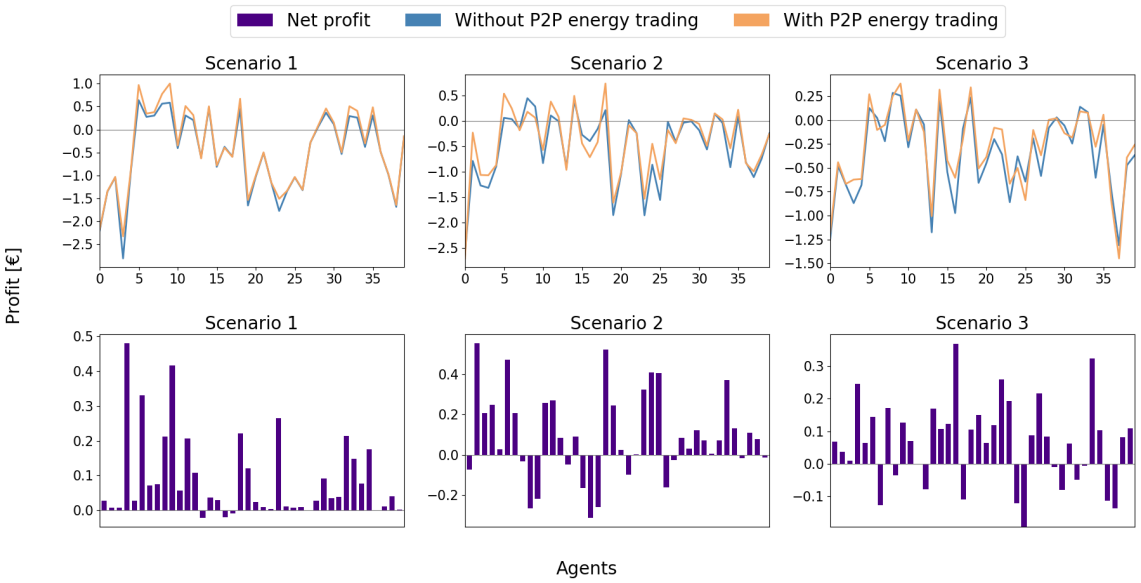

Figure 5.9: Agents profit comparison between using P2P energy trading or not for different scenarios

requires a deep analysis separately. However, the baseline to compare future algorithm improvements has been established in the previous section.

The two-stage stochastic programming model formulation also could be extended or modified. For example, the formulation could include the reactive power provided by the DERs or measure the reactive power that the energy community could provide to the DSO as an ancillary service. The DSO entirely supply the reactive power in the current formulation; hence, this consideration could significantly improve the model proposed. Likewise, the formulation could be extended to include the intraday market within the second stage variables and use the electric vehicles or demand response from the users to face the mismatches between the day-ahead and intraday market. Besides, the second-order cone programming approach could be implemented to address the non-linearities and non-convexity related to the network technical constraints and contrast the running times with the model proposed in this section.

In addition, the objective function presented in the formulation considers only first-stage variables related to the total energy bought/sold from/to the grid. However, the results show that the individual profit is sometimes affected when the model is under a two-stage approach because the agents with higher flexibility must absorb the energy surplus bought to the grid when the uncertainty disappears. Therefore, future works could include part of the individual cost to mitigate these events and avoid disincentives to trade energy in the LEM by users with high flexibility levels.

5.6 Chapter conclusions

This chapter proposes a two-stage stochastic programming model to represent an energy community operating in a day-ahead market under a P2P energy trading scheme. The benders decomposition method has been used to reduce the information provided by the users to operate in the LEM. A new family cut has been introduced in the decomposition method to manage the binary variables related to users' simultaneous energy buying/selling and battery operations presented in the SPs, which prevent the classic Bender implementation.

The 69-bus system has been used to contrast the model with the Benders algorithm considering from 3 to 39 agents trading energy under three scenarios of 24 hours, showing that the proposed decomposition method using the new Strengthened Benders cuts converge to the same optimal value provided by the model which follows a centralized market design. i.e., the proposed methodology reduces the LEM's shared information without increasing the energy community cost. Besides, the non-use of binary variables to model the battery behavior or prevent the selling/buying energy simultaneously in the LEM underestimates or overestimates the energy traded in the community market, respectively.

Chapter 6

A stochastic model to measure the reactive power supplied by DERs under a P2P energy trading scheme

6.1 Introduction

The electricity market deregulation to promote the deployment of DERs at the distribution level has opened new consumer-centric market opportunities where prosumers can be part of the daily market operation through transactive energy (TE) schemes. The benefits provided by a high DERs penetration in DN have been widely studied over the last few years [156], focusing mainly on the active power provided by these resources. However, The DERs' capability to provide reactive power through smart inverters opens a new benefit dimension associated with the AS that an energy community could provide to the distribution system operator DSO.

Traditionally, the network stability and the power quality are managed at the transmission level through large synchronous generators [157]. However, with the small-scale DERs emergence at a local level, some control mechanisms, as local AS offered by local energy communities, could be translated to the DN to increase the efficiency of the transmission system and reduce the cost of the DSO. Thus, the ASs provided by a local energy community with high DERs penetration could support the balancing market through demand/generation management and could even provide frequency regulation and local reactive power control for voltage stability [158]. Besides, they could reduce line losses, increase available line capacity and allow higher peak electrical load [159].

P2P energy trading arises as a solution for a LEM where prosumers and consumers are willing to trade energy to minimize the individual or the community cost (resp. maximize welfare). The community market operation to allow energy trading and how the users' information is managed have been the focus of research in the last few years, leading to three different schemes. The first design corresponds to a centralized market fully controlled by a CM or coordinator who decides the energy exchanges to maximize the community's social welfare. On the other hand, in the decentralized scheme, the users have complete control of their information, and they decide when and how much to sell/buy. The distributed design mix the two above, and the CM suggests the system's pricing and control and the users control their information [160].

This chapter follows the P2P energy trading research line mentioned above through a centralized market-based stochastic model to simultaneously study the energy trading and the reactive power potential supplied by the DERs as ASs to the DSO, considering the day-ahead and intraday markets. Besides, the two-stage stochastic formulation proposed contributes to filling the current research gap of P2P energy trading under uncertainty since most articles manage energy trading using deterministic approaches.

The chapter structure is summarized as follows. Section 6.2 presents the literature review, the research gap, and the main chapter contributions. Section 6.3 describes the community framework, the markets addressed in the chapter, and the proposed model assumptions, to then presents the stochastic model in Section 6.4. The case study and the computational results are presented in Section 6.5, and the conclusions are discussed in Section 6.6.

6.2 Literature review

This section contains a literature review of the P2P energy trading models based on optimization techniques and articles that consider the reactive power provision, not necessarily under a transaction energy scheme. In this regard, the literature review is summarized in Table 6.1 to identify the relevant works with the model proposed in this chapter and the gaps in the literature.

A broad interest in addressing P2P energy trading from different approaches has been reported in the literature in the last few years; however, few articles have addressed the topic from a stochastic programming-based perspective. For instance, the authors in [122] present a two-stage robust optimization model to address uncertainties in a day-ahead and real-time spot market using the Benders decomposition

Table 6.1: Mathematical formulations for the reactive power provided by DERs

Ref	Nature	Objective Function	Type Optimization problem	Technique	Market structure	Market Type	Privacy	Market clearing methods	Tech. limit	Q	BSS	Test system
[161]	Deterministic	Max prosumers welfare	MINLP	Algorithm	Decentralized.	Day-ahead	✓	ADMM	✓	✓	Linear	IEEE-33
[162]	Deterministic	Max utility function	Game-theoretic	Algorithm	Decentralized	Day-ahead	✓	Price-updating strategy	×	✓	×	Individual agents
[163]	Deterministic	Min cost and line losses	MINLP	SOCP	-	-	×	Optimization	✓	✓	×	IEEE-123
[164]	Deterministic	Max prosumers welfare	Linear	Solver	Centralized	Balancing and AS Market	×	Given	×	✓	×	Simulink
[107]	Deterministic	Max prosumers welfare	MINLP	SOCP	Decentralized	Real-time market	✓	ADMM	✓	✓	×	144 Bus System
[165]	Deterministic	Min losses	LP	Methaheuristic algorithm	Centralized	Day-ahead	×	Given	✓	✓	×	MV Distribution System
[166]	Deterministic	Max reactive power	MINLP	Benders Decomposition	Centralized	Day-ahead	×	Algorithm	✓	✓	×	IEEE-33
[167]	Deterministic	Min MG cost	MINLP	GA	Centralized	×	×	×	×	✓	Binary	MG
[168]	Deterministic	Min MG cost	MINLP	Simulation	Centralized	×	×	×	✓	✓	Binary	Simulation MG
[169]	Deterministic	Min cost	MINLP	Solver	Centralized	Day-ahead	×	Given	✓	✓	Binary	IEEE 33 69
[98]	Deterministic	Min MG cost	NLP	Interior point algorithm	Centralized	-	×	Algorithm	×	×	Linear	LV Network
[103]	Deterministic	Min MG cost	MILP	Decomposition method	Decentralized	Day-ahead	✓	ADMM	×	×	Binary	Individual agents
[170]	Deterministic	Max the welfare	LP	Decomposition method	Decentralized	-	×	Algorithm	×	×	Linear	Individual agents
[122]	Stochastic	Max profit	Robust optimization	Benders Decomposition	Centralized	Day-ahead and Intraday market	×	Given	×	×	Linear	MG
[171]	Stochastic	Max profit	MINLP	Linearization of binary variables	Centralized	Balancing and AS market	×	Optimization	×	×	Linear	Simulation
[125]	Stochastic	Min cost	MILP	Benders Decomposition	Decentralized	Day-ahead and Intraday market	✓	ADMM	×	×	Linear	Individual agents
[126]	Stochastic	Min social and operation cost	Robust optimization	Decomposition method	Decentralized	Day-ahead and Intraday market	×	ADMM	✓	✓	Linear	IEEE 123

approach to protect the users' information. In the same line, a distributionally robust co-optimization model for the P2P energy trading and network operation of interconnected MGs is presented in [126]. The model considers voltage and reactive power as well as the battery constraints through continuous variables. Likewise, the authors in [125] propose a two-stage stochastic programming problem to manage the day-ahead and intraday market under a P2P energy trading scheme, which preserves the private user information. However, none of the above articles include the capability of DERs to provide reactive power in the formulation.

On the other hand, the work done by [170] proposes a deterministic two-stage bidding strategy for P2P trading of nanogrid. The model does not consider the technical constraints and is tested on individual houses only. Likewise, the authors in

[98] propose a deterministic two-stage aggregated control for P2P energy sharing in community MGs, where an energy sharing coordinator controls the batteries allowing simultaneous energy charging/discharging without including network constraints or reactive power. Similarly, a two-stage formulation based on the ADMM is presented by [103] to address an eventual day-ahead market in a P2P energy trading community.

Few articles have started to include the reactive power from DERs to provide AS to DSO. The work developed by [162] proposes a framework where agents/users can trade active and reactive power using the game-theoretical framework (Stackelberg game) to model the tradings under a decentralized scheme and operating in a day-ahead market. However, despite considering the reactive power trading, the formulation does not include batteries, and it is not based on the power flow equations. In [161], a non-convex nonlinear model is proposed to address a P2P energy trading framework in a DN considering the network technical limitation and maintaining the users' information private. The model operates for a day-ahead market, decomposing the problem into two nodal agent and prosumer problems and using the ADMM to clear the market, which considers the batteries as a linear formulation allowing its simultaneous charging and discharging process. In [163], a reactive power market at the distribution level is proposed through a MINLP based on the optimal power flow equations. The model is tested in a New England case study to minimize the line losses and total costs, where the DGs participating in the market can increase their revenues. However, the article in [163] focuses on modeling a reactive power market at the distribution level rather than modeling a P2P energy trading providing reactive power as ASs.

Additionally, the work done by [164] presents multi-market nanogrids based on the P2P energy trading scheme, which provides ASs such as balancing and frequency regulation. The deterministic and linear formulation considers the reactive power but does not use the power flow equations as a base. On the contrary, the article developed by [171] proposes a MILP to model the aggregator operation in an ASs market using a stochastic approach. The formulation includes only the balancing services through a load and generation modification, excluding the reactive power and the technical constraints, and considering the BESS as a linear formulation under a centralized market. In [107], a collaborative market design is proposed to address the ASs provided by prosumers under a P2P energy trading architecture. The formulation operates in a real-time market considering a fully distributed peer-centric market-clearing and the network technical limitations. The ADMM method is used to clear

the market and maximize the prosumer welfare. In addition, the formulation does not consider storage devices that simplify the problem complexity.

Other researchers have addressed the active/reactive power dispatched from DERs, but not under a P2P energy trading scheme or from a reactive power market perspective. For instance, [169] presents a deterministic approach based on the power flow equations to model the active and reactive power dispatched by batteries considering voltage source converters for a day-ahead market. In [166], a deterministic MINLP is presented to model the DERs based on synchronous generation in a reactive power market. The formulation uses the Benders decomposition method to divide the model into a master problem, which determinates the total payments, and subproblems, that indicate the solution feasibility provided by the master problem. However, the formulation proposed in [166] does not consider storage devices, nor P2P energy trading schemes.

In addition, the work developed by [167] presents a model for the active-reactive power dispatch of PV-battery hybrid systems based on an economic model predictive controller (EMPC) considering the battery life in the formulation, which concludes that providing reactive power locally is more cost-effective than importing it from the main grid, and the PV-inverter can generate reactive power at a meager cost than the battery inverter. However, the formulation does not operate under a P2P scheme, and the technical constraints are not included. Likewise, the article [168] proposed an MINLP for the optimal control scheme based on MPC considering PV-battery hybrid systems, including network technical limitations, but do not operate under a transactive energy scheme. Work in [165] proposes an optimal-centralized control formulation for a microgrid's day-ahead operation with power-electronic converters that can offer reactive power services to DSO, minimizing the energy losses and managing the voltage level within the operational limits.

The literature review shows increasing attention regarding P2P energy trading designs to improve the DN efficiency, reduce the operational cost and increase the users' participation in the electricity markets. Nevertheless, few articles have studied the potential economic and operational benefits derived from the DERs' capability to provide reactive power through smart-inverters. In this regard, different approaches have been implemented, considering either aggregators or TE schemes under an eventual reactive market at the distribution level. However, most formulations are based on a deterministic approach and do not consider the two-stage stochastic programming framework to address the day-ahead and intraday market.

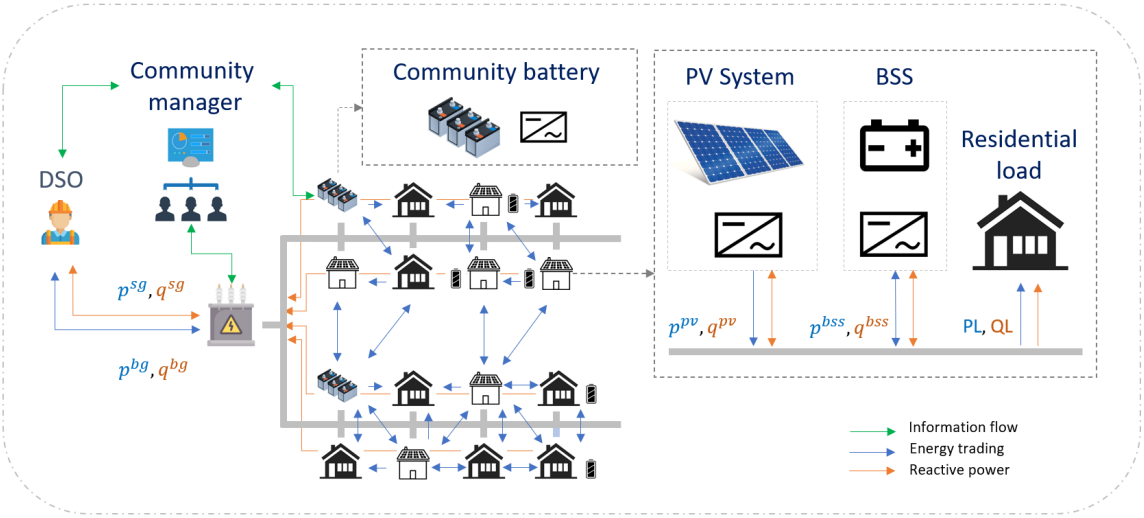

Figure 6.1: P2P energy trading scheme considering community battery bank and reactive power

In fact, from the deterministic perspective, the works presented by [166], [162], and [161] are close to what is proposed in this chapter. However, they do not consider batteries or, if it is included, are modeled through non-binary variables allowing the simultaneous charging and discharging, which may imply unrealistic solutions. On the contrary, the few articles that address the problem described from a stochastic perspective [122, 171, 125, 126] also consider battery through linear formulation and [122, 171, 125] do not include the reactive power and the technical network constraints (detail in Table 6.1).

6.3 System description

This section explains the market composition modeled through the two-stage stochastic programming approach. Specifically, the components required by the energy community are established to identify the first and second-stage variables in order to visualize the reactive power capability provided by the DERs under different active power generation scenarios.

6.3.1 Two-stage stochastic programming approach

The two-stage stochastic programming is defined by [172] as a versatile modeling tool for decision-making under uncertainty. In the first stage, decisions "here-and-now" must be made when some parameters are random. When the uncertain parameters

are revealed, the second-stage variables are decided to minimize the expected total cost or maximize the profit. Thus, for uncertainty parameters like the users' load consumption or the power generated by the PV systems, some decisions regarding the total reactive power provided by the DERs and the energy bought/sold from/to the grid must be taken without knowing the final consumption/generation. These decisions represent the first stage variables and, in this chapter, are related to the day-ahead market. On the other hand, the second-stage variables represent the decisions once the uncertainty is realised, in this case, corresponding to the real-time market operation, and they are represented by the energy traded in the LEM and the battery behavior.

6.3.2 Market framework

The community modeled in this chapter belongs to a centralized P2P energy trading scheme, which comprises prosumers and consumers. Specifically, in this chapter, a prosumer is an agent who possesses a PV and or an energy storage system, which allows them to act as a small generator when the load consumption is lower than the energy self-generated or as a consumer when it has an energy deficit. Likewise, a prosumer can sell (resp. buy) its energy surplus (resp. deficit) to the LEM or the grid, establishing a difference with models that set fixed sellers and buyers groups.

This chapter uses two centralized collaborative frameworks to study the P2P energy trading and the reactive power provided by the system while the total community cost is minimized. The first one corresponds to the traditional energy community integrated by prosumers, consumers, and a CM who coordinates the energy and the information between the agents and the DSO. Besides, the CM determines the energy sold/bought to/from the grid in the day-ahead market and for the intraday market, defines the energy traded in the LEM, the batteries behaviors, and the reactive power provided by the DERs to offer as ASs and keep the local system balanced. The second framework considers the same previous structure but includes community batteries. Adding community storage devices aims to study their effect on the individual profit when the community cost is minimized and explore their potential to provide reactive power as ASs. Fig. 6.1 shows a schematic diagram of an energy community composed of consumers, prosumers, and community batteries trading active power and providing reactive power to the DSO.

It is worth noting that when community welfare is studied, the individual benefit may be affected for the sake of the global benefit. Specifically, under a two-stage stochastic framework and considering the total energy sold/bought to/from the grid

as first-stage variables, the users with high storage capacity (high flexibility) must face the uncertainty of the second-stage variables (intraday market) absorbing or injecting the required energy to meet the energy compromised in the day-ahead market. This extra energy absorbed or injected could affect its benefit because it would be absorbing (resp. injected) more energy than the individual requirement. Therefore, a framework with community batteries could reduce the adverse effects over the agents with high ESS capacity. Nevertheless, the extra energy absorbed (resp. injected) by agents with high BESS capacity to face the intraday market is differentiated into two additional frameworks. Thus, the community services offered by these agents can be quantified for eventual economic compensation.

Fig. 6.2 summarizes schematically the four frameworks addressed in this paper. The A and B structures correspond to the main two frameworks regarding an energy community trading energy without and with community battery. Under this scheme, the flexibility provided by the agents' batteries is not detected. Therefore, some users see their cost function reduced because they must absorb (resp. inject) additional energy to face the uncertainty of the community electricity consumption. Thus, with the end to identify the extra energy managed by these users, the frameworks A' and B' are presented.

6.3.3 Pricing

The authors in [173] present a review regarding the reactive power pricing in a power market for transmission and distribution level addressing the methods based on the lost opportunity cost (LOC) and the OPF mostly. The price used in the LOC-based method depends on the power factor (PF) operational range, which usually is defined as 0.95. Thus, a penalty cost associated with the active power not being provided is included in the objective function outside of this range. However, in a power system with high DERs penetration and a constantly changing PF, this mechanism does not seem to be suitable [163]. The second alternative simultaneously determines the reactive and active marginal price through the power flow equations. This method considers the Lagrange multipliers corresponding to the active and reactive power nodal constraints to identify the marginal cost to maintain the network balance respecting the voltage levels [140, 141], which is the mechanism used in this chapter.

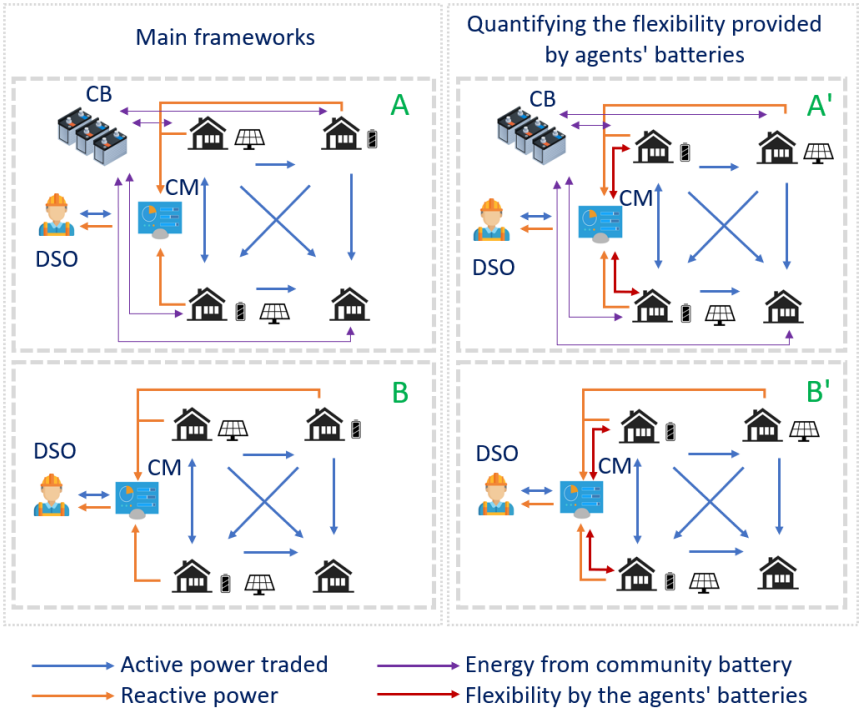

Figure 6.2: P2P energy trading frameworks. A: P2P energy trading with CB, B: P2P energy trading without CB, A': P2P energy trading with CB and detecting the flexibility provided by the agents' batteries, and B': P2P energy trading detecting the flexibility provided by the agents' batteries.

6.3.4 Assumptions

A P2P energy trading architecture includes between six [174], or four [175] layers for proper implementation. These layers comprise the grid infrastructure, participants in the LEM, and the communication and control systems. The model proposed in this article assumes that the money transaction is safe, and the DN contains the monitors required to read the generation and the electricity demand in real-time. Thus, the formulation focuses on allowing the energy traded between agents belonging to a LEM, quantifying the eventual reactive power provided by the DERs to the DSO for different scenarios, and maintaining the technical constraints in the operational limits. Likewise, the ASs covered by the model includes reactive power service provided from DERs based on smart-inverters to the DSO and the increase/decrease demand/generation from the prosumers and DERs.

6.4 Mathematical formulation

The two-stage stochastic mixed-integer second-order conic programming (MISOCP) P2P energy trading model presented in this section minimizes the total energy community cost considering i) the day-ahead and intraday markets, ii) the self-generation and load consumption as uncertainty parameters, iii) the active power traded between agents, iv) the reactive power provided by DERs as ASs and for internal network stability, v) different battery constraints for community batteries and to detect the flexibility provided by the agents' batteries to face the intraday market, and vi) the network technical limitation. Therefore, the objective function is defined as follows:

$$minimize \;\; z = \sum_{t\in\mathcal{T}} \sum_{s\in\mathcal{S}} \rho_s(\lambda^{bg}_{t,s} p\kappa^{bg}_t - \lambda^{sg}_{t,s} p\kappa^{sg}_t - \lambda^{as}_{t,s} q\kappa^{as}_t). \tag{6.1}$$

Eq. (6.1) minimizes the total energy community cost, including the active power bought ($p\kappa^{bg}$) and sold ($p\kappa^{sg}$) to the grid and the reactive power ($q\kappa^{as}$) that the energy community can offer to the main grid as an AS. It is worth remarking that the variables involved in the objective function correspond to first-stage variable decisions, which implies that the uncertainty is represented through the occurrence probability (ρ_s) of every scenario s, such that $\rho_s \in [0, 1]$ is the likelihood of occurrence of the scenario $s \in S$ with $\sum_{s\in S} \rho_s = 1$. Likewise, the pricing related to the electricity provided by the grid, the feed-in tariff price, and the economic compensation of providing reactive power to the DSO is represented respectively by $\lambda^{bg}_{t,s}$, $\lambda^{sg}_{t,s}$, and $\lambda^{as}_{t,s}$.

6.4.1 Local energy market constraints

The objective function presented previously is subject to the following market limitations. Therefore; $\forall i \in \mathcal{A}, \forall t \in \mathcal{T}, \forall s \in \mathcal{S}$

$$\Delta p_{i,t,s} = pg_{i,t,s} + ds_{i,t,s} - ch_{i,t,s} - PL_{i,t,s}, \tag{6.2a}$$
$$\Delta q_{i,t,s} = qg_{i,t,s} + qds_{i,t,s} - QL_{i,t,s}, \tag{6.2b}$$
$$\Delta p_{i,t,s} = \Delta p^{+}_{i,t,s} + \Delta p^{-}_{i,t,s}, \tag{6.2c}$$
$$\Delta p^{+}_{i,t,s} = p^{sm}_{i,t,s} + p^{sg}_{i,t,s} + ch^{cb'}_{i,t,s}, \tag{6.2d}$$
$$\Delta p^{-}_{i,t,s} = p^{bm}_{i,t,s} + p^{bg}_{i,t,s} - ds^{cb'}_{i,t,s}, \tag{6.2e}$$
$$\Delta p^{+}_{i,t,s} \leq M(y_{i,t,s}), \tag{6.2f}$$
$$\Delta p^{-}_{i,t,s} \geq M(y_{i,t,s} - 1), \tag{6.2g}$$
$$\Delta p^{-}_{i,t,s}, p^{bm}_{i,t,s} \leq 0; \quad \Delta p^{+}_{i,t,s}, p^{sg}_{i,t,s}, p^{sm}_{i,t,s}, p^{bg}_{i,t,s} \geq 0, \tag{6.2h}$$

The previous equations (6.2) establish the market rules for the agents who trade energy in the LEM. Thus, Eqs. (6.2a) and (6.2b) defines Δp and Δq respectively, which represent the difference between the load consumption and the active or reactive power self-generated, including the power provided by the PV panels and the BSS. On the other hand, Δp is also defined in Eq. (6.2c) as a positive or negative value, indicating that an agent can have a surplus or deficit of energy, respectively. If there is an energy surplus, the agents must sell their surplus to the LEM, to the grid, or store it in the battery as indicated Eq. (6.2d). In the opposite case, if the agents have a deficit, the energy must come from the LEM, the grid, or the battery (6.2e). Besides, to prevent simultaneous selling/buying by the agents in the LEM and/or the gird, the binary variables are defined in Eqs. (6.2f) and (6.2g). Thus, when y takes positive values, the agent has an energy surplus; otherwise, it takes value zero.

Once defined, the individual agent's behavior corresponds to defining the global market constraints and identifying the energy traded in the LEM, the energy bought/sold to the grid, and the reactive power capability provided by the agents to the DSO through the following constraints. Therefore; $\forall t \in \mathcal{T}, \forall s \in \mathcal{S}$

$$\sum_{i \in \mathcal{A}} p^{sm}_{i,t,s} + \sum_{i \in \mathcal{A}} p^{bm}_{i,t,s} = 0, \tag{6.3a}$$

$$\sum_{i \in \mathcal{A}} p^{sg}_{i,t,s} \geq p\kappa^{sg}_{t}, \tag{6.3b}$$

$$\sum_{i \in \mathcal{A}} -p^{bg}_{i,t,s} \leq p\kappa^{bg}_{t}, \tag{6.3c}$$

$$q\kappa^{as}_{t} \leq \sum_{i \in \mathcal{A}} \Delta q_{i,t,s} + \sum_{i \in \mathcal{C}} q ds^{cb}_{i,t,s}. \tag{6.3d}$$

Eq. (6.3a) represents the local market balance constraints such that all the energy sold in the LEM is bought. Eq. (6.3b) indicates that the sum of the energy sold to the grid by agents must be greater or equal to the total energy exported through the substation ($p\kappa^{sg}$). Likewise, Eq. (6.3c) represents the same situation but for the energy bought from the grid. It is worth noting that these terms are not necessarily equal due to the line losses. Eq. (6.3d) identifies the reactive power provided through the substation ($q\kappa^{as}$) by the agents and the community battery.

6.4.2 Agents battery modeling

The following set of constraints models the battery behavior. Therefore; $\forall i \in \mathcal{A}, \forall t \in \mathcal{T}, \forall s \in \mathcal{S}$:

$$soc_{i,t+1,s} = soc_{i,t,s} + [\varphi^{ch}\varphi^{bss}ch_{i,t,s} - \frac{1}{\varphi^{ds}\varphi^{bss}}ds_{i,t,s}]\Delta t, \tag{6.4a}$$

$$SOC^{min}BT_i \leq soc_{i,t,s} \leq SOC^{max}BT_i, \tag{6.4b}$$

$$ch_{i,t,s} \leq PB(w_{i,t,s}), \tag{6.4c}$$

$$ds_{i,t,s} \leq PB(1 - w_{i,t,s}), \tag{6.4d}$$

$$(ds_{i,t,s})^2 + (qds_{i,t,s})^2 \leq (\gamma_i^{bss})^2, \tag{6.4e}$$

$$(ch_{i,t,s})^2 + (qds_{i,t,s})^2 \leq (\gamma_i^{bss})^2. \tag{6.4f}$$

Eq. (6.4a) represents the battery SOC for the next period, which depends on the current SOC plus (resp. minus) the energy-charged (resp. discharged) as appropriate. Eq. (6.4b) establishes the operational range of the battery multiplied by its installed capacity. Note that if an agent does not have a battery, its energy storage capacity is zero, forcing the other battery variables to zero. The formulation uses a binary variable to model the charge and discharge battery process because both actions cannot be executed simultaneously. Thus, Eq. (6.4c) represents the charging process, and Eq. (6.4d) the battery discharge. Eqs. (6.4e) and (6.4f) indicate the reactive power capability provided by the batteries in the discharging and charging processess.

6.4.3 Community battery modeling

The constraints related to the community battery operation are similar to the agent batteries with two additional restrictions. Therefore; $\forall i \in \mathcal{A}, \forall t \in \mathcal{T}, \forall s \in \mathcal{S}$,

$$soc^{cb}_{i,t+1,s} = soc^{cb}_{i,t,s} + [\varphi^{ch}\varphi^{bss}ch^{cb}_{i,t,s} - \frac{1}{\varphi^{ds}\varphi^{bss}}ds^{cb}_{i,t,s}]\Delta t, \tag{6.5a}$$

$$SOC^{min}BT_i^{cb} \leq soc_{i,t,s} \leq SOC^{max}BT_i^{cb}, \tag{6.5b}$$

$$ch^{cb}_{i,t,s} \leq PB^{cb}(w^{cb}_{i,t,s}), \tag{6.5c}$$

$$ds^{cb}_{i,t,s} \leq PB^{cb}(1 - w^{cb}_{i,t,s}), \tag{6.5d}$$

$$(ds^{cb}_{i,t,s})^2 + (qds^{cb}_{i,t,s})^2 \leq (\gamma_i^{cbss})^2, \tag{6.5e}$$

$$(ch^{cb}_{i,t,s})^2 + (qds^{cb}_{i,t,s})^2 \leq (\gamma_i^{cbss})^2, \tag{6.5f}$$

$$\sum_{i \in \mathcal{A}} ds^{cb'}_{i,t,s} \geq \sum_{i \in \mathcal{A}} ds^{cb}_{i,t,s}, \tag{6.5g}$$

$$\sum_{i \in \mathcal{A}} ch^{cb'}_{i,t,s} \leq \sum_{i \in \mathcal{A}} ch^{cb}_{i,t,s}. \tag{6.5h}$$

Eq. (6.5g) represents that the total energy discharged from the community battery must be greater or equal to the energy delivered to the agents, and Eq. (6.5h) indicates the total energy absorbed by the community battery must be less or equal to the energy provided by the agents.

6.4.4 Battery flexibility detection

Two continuous variables must be included in the battery formulation to separate the energy used by agents for self-consumption and the energy to face the community electricity load uncertainty. Therefore; $\forall i \in \mathcal{A}, \forall t \in \mathcal{T}, \forall s \in \mathcal{S}$:

$$soc_{i,t+1,s} = soc_{i,t,s} + [\varphi^{ch}\varphi^{bss}(ch_{i,t,s} + \Delta ch_{i,t,s}) - \frac{1}{\varphi^{ds}\varphi^{bss}}(ds_{i,t,s} + \Delta ds_{i,t,s})]\Delta t, \tag{6.6a}$$

$$SOC^{min}BT_i \leq soc_{i,t,s} \leq SOC^{max}BT_i, \tag{6.6b}$$

$$ch_{i,t,s} + \Delta ch_{i,t,s} \leq PB(w_{i,t,s}), \tag{6.6c}$$

$$ds_{i,t,s} + \Delta ds_{i,t,s} \leq PB(1 - w_{i,t,s}), \tag{6.6d}$$

$$(ds_{i,t,s} + \Delta ds_{i,t,s})^2 + (qds_{i,t,s})^2 \leq (\gamma_i^{bss})^2, \tag{6.6e}$$

$$(ch_{i,t,s} + \Delta ch_{i,t,s})^2 + (qds_{i,t,s})^2 \leq (\gamma_i^{bss})^2. \tag{6.6f}$$

The set of equations (6.6) represents the same operations as (6.4), with the only difference that the charging and discharging battery process identify the flexibility provided for the energy community through (Δch) and (Δds), respectively. However, when the flexibility variables are considered in the model, Eqs. (5.9a) and (5.9b) must be rewritten as follows:

$$\sum_{i \in \mathcal{A}} p_{i,t,s}^{sg} + \sum_{i \in \mathcal{A}} \Delta ds_{i,t,s} \geq p\kappa_t^{sg}, \tag{6.7a}$$

$$\sum_{i \in \mathcal{A}} -p_{i,t,s}^{bg} + \sum_{i \in \mathcal{A}} \Delta ch_{i,t,s} \leq p\kappa_t^{bg}, \tag{6.7b}$$

6.4.5 Network technical limitation

The second-order cone relaxation for the AC OPF problem is used to model the network constraints. Therefore; $\forall t \in \mathcal{T}, \forall s \in \mathcal{S}$

$$\sum_{(i,j) \in \mathcal{L}} p_{t,s}^{i,j} - \sum_{(j,i) \in \mathcal{L}} (p_{t,s}^{j,i} - R_{j,i} l_{j,i}) = \begin{cases} \Delta p_{i,t,s} & \forall i \in \mathcal{A}, \\ ds_{i,t,s}^{cb} - ch_{i,t,s}^{cb} & \forall i \in \mathcal{C}, \\ p\kappa_t^{bg} - p\kappa_t^{as} & \text{Sub}, \end{cases} \tag{6.8}$$

$$\sum_{(i,j)\in\mathcal{L}} q_{t,s}^{i,j} - \sum_{(j,i)\in\mathcal{L}} (q_{t,s}^{j,i} - X_{j,i} l_{j,i}) = \begin{cases} \Delta q_{i,t,s} & \forall i \in \mathcal{A}, \\ q ds_{i,t,s}^{cb} & \forall i \in \mathcal{C}, \\ -q\kappa_t^{sg} & \text{Sub}, \end{cases} \tag{6.9}$$

$$v_{j,t,s} = v_{i,t,s} - 2(R_{i,j} p_{t,s}^{i,j} + X_{i,j} q_{t,s}^{i,j}) + (R_{i,j}^2 + X_{i,j}^2) l_{i,j}, \tag{6.10}$$

$$(p_{t,s}^{i,j})^2 + (q_{t,s}^{i,j})^2 \leq l_{i,j} v_{i,t,s}. \tag{6.11}$$

The active and reactive power balance equations are represented in (6.8) and (6.9), respectively. The right-hand side of both constraints will depend on if the bus possesses a user trading energy in the LEM, a community battery, or is the substation (Sub). Thus, for buses with agents, Eq. (6.8) considers the difference between the power self-generation and the agent load consumption. On the contrary, if the bus has a community battery, Eq. (6.8) only includes the power injected or absorbed by the battery. Likewise, the substation bus controls the total active power entering ($p\kappa^{bg}$) and leaving ($p\kappa^{sg}$) the system. However, in the substation bus, the reactive power in Eq. (6.9) is considered a variable load ($q\kappa^{as}$) to measure the energy community's reactive power capability to provide to the DSO through the DERs. Eq. (6.10) and (6.11) correspond to the classical line power flow equations, which do not present variation. Note that if the model detects the flexibility provided by the agents' batteries, the right-hand side of Eq. (6.8) for buses with agents must include Δch and Δds, because these values are available to the community to be used as appropriate.

The following equations (6.12) bound the voltage, the active and reactive power provided from the PV systems, and the line flow capacity. Thus; $\forall s \in \mathcal{S}, \forall t \in \mathcal{T}$

$$(V^{min})^2 \leq v_{i,t,s} \leq (V^{max})^2 \qquad \forall i \in \mathcal{B}, \tag{6.12a}$$

$$0 \leq pg_{i,t,s} \leq \varphi^{pv} PG_{t,s}^{max} \gamma_i^{pv} \qquad \forall i \in \mathcal{A}, \tag{6.12b}$$

$$(pg_{i,t,s})^2 + (qg_{i,t,s})^2 \leq (\gamma_i^{pv})^2 \qquad \forall i \in \mathcal{A}, \tag{6.12c}$$

$$(p_{t,s}^{i,j})^2 + (q_{t,s}^{i,j})^2 \leq (S_{i,j}^{max})^2 \qquad \forall (i,j) \in \mathcal{L}. \tag{6.12d}$$

6.5 Computational results

In this section, the model presented in Section 6.4 is tested in a modified version of the well-known IEEE 33- bus system, considering the different frameworks explained in Section 6.3.2 under different scenarios. The optimization model has been programmed in Python-Pyomo using Gurobi as the solver in an Intel Core i7 2.3 GHz CPU and 16 GB RAM.

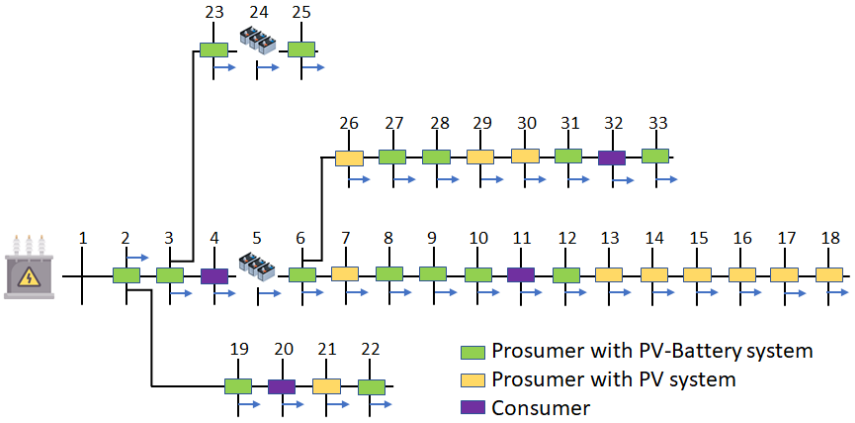

Figure 6.3: Test system

6.5.1 System data

The model proposed in this chapter has been tested in the IEEE 33-bus radial distribution system [176], modifying the maximum active power load and respecting the proportion reactive power load from the original system. Thus, the total active load is 105 kW and 75.6 kVAr, and the lower and upper voltage bound are 0.95 p.u. and 1.05 p.u., respectively. We have considered 22 different load profiles for the 32 electricity demands of the test system, considering three scenarios of 24 hours. In this regard, the load consumption profiles have been obtained from [69] and the weather condition from [70]. Likewise, Table 6.2 shows the DERs location and capacity for every bus, such that 15 prosumers have PV-Battery systems, 11 PV systems, and the remaining buses possess traditional consumers. The total PV capacity installed arises to 136.5 kW, 186 kWh for the agents' batteries, and 200 kWh for the community batteries when they are considered. Because there is currently no reactive power wholesale market, the prices for the reactive power have been assumed as one-sixth of the electricity price provided by the DSO and the FIT price as one-third of the day-ahead market price.

6.5.2 Numerical results

The model has been tested following the frameworks presented in Section 6.3.2 and schematically described in Fig. 6.2. Besides, we have decomposed the models for every framework into three different formulations to measure the energy traded and the ASs effect over the community cost and compare the improvement of the proposed model with the current literature. Thus, Table 6.3 summarizes the formulation testing in

Table 6.2: Load consumption and DERs capacity parameters for the case study

Bus	PL	QL	PV	BT	BT^{cb}	**Bus**	PL	QL	PV	BT	BT^{cb}
2	4	2.97	6	12	0	18	3	2.14	4.5	0	0
3	4	2.88	6	12	0	19	4	2.86	6	12	0
4	4	2.93	0	0	0	20	4	2.86	0	0	0
5	0	0	0	0	100	21	3	2.14	4.5	0	0
6	5	3.59	7.5	15	0	22	3	4.42	4.5	9	0
7	3	2.15	4.5	0	0	23	3	2	4.5	10	0
8	5	3.13	7.5	15	0	24	0	0	0	0	100
9	5	3.44	7.5	15	0	25	4	2.85	6	12	0
10	4	2.64	6	12	0	26	4	2.83	6	0	0
11	3	1.75	0	0	0	27	5	3.54	7.5	15	0
12	2	1.17	3	12	0	28	2	1.67	3	8	0
13	2	1.2	3	0	0	29	2	1.43	3	0	0
14	5	3.55	7.5	0	0	30	4	2.68	6	0	0
15	3	2.1	4.5	0	0	31	2	1.34	3	12	0
16	3	2.14	4.5	0	0	32	3	2.14	0	0	0
17	5	3.57	7.5	0	0	33	2	1.43	3	15	0

Table 6.3: Models addressed in the computational results

	Without energy trading (α)	With energy trading (β)	Energy trading and ASs (γ)
Framework A	αA	βA	γA
Framework B	αB	βB	γB
Framework A'	αA'	βA'	γA'
Framework B'	αB'	βB'	γB'

this section, and Table 6.4 presents the results for every framework with its respective model.

6.5.2.1 Case A and B analysis

The results show significant improvements at every framework when the energy community trades energy and provides ASs. However, before analyzing the objective function result, an improvement point is established as a reference to compare the results obtained by the model proposed with the literature. Thus, the total community cost reduction when the system operates under a P2P energy trading scheme (without ASs consideration) is on average 15.5%. This percentage is obtained by comparing the objective function when the agents do not trade energy (αA) with the models considering energy trading (βA). Likewise, the rate at which the objective function decreases is consistent with the results obtained by [98] and [107]. Specifically, the

Table 6.4: First and second stage variables performance by model

	Objective Function Components				Energy from/to the grid				LEM	Agents' Batteries		Community Batteries		Flexibility service	
Model	OF Cost [€]	$p\kappa^{bg}$ [kWh]	$p\kappa^{bg}$ [kWh]	$q\kappa^{as}$ [kVAr]	p^{bg} [€]	p^{sg} [€]	p^{bg} [kWh]	p^{sg} [kWh]	p^{sm}/p^{bm} [kWh]	ch [kWh]	ds [kWh]	ds^{cb} [kWh]	ch^{cb} [kWh]	Δch [kWh]	Δds [kWh]
αA	16.41	548.01	502.81	0	26.34	9.94	547.99	502.91	0	434.1	553.32	695.53	584.54	-	-
βA	14.07	499.69	486.89	0	23.7	9.63	499.67	487	317.24	512.53	615.77	629.54	505.7	-	-
γA	-51.61	499.69	479.06	2393	23.7	9.41	499.69	479.17	459.03	441.97	556.99	592.86	459.03	-	-
αB	48.85	1343.4	1218.2	0	72.44	23.59	1343.4	1218.2	0	445.75	572.11	0	0	-	-
βB	40.7	1147.8	1020.2	0	60.46	19.77	1147.8	1020.3	472.63	560.83	663.88	0	0	-	-
γB	18.61	1147.8	1014.9	804.6	60.38	19.66	1147.7	1014.9	411.55	534.63	641.74	0	0	-	-
αA'	16.41	548.01	502.82	0	23.37	8.39	483.7	412.52	0	359.83	456.44	720.44	615.63	64.34	90.47
βA'	14.07	499.69	486.89	0	20.39	8.67	427.5	432.63	330.76	416.34	544.56	606.94	480.44	72.19	54.44
γA'	-51.61	499.69	479.06	2393	20.63	8.48	434.05	424.88	336.24	398.14	584.02	584.02	448.23	65.64	54.36
αB'	48.83	1343.5	1219.3	0	67.69	20.82	1237.5	1069.7	0	323.84	408.98	0	0	105.9	149.7
βB'	40.7	1147.8	1020.2	0	55.1	18.4	1027.9	944.18	446.97	421.32	571.64	0	0	119.8	76.11
γB'	18.61	1147.8	1014.9	804.6	54.21	18.37	1009.9	943.3	450.33	415.93	585.62	0	0	137.8	71.63

work done by [98] reports a reduction in community cost by 30% and [107] an 18%. However, both works present deterministic approaches. They do not consider the network technical limitation, and the batteries are modeled through continuous variables; therefore, their cost reduction could be overestimated, and the 15.5% obtained by the model proposed in this chapter is considered an acceptable reference point.

On the contrary, when the energy community trades energy and receives economic compensation by providing reactive power to the DSO, the objective function decreases 54.3% without including community batteries (βB Vs. γB) and presents profit when they are considered (βA Vs. γA). In other words, the DERs' capability to provide AS through reactive power to the DSO could significantly affect the total community cost, even generating positive surpluses. However, it is worth remembering that the reactive power price is defined in this case study as one-sixth of the electricity price and half of the FIT.

Note that the reactive power inclusion as ASs does not change the first-stage variables corresponding to the active power bough/sold to the grid. In fact, the objective function reduction is explained uniquely by the reactive power provided to the DSO; however, the energy traded in the LEM and the community/agents batteries change when the ASs are included showing a LEM activity increase of 44.7%, and a reduction of the batteries use of around 9.5%. On the other hand, when the community batteries are not included, the LEM activity decreases 12.9% and the agents' battery operation around 4%.

6.5.2.2 Case A' and B' analysis

In the previous cases A and B, it is impossible to distinguish the extra energy that some agents must absorb or inject to ensure the energy engaged in first stage decisions. This additional battery use is a flexible service supplied by users with storage devices to the community when they operate in a two-stage framework in the day-ahead

and intraday market. Therefore, although cases A and B show a reduction in the community cost function, the individual cost could be affected by this additional use of batteries, discouraging users' participation in the LEM. Therefore, cases A' and B' represent cases A and B, respectively, but A' and B' distinguish the flexible services supplied by the users with BSS.

The total energy bought and sold to the grid and the reactive power provided to the DSO is equal to cases A and B; however, the agents' energy bought and sold to the grid change. In fact, in this case, to obtain the total energy bought to the grid ($p\kappa^{bg}$) we must sum the energy bought to the grid by the users (p^{bg}) plus the users' batteries charging (Δch). i.e., a percentage of the total energy that enters the system goes to the users, and the remaining is stored in the users' batteries. For example, In the case γB', the total energy bought to the grid is 499.69 kWh, of which 434.05 kWh are consumed by the agents, and 65.64 kWh corresponding to 13.1% are absorbed by the batteries. Similar behavior occurs for the total energy leaving the system ($p\kappa^{sg}$), where the users' batteries discharge 11.3% of the total energy sold to the grid. These percentages, related to the flexible services provided by the agents' batteries, decrease when the community batteries are considered in the model (γA'); however, their participation continues to be 12% and 7.1% respectively, which suggests a non-negligible value to take into account.

6.5.2.3 Local energy market share

Fig. 6.4 shows how the agents meet their electricity load through the different mechanisms available in the local market, for the first scenario and considering community batteries. The bars in Fig. 6.4 have been sorted from agents whom more energy buy to the LEM (left) and agents that more energy provides to the LEM (right). Thus, when the bar takes positive values indicates that the agents consume the energy supplied by the LEM, the grid, or the battery; otherwise, in case of negative values, the agents provide energy to the LEM, to the gird, or charge the community batteries. In this regard, at least ten agents generate enough energy to self-satisfied their consumption and supply energy to the community or the DSO, being the power generated through the PV systems responsible for more than 90% of the energy self-consumed and injected into the grid. On the other hand, agents without DERs installed (4, 20, 32, 11) meet their demand by buying the energy in the LEM and from the community batteries. Note that the batteries share show is small because it corresponds to the aggregated energy discharge and charging in 24 h. i.e., when the battery indicates a positive value, the battery in 24 h discharged more energy than charged.

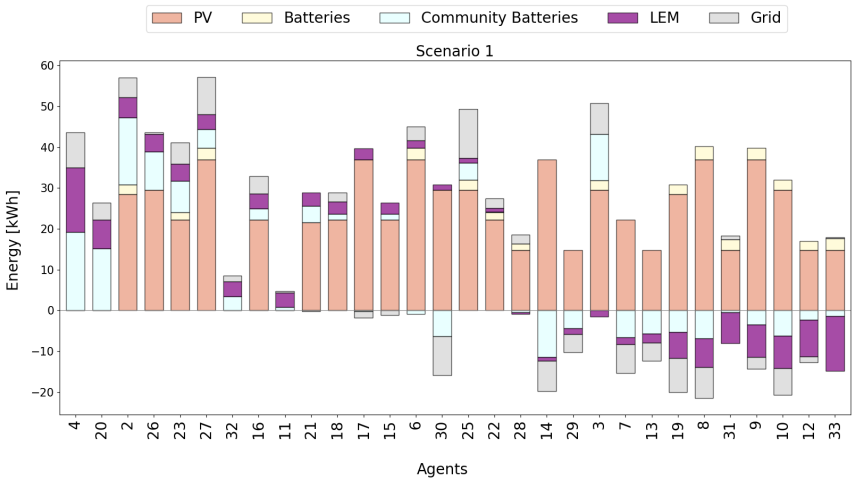

Figure 6.4: Energy share by agents

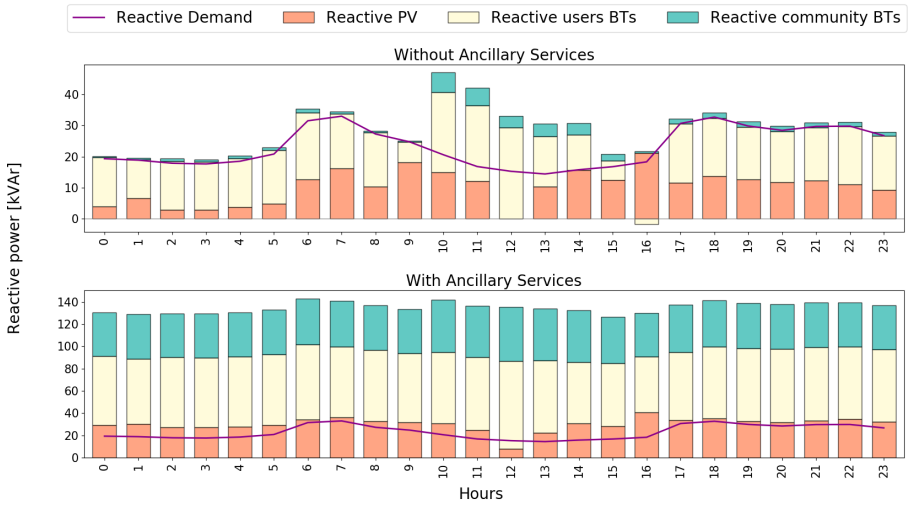

Figure 6.5: Reactive power supplied with and without ASs

6.5.2.4 Reactive power capability

The DERs capability to supply reactive power is shown in Fig. 6.5, contrasting scenario 1 when the system provides ASs (below) and when do not (up). Thus, when the DERs do not provide ASs, the community battery usage for reactive power is marginal, and the reactive power corresponds to the reactive demand, except when the PV systems operate. On the contrary, under the same load and weather conditions, when the DERs provide ASs, the reactive power provided by the inverters associated with the PV systems supply almost the total reactive power, and the remaining is provided by the individual and community batteries.

6.5.2.5 Community battery role

The results in Table 6.4 show that when the community batteries operate in a P2P energy trading scheme, the agents' batteries use decreases, and the total community cost is reduced mainly through the reactive power provided by these community devices. Besides, following the hourly community battery operation in Fig. 6.6, when they are considered (second charts row) operates at the end of the day, discharging energy and charging when the PV systems are generating electricity. Note that the negative value corresponds to when the energy goes out of the system (charging batteries and selling to the grid), and when it is positive represents the discharging battery process and the agents' load consumption.

On the contrary, when the community batteries are not included (first charts row), the agents' batteries in the second and third scenarios must absorb all the energy provided by the grid over the load consumption. This extra energy absorbed is adequately commented in the following subsection, but is the flexible service provided by users with storage devices to the community to face the energy compromised in the day-ahead market (first-stage variables). For example, following the second chart of the first row, the energy over the demand line is the energy absorbed by the battery; this surplus corresponds to the energy compromised in the first stage, where the first scenario fixes the maximum due to its most demanded. Under the same logic, this situation does not occur in the first stage, where the agents' batteries charge only when the PV systems are generating electricity.

6.5.3 Individual profit

The dual variables related to Eq. 5.2 have been used as the LEM price in order to compare the agents' profit when they trade energy and when they do not. Thus, Fig. 6.7 shows the agents' profit comparison when the energy community operates without energy trading, with energy trading, and when they provide ASs through reactive power. Besides, the results contrast the community battery impact on the users' profit, while the opening in scenarios show the second-stage variables change. Therefore, if the first scenario occurs, the individual profit with energy trading slightly improves due to the first being the most demanded scenario. However, when the system provides reactive power, users 3, 19, 22, and 23 improve their profit in the first scenario significantly regarding others, and many users with DERs also improve their cost function for the second and third scenarios. On the contrary, traditional consumers without DERs installed, like 4, 11, 20, and 32, show a very slight profit

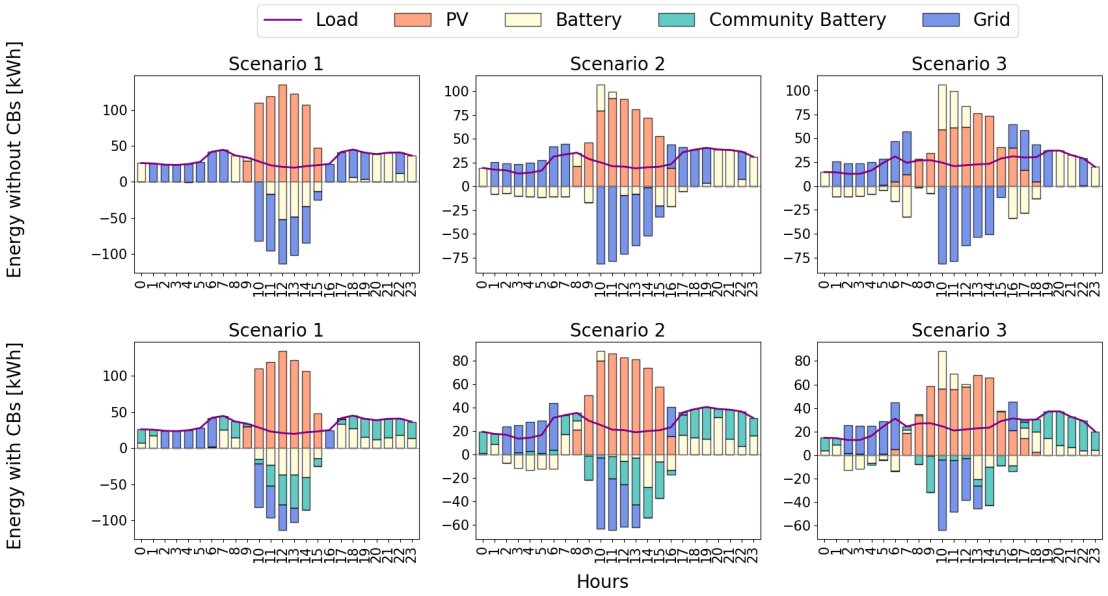

Figure 6.6: Community batteries effect on the second stage variables

increase compared with users with DERs when the ASs are provided through reactive power. For users without DERs, this minor improvement is explained because when they buy energy in the LEM, they are doing it at a lower price than the electricity price provided by the grid, and they do not have access to provide reactive power, which is the main factor to increase the profit of agents with DERs.

On the other hand, some users like 17, 10, 28, and 29 with a PV-BSS system reduce their profit when they trade energy in the LEM compared to when they do not. This negative increase is explained because some agents must absorb or inject from their batteries more energy than they require to meet the total community energy compromised in the day-ahead market. Therefore, they provide a flexible service that is not compensated in this model, but the energy amount involved is quantified to justify that a minimal compensation increase this negative value to make it positive and promote their participation in the LEM. In other words, a minimal price for the extra use of batteries under an energy trading scheme can further encourage the participation of agents with DERs through the individual profit increase regarding when they do not trade energy.

In addition, when the profit is studied at an average level separating between consumers and prosumers with PV, PV-battery systems, and considering the community batteries, we found that users with PV system increase their profit at average in a 34 %, agents with PV-Battery system a 7% and traditional consumer in 9%. These

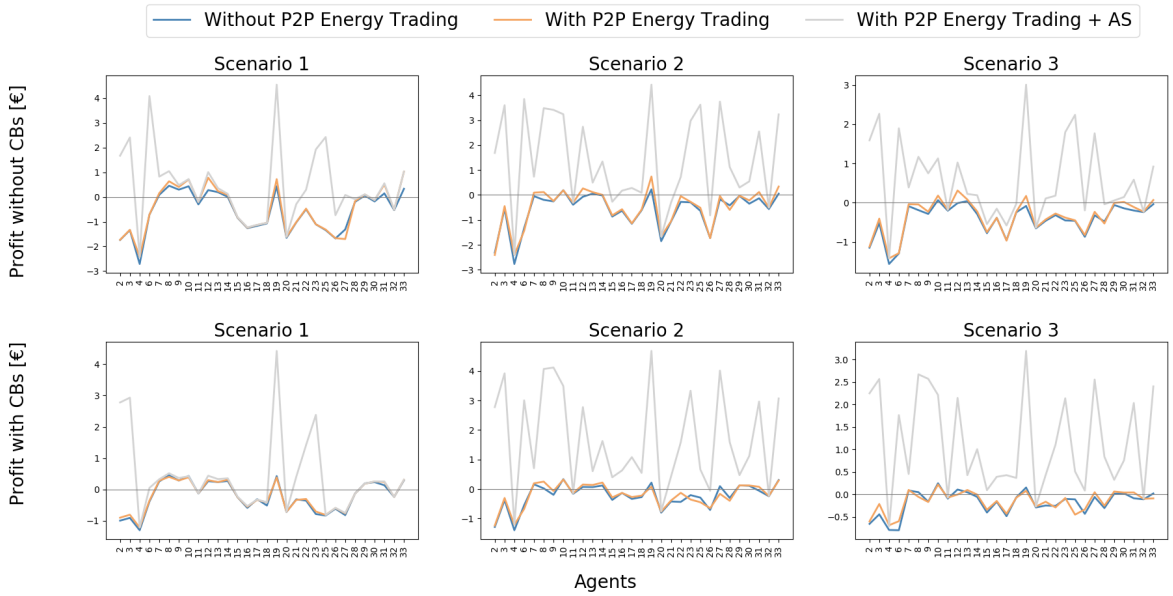

Figure 6.7: Agents profit comparison when they operate under P2P energy trading providing ASs and when they not

results show that users with flexibility perceive lower improvement than a traditional consumer, and the explanation is related to the flexibility service provided by the battery for the energy community in a two-stage context. However, when the DERs provide ASs to DSO through reactive power, users with DERs increase their profit more than five times on average.

6.6 Chapter conclusions

This chapter has presented a two-stage stochastic MISOCP model to address the day-ahead and intraday market of a local energy community trading active power under a centralized marker design, considering the DERs' capability to provide reactive power. Different frameworks have been considered to include community batteries and measure the service provided by users with storage devices to the energy community in the intraday market to face the energy committed in the day-ahead market.

The formulation proposed has been tested in the IEEE-33 bus distribution system considering three simultaneous scenarios of 24 hours showing the significant effect of the reactive power supplied by the DERs on the community welfare when the users perceive an economic remuneration by the reactive power provided. Likewise, the community batteries have shown a relevant role to support a two-stage framework related to the day-ahead and intraday markets, helping the users without battery

systems to commit energy in the day-ahead market. Besides, the energy quantification stored in the users' batteries to support the two-stage framework has been presented as alternative mechanisms to promote the collaborative local market scheme.

Chapter 7

Conclusions

This thesis has addressed significant challenges related to the expected share increase of DERs in DN due to renewables cost decreasing and the power systems decarbonization. In this regard, three topics have been reviewed, and different optimization techniques have been applied to support planning and operation decisions regarding the DN' restructuring process. The first topic managed the optimal location and sizing of DERs into DN from a deterministic and stochastic perspective. Then, the unexpected main grid failure in the electricity provision for DN with high DERs penetration was addressed under a deterministic formulation providing the topology to face these unlikely events minimizing the load curtailment. In the third topic, the potential TE has been modeled and simulated through a P2P energy trading scheme considering different frameworks and markets.

Regarding the first two objectives (O1 and O2) related to the optimal DERs location and sizing problem, a novel algorithm has been developed using the GA logic to manage the binary variables related to the location problem, so extending the sizing and location problem for multiperiod scenarios greater than 24 hours. In this regard, it has been proved that the formulation proposed allows the planning of 100% autonomous systems since finding a feasible solution to the DG and BESS capacity problem for a time horizon of 8760 h through a reduced scenario of 168 hours. Besides, the deterministic approach has been used to compare the optimal DG and BSS capacity considering a system under grid-connected and off-grid modes, proving that the capacity required to supply the entire electricity demand in an islanded network increases the investment cost significantly. However, it has been shown that when the external grid provides electricity only in the most critical hours (hours with poor weather conditions), the investment and the operational cost decrease significantly. Thus, the formulation presented provides the needed flexibility to measure

the trade-off between the investment required in DERs and the expected energy supplied by these resources under one year of operation in a single model. Likewise, the results have shown that considering one year of operation and under the cost batteries assumptions, the model always installs lead-acid batteries instead of lithium-ion, putting investment before battery efficiency.

In addition, the location and sizing problem of DERs have been addressed under a two-stage stochastic approach considering the effect of the DR and the EVs on the optimal sizing. In this regard, different sets of scenarios have been determined using the backward algorithm to show that the DERs capacity installed is highly sensible to the case selected. i.e., when the cases had more wind resources, the model installed more wind turbines than solar panels and vice versa; however, when these capacities were tested in a complete scenario of 8760, the energy provided by the system was low compared with cases where the irradiation and the wind speed were considered in the same proportion. Thus, the better results in terms of investment, operational cost, and energy provided by the DERs were under scenarios with high irradiation and wind speed levels.

Besides, and corresponding to objective 3 (O3), the EVs' presence suggests a reducing operational cost related to the energy provided by the main grid due to their capacity to inject energy in hours with a high price; however, a high EVs penetration might increase DERs capacity installation. On the other hand, the DG's capability to provide reactive power indicates that it might be possible to supply a high percentage of the reactive power load from renewable resources and provide ASs to the utility grid. The proposed algorithm and formulation have been tested in different IEEE networks proving their efficiency and convergence.

From the operational perspective and related to objective 4 (O4), a VMs topology scheduling model has been presented to minimize the active and reactive power not supplied in DN with high DERs penetration with temporal failures in the electricity provision from the external grid. In this regard, the consumption points where the electricity demand is not satisfied or nodes that do not have enough demand flexibility to decrease their consumption to face a lower energy provision scenario have been considered the VMs boundaries. The results have shown that under the scheme proposed, the DR may decrease the load curtailment considerably, and the boundaries point usually corresponds to nodes far away from a DG or storage devices. Likewise, the VMs' topologies have been validated using the classic AC OPF formulation to ensure that the solution provided by the model is an optimal solution of the AC OPF.

The P2P energy trading scheme has been addressed in this thesis under two different stochastic programming formulations. The first approach (O5) focused on modeling a scheduling energy trading day-ahead market, preserving the users' information private considering the network technical limitation and the active power as a tradable commodity without considering reactive power provided by the DERs. In this regard, the Benders algorithm was implemented, separating the original formulation into a MP that manages the network necessities and multiple SPs that address the energy traded by the users in the LEM. The strengthened Bender cuts have been used to manage the binary variables related to the SPs ensuring the optimality of the solution found by the algorithm. Thus, it has been proved that the algorithm proposed to converge to the same objective function of the centralized model, being the computational time, the only cost paid by the users to keep their information private. Besides, it has been quantified that a P2P energy trading scheme, under the assumptions considered in the case study, could decrease the global community cost by 18.2% on average. However, the results have shown that maximizing global welfare could reduce the individual profit of users with batteries, which could discourage collaborative energy trading among community users.

Finally, the second approach (O6) addressed the P2P energy trading scheme under a centralized market design modeling a day-ahead and intraday market quantifying the reactive power provided by the DERs to the DSO as ASs. The formulation has measured the community batteries' effects on the energy trading in the LEM and the reactive power provided by these devices. The results have shown that ASs provided by the energy community users through reactive power may increase the community welfare significantly and provide positive incentives to promote the users' participation in the local market. Besides, the flexibility provided by the users' batteries has been quantified to measure the services provided by users with storage devices to the community to face the energy compromised by the community in the day-ahead market.

7.1 Further work

The following research works are suggested to extend, compare or improve the topics addressed in this thesis.

Related to the optimal sizing and allocation of DERs

- The algorithm proposed in this thesis to address the binary variables related to the DERs location decreases the execution time considerably, allowing extensive

multiperiod scenarios. However, the algorithm could be improved or contrasted using decomposition methods techniques.

- Although the thesis uses the Backward algorithm to reduce the number of scenarios, a new algorithm could be designed to improve the scenario selection based on the capacity of the scenarios to generate energy rather than on the statistical difference between them.

- The two-stage stochastic approach could be contrasted with a bi-level and/or a robust optimization and study the best alternative to handle the DERs' uncertainty in the decision related to their location and capacity.

Related to the models to simulate a P2P energy trading market

- Investigate an alternative method or improve the computational times of the Bender decomposition algorithm presented to solve the P2P energy trading model from a decentralized market design perspective.

- Extend the two-stage stochastic model presented in Chapter 5 to manage the day-ahead market, and include the intraday market, but under a multistage approach including EVs, DR, and ASs.

- Based on the P2P energy trading models presented in this thesis, develop a multimarket pricing algorithm. Thus, the different potential markets applied for an EC like day-ahead, intraday, ASs, and flexibility market could be formulated considering the proper economic incentives for the users to trade energy.

Bibliography

[1] IRNEA. *Renewable Power Generation Costs in 2020*. 2020.

[2] M. A. Hannan, S. B. Wali, P. J. Ker, M. S.Abd Rahman, M. Mansor, V. K. Ramachandaramurthy, K. M. Muttaqi, T. M.I. Mahlia, and Z. Y. Dong. Battery energy-storage system: A review of technologies, optimization objectives, constraints, approaches, and outstanding issues. *Journal of Energy Storage*, 42(July):103023, 2021.

[3] International Renewable Energy Agency (IRENA). *Global Energy Transformation (GET): A Roadmap to 2050*. 2019.

[4] M. Nijhuis, M. Gibescu, and J. F.G. Cobben. Assessment of the impacts of the renewable energy and ICT driven energy transition on distribution networks. *Renewable and Sustainable Energy Reviews*, 52:1003–1014, 2015.

[5] Shuying Zhen, Yiwei Ma, Fred Wang, and Leon M. Tolbert. Operation of a flexible dynamic boundary microgrid with multiple islands. *Conference Proceedings - IEEE Applied Power Electronics Conference and Exposition - APEC*, 2019-March:548–554, 2019.

[6] IRENA. Electricity trading arrangements. 2020.

[7] Esther Mengelkamp, Philipp Staudt, Johannes Garttner, and Christof Weinhardt. Trading on local energy markets: A comparison of market designs and bidding strategies. *International Conference on the European Energy Market, EEM*, 2017.

[8] Breyer C. Ram M., Bogdanov D., Aghahosseini A., Oyewo A.S., Gulagi A., Child M., Fell H.-J. *Global Energy System Based On 100% Renewable Energy - Power Sector*, volume 1. 20178.

[9] IRENA. *Global energy transformation: A roadmap to 2050 (2019 edition)*. 2019.

[10] Zhifang Yang, Haiwang Zhong, Anjan Bose, Tongxin Zheng, Qing Xia, and Chongqing Kang. A Linearized OPF Model with Reactive Power and Voltage Magnitude: A Pathway to Improve the MW-Only DC OPF. *IEEE Transactions on Power Systems*, 33(2):1734–1745, 2018.

[11] Zhifang Yang, Haiwang Zhong, Qing Xia, Anjan Bose, and Chongqing Kang. Optimal power flow based on successive linear approximation of power flow equations. *IET Generation, Transmission and Distribution*, 10(14):3654–3662, 2016.

[12] Nasim Nezamoddini and Yong Wang. Robust optimization of energy storage system allocation and sizing. *67th Annual Conference and Expo of the Institute of Industrial Engineers 2017*, pages 914–919, 2017.

[13] H Nazaripouya, Y Wang, P Chu, H R Pota, and R Gadh Members. Optimal Sizing and Placement of Battery Energy Storage in Distribution System Based on Solar Size for Voltage Regulation. 2015.

[14] Khawaja Khalid Mehmood, Saad Ullah Khan, Soon Jeong Lee, Zunaib Maqsood Haider, Muhammad Kashif Rafique, and Chul Hwan Kim. Optimal sizing and allocation of battery energy storage systems with Wind and solar power DGs in a distribution network for voltage regulation considering the lifespan of batteries. *IET Renewable Power Generation*, 11(10):1305–1315, 2017.

[15] Yongxi Zhang, Shuyun Ren, Zhao Yang Dong, Yan Xu, Ke Meng, and Yu Zheng. Optimal placement of battery energy storage in distribution networks considering conservation voltage reduction and stochastic load composition. *IET Generation, Transmission & Distribution*, 11(15):3862–3870, 2017.

[16] Siqi Lu, Xiaorong Wang, and Junyong Wu. Location and Size Planning of Distributed Photovoltaic Generation in Distribution network System Based on K-means Clustering Analysis. *IOP Conference Series: Earth and Environmental Science*, 108(5), 2018.

[17] E. S. Ali, S. M. Abd Elazim, and A. Y. Abdelaziz. Optimal allocation and sizing of renewable distributed generation using ant lion optimization algorithm. *Electrical Engineering*, 100(1):99–109, 2018.

[18] R. Mena, Y. Li, E. Zio, M. Hennebel, and C. Ruiz. Optimal sizing and allocation of distributed generation for reliable energy distribution accounting for uncertainty. *Safety, Reliability and Risk Analysis: Beyond the Horizon - Proceedings of the European Safety and Reliability Conference, ESREL 2013*, pages 2899–2907, 2014.

[19] Rabbia Siddique, Safdar Raza, Abdul Mannan, Linta Khalil, Nashitah Alwaz, and Mughees Riaz. A modified NSGA approach for optimal sizing and allocation of distributed resources and battery energy storage system in distribution network. *Materials Today: Proceedings*, (xxxx), 2020.

[20] Yasin Gilasi, Seyed Hamid Hosseini, and Hossein Ranjbar. Resiliency-oriented optimal siting and sizing of distributed energy resources in distribution systems. *Electric Power Systems Research*, 208(February):107875, 2022.

[21] E. E. Sfikas, Y. A. Katsigiannis, and P. S. Georgilakis. Simultaneous capacity optimization of distributed generation and storage in medium voltage microgrids. *International Journal of Electrical Power and Energy Systems*, 67:101–113, 2015.

[22] Juan Camilo López, Kaio Vieira dos Santos, Luiza Higino Silva, Nataly Banol Arias, Marcos J. Rider, and Luiz C. P. da Silva. Optimal Sizing and Allocation of Distributed Energy Resources in Microgrids Considering Internal Network Reinforcements. *SSRN Electronic Journal*, 2021.

[23] Mohammad Sadegh Javadi, Matthew Gough, Seyed Amir Mansouri, Amir Ahmarinejad, Emad Nematbakhsh, Sergio F. Santos, and João P.S. Catalão. A two-stage joint operation and planning model for sizing and siting of electrical energy storage devices considering demand response programs. *International Journal of Electrical Power and Energy Systems*, 138(June 2021), 2022.

[24] Mukesh Gautam, Narayan Bhusal, and Mohammed Benidris. A cooperative game theory-based approach to sizing and siting of distributed energy resources. In *2021 North American Power Symposium (NAPS)*, pages 01–06, 2021.

[25] Abdulbari Ali Mohamed Frei and Muhammet Tahir Guneser. Optimal Accommodation of DERs in Practical Radial Distribution Feeder for Techno-Economic with Artificial Bee Colony Algorithm. *3rd International Conference on Electrical, Communication and Computer Engineering, ICECCE 2021*, (June):12–13, 2021.

[26] Amin Foroughi Nematollahi, Hossein Shahinzadeh, Hamed Nafisi, Behrooz Vahidi, Yassine Amirat, and Mohamed Benbouzid. Sizing and sitting of ders in active distribution networks incorporating load prevailing uncertainties using probabilistic approaches. *Applied Sciences*, 11(9), 2021.

[27] Muhammad Khalid, Umer Akram, and Saifullah Shafiq. Optimal planning of multiple distributed generating units and storage in active distribution networks. *IEEE Access*, 6(c):55234–55244, 2018.

[28] Di Hu, Ming Ding, Rui Bi, Xianfang Liu, and Xiuting Rong. Sizing and placement of distributed generation and energy storage for a large-scale distribution network employing cluster partitioning. *Journal of Renewable and Sustainable Energy*, 10(2), 2018.

[29] Farhad Samadi Gazijahani and Javad Salehi. Stochastic multi-objective framework for optimal dynamic planning of interconnected microgrids. *IET Renewable Power Generation*, 11(14):1749–1759, 2017.

[30] Jennifer F. Marley, Daniel K. Molzahn, and Ian A. Hiskens. Solving Multiperiod OPF Problems Using an AC-QP Algorithm Initialized with an SOCP Relaxation. *IEEE Transactions on Power Systems*, 32(5):3538–3548, 2017.

[31] Carleton Coffrin, Hassan L. Hijazi, and Pascal Van Hentenryck. The QC Relaxation: Theoretical and Computational Results on Optimal Power Flow. *Ieee Transactions on Power Systems*, 31(4):3008–3018, 2016.

[32] James A. Momoh, M. E. El-Hawary, and Ramababu Adapa. A review of selected optimal power flow literature to 1993 part i: nonlinear and quadratic Programming Approaches. *IEEE Transactions on Power Systems*, 14(1):96–103, 1999.

[33] James A. Monoh, M. E. Ei-Hawary, and Ramababu Adapa. A review of selected optimal power flow literature to 1993 part ii: newton, linear programming and Interior Point Methods. *IEEE Transactions on Power Systems*, 14(1):105–111, 1999.

[34] F. García-Muñoz, F. Díaz-Gonzalez, C. Corchero, and C. Nuñez-De-Toro. Optimal Sizing and Location of Distributed Generation and Battery Energy Storage System. In *Proceedings of 2019 IEEE PES Innovative Smart Grid Technologies Europe, ISGT-Europe 2019*, 2019.

[35] John H. Holland. *Adaptation in natural and artificial systems: an introductory analysis with applications to biology, control and artificial intelligence*. 1975.

[36] M. S. Osman, M. A. Abo-Sinna, and A. A. Mousa. A solution to the optimal power flow using genetic algorithm. *Applied Mathematics and Computation*, 155(2):391–405, 2004.

[37] A. G. Bakirtzis, P. N. Biskas, C. E. Zoumas, and V. Petridis. Optimal Power Flow by Enhanced Genetic Algorithm. *IEEE Power Engineering Review*, 22(2):60–60, 2008.

[38] Pvwatts, 2018.

[39] Data real-time - historic, 2018.

[40] A Wazir and Naeem Arbab. Analysis and optimization of ieee 33 bus radial distributed system using optimization algorithm. 2016.

[41] Expósito Antonio Gómez, Antonio J. Conejo, and Can nizares Claudio. *Electric energy systems analysis and operation*. CRC Press, 2018.

[42] Francisco Díaz-González, Andreas Sumper, Oriol Gomis-Bellmunt, and Roberto Villafáfila-Robles. A review of energy storage technologies for wind power applications. *Renewable and Sustainable Energy Reviews*, 16(4):2154–2171, 2012.

[43] International Renewable Energy Agency. *Renewable Power Generation Costs in 2018*. 2018.

[44] Volume Power Sector. Wind Power. *Green Energy and Technology*, 20(5):231–256, 2012.

[45] Energy iberian market operator - omie, anual spot market prices, 2018.

[46] Walter Gil-González, Alejandro Garces, Oscar Danilo Montoya, and Jesus C. Hernández. A mixed-integer convex model for the optimal placement and sizing of distributed generators in power distribution networks. *Applied Sciences (Switzerland)*, 11(2):1–15, 2021.

[47] Ehsan Hooshmand and Abbas Rabiee. Robust model for optimal allocation of renewable energy sources, energy storage systems and demand response in distribution systems via information gap decision theory. *IET Generation, Transmission and Distribution*, 13(4):511–520, 2019.

[48] Ali Ehsan and Qiang Yang. Optimal integration and planning of renewable distributed generation in the power distribution networks: A review of analytical techniques. *Applied Energy*, 210(October 2017):44–59, 2018.

[49] Kai Gong, Xu Wang, Chuanwen Jiang, Mohammad Shahidehpour, Xiaolin Liu, and Zean Zhu. Security-Constrained Optimal Sizing and Siting of BESS in Hybrid AC/DC Microgrid Considering Post-Contingency Corrective Rescheduling. *IEEE Transactions on Sustainable Energy*, 3029(c):1–1, 2021.

[50] H. Nazaripouya, Y. Wang, P. Chu, H. R. Pota, and R. Gadh. Optimal sizing and placement of battery energy storage in distribution system based on solar size for voltage regulation. *IEEE Power and Energy Society General Meeting*, 2015-September:9–13, 2015.

[51] Omid Sadeghian, Morteza Nazari-Heris, Mehdi Abapour, S. Saeid Taheri, and Kazem Zare. Improving reliability of distribution networks using plug-in electric vehicles and demand response. *Journal of Modern Power Systems and Clean Energy*, 7(5):1189–1199, 2019.

[52] Pierluigi Siano. Demand response and smart grids - A survey. *Renewable and Sustainable Energy Reviews*, 30:461–478, 2014.

[53] Pavani Ponnaganti, Jayakrishnan R. Pillai, and Birgitte Bak-Jensen. Opportunities and challenges of demand response in active distribution networks. *Wiley Interdisciplinary Reviews: Energy and Environment*, 7(1), 2018.

[54] German Bundestag. Innovation Outlook Charging for Electric. 2019.

[55] Abdullah S. Bin Humayd and Kankar Bhattacharya. Distribution system planning to accommodate distributed energy resources and PEVs. *Electric Power Systems Research*, 145:1–11, 2017.

[56] Majid Abdi-Siab and Hamid Lesani. Distribution expansion planning in the presence of plug-in electric vehicle: A bilevel optimization approach. *International Journal of Electrical Power and Energy Systems*, 121(October 2019):106076, 2020.

[57] Fernando García-Muñoz, Francisco Díaz-González, and Cristina Corchero-García. A novel algorithm based on the combination of AC-OPF and GA for the optimal sizing and location of DERs into distribution networks. *Sustainable Energy, Grids and Networks*, 27:100497, 2021.

[58] Duong Quoc Hung, Student Member, Nadarajah Mithulananthan, and Senior Member. Determining PV Penetration for Distribution Determining PV Penetration for Distribution Systems With Time-Varying Load Models. *Power Systems, IEEE Transactions on*, 29(July):3048–3057, 2016.

[59] Y. M. Atwa, E. F. El-Saadany, M. M.A. Salama, and R. Seethapathy. Optimal renewable resources mix for distribution system energy loss minimization. *IEEE Transactions on Power Systems*, 25(1):360–370, 2010.

[60] Juan M. Morales, Salvador Pineda, Antonio J. Conejo, and Miguel Carrión. Scenario reduction for futures market trading in electricity markets. *IEEE Transactions on Power Systems*, 24(2):878–888, 2009.

[61] Nicole Gröwe-Kuska, Holger Heitsch, and Werner Römisch. Scenario reduction and scenario tree construction for power management problems. *2003 IEEE Bologna PowerTech - Conference Proceedings*, 3:152–158, 2003.

[62] Zhongwen Li, Chuanzhi Zang, Peng Zeng, and Haibin Yu. Combined two-stage stochastic programming and receding horizon control strategy for microgrid energy management considering uncertainty. *Energies*, 9(7), 2016.

[63] Vassilis Kekatos, Gang Wang, Antonio J. Conejo, and Georgios B. Giannakis. Stochastic Reactive Power Management in Microgrids with Renewables. *IEEE Transactions on Power Systems*, 30(6):3386–3395, 2015.

[64] Brett A. Robbins, Christoforos N. Hadjicostis, and Alejandro D. Domínguez-García. A two-stage distributed architecture for voltage control in power distribution systems. *IEEE Transactions on Power Systems*, 28(2):1470–1482, 2013.

[65] Abouzar Samimi, Ahad Kazemi, and Pierluigi Siano. Economic-environmental active and reactive power scheduling of modern distribution systems in presence of wind generations: A distribution market-based approach. *Energy Conversion and Management*, 106:495–509, 2015.

[66] Oktoviano Gandhi, Carlos D. Rodríguez-Gallegos, Wenjie Zhang, Dipti Srinivasan, and Thomas Reindl. Economic and technical analysis of reactive power provision from distributed energy resources in microgrids. *Applied Energy*, 210(March 2017):827–841, 2018.

[67] Pramuk Unahalekhaka and Panot Sripakarach. Reduction of Reverse Power Flow Using the Appropriate Size and Installation Position of a BESS for a PV Power Plant. *IEEE Access*, 8:102897–102906, 2020.

[68] Ray Daniel Zimmerman, Carlos Edmundo Murillo-sánchez, and Robert John Thomas. MATPOWER : Steady-State Operations , Systems Research and Education. *IEEE Transactions on Power Systems*, 26(1):12–19, 2011.

[69] OpenEI. Commercial and residential load data, 2004.

[70] European Commission. European photovoltaic geographical information system, 2017.

[71] Constance Crozier, Thomas Morstyn, and Malcolm McCulloch. A Stochastic Model for Uncontrolled Charging of Electric Vehicles Using Cluster Analysis. 14(8):1–9, 2019.

[72] Laya Das, Sai Munikoti, Balasubramaniam Natarajan, and Babji Srinivasan. Measuring smart grid resilience: Methods, challenges and opportunities. *Renewable and Sustainable Energy Reviews*, 130(May):109918, 2020.

[73] Camilo A. Cortes, Sergio F. Contreras, and Mohammad Shahidehpour. Microgrid topology planning for enhancing the reliability of active distribution networks. *IEEE Transactions on Smart Grid*, 9(6):6369–6377, 2018.

[74] Mostafa Barani, Jamshid Aghaei, Mohammad Amin Akbari, Taher Niknam, Hossein Farahmand, and Magnus Korpas. Optimal partitioning of smart distribution systems into supply-sufficient microgrids. *IEEE Transactions on Smart Grid*, 10(3):2523–2533, 2019.

[75] Dan T. Ton I. and Merrill A. Smith. Doi:10.1016/J.Tej.2012.09.013. 2012.

[76] Yuhua Du, Xiaonan Lu, Jianhui Wang, and Srdjan Lukic. Distributed Secondary Control Strategy for Microgrid Operation with Dynamic Boundaries. *IEEE Transactions on Smart Grid*, PP(c):1, 2018.

[77] Hossein Haddadian and Reza Noroozian. Multi-microgrids approach for design and operation of future distribution networks based on novel technical indices. *Applied Energy*, 185:650–663, 2017.

[78] Ieee guide for design, operation, and integration of distributed resource island systems with electric power systems. *IEEE Std 1547.4-2011*, pages 1–54, 2011.

[79] X. Xu, F. Xue, S. Lu, H. Zhu, L. Jiang, and B. Han. Structural and hierarchical partitioning of virtual microgrids in power distribution network. *IEEE Systems Journal*, 13(1):823–832, 2019.

[80] Mohammed E. Nassar and M. M.A. Salama. Adaptive self-adequate microgrids using dynamic boundaries. *IEEE Transactions on Smart Grid*, 7(1):105–113, 2016.

[81] Joel Jose, Anupama Kowli, Vaibhav Bhalekar, Krishna V. Prasad, and Narayanan Rajagopal. Dynamic microgrid-based operations: A new operational paradigm for distribution networks. *IEEE PES Innovative Smart Grid Technologies Conference Europe*, pages 564–569, 2016.

[82] B. Meyer, M. Fiedeldey, H. Mueller, C. Hoffman, R. Koeberle, and J. Bamberger. Impact of large share of renewable generation on investment costs at the example of aÜw distribution network. In *22nd International Conference and Exhibition on Electricity Distribution (CIRED 2013)*, pages 1–4, 2013.

[83] Dongkuan Xu and Yingjie Tian. A Comprehensive Survey of Clustering Algorithms. *Annals of Data Science*, 2(2):165–193, 2015.

[84] Ulrik Brandes, Daniel Delling, Marco Gaertler, Robert Görke, Martin Hoefer, Zoran Nikoloski, and Dorothea Wagner. On modularity clustering. *IEEE Transactions on Knowledge and Data Engineering*, 20(2):172–188, 2008.

[85] Saman Korjani, Angelo Facchini, Mario Mureddu, and Alfonso Damiano. A Genetic Algorithm Approach for the Identification of Microgrids Partitioning into Distribution Networks.

[86] Emprise Y.K. Chan and Dit Yan Yeung. A convex formulation of modularity maximization for community detection. *IJCAI International Joint Conference on Artificial Intelligence*, pages 2218–2225, 2011.

[87] Bo Zhao, Zhicheng Xu, Chen Xu, Caisheng Wang, and Feng Lin. Network Partition-Based Zonal Voltage Control for Distribution Networks with Distributed PV Systems. *IEEE Transactions on Smart Grid*, 9(5):4087–4098, 2018.

[88] G J Fang and H Bao. A calculation method of electric distance and subarea division application based on transmission impedance. *IOP Conference Series: Earth and Environmental Science*, 104:012006, dec 2017.

[89] Eduardo Cotilla-Sanchez, Paul D.H. Hines, Clayton Barrows, Seth Blumsack, and Mahendra Patel. Multi-attribute partitioning of power networks based on electrical distance. *IEEE Transactions on Power Systems*, 28(4):4979–4987, 2013.

[90] Saeed D. Manshadi and Mohammad E. Khodayar. Expansion of Autonomous Microgrids in Active Distribution Networks. *IEEE Transactions on Smart Grid*, 9(3):1878–1888, 2018.

[91] Abdollah Kavousi-Fard, Alireza Zare, and Amin Khodaei. Effective dynamic scheduling of reconfigurable microgrids. *IEEE Transactions on Power Systems*, 33(5):5519–5530, 2018.

[92] Antonio Gomez-Exposito, Antonio J Conejo, and Claudio Cañizares. *Electric energy systems: analysis and operation*. CRC press, 2018.

[93] Matthias Resch. Impact of operation strategies of large scale battery systems on distribution grid planning in Germany. *Renewable and Sustainable Energy Reviews*, 74(December 2016):1042–1063, 2017.

[94] Seyedmohsen Hosseini, Kash Barker, and Jose E. Ramirez-Marquez. A review of definitions and measures of system resilience. *Reliability Engineering and System Safety*, 145:47–61, 2016.

[95] Xiaodong Yang, Youbing Zhang, Haibo He, Shuaijie Ren, and Guoqing Weng. Real-Time Demand Side Management for a Microgrid Considering Uncertainties. *IEEE Transactions on Smart Grid*, 10(3):3401–3414, 2019.

[96] Mohsen Khorasany, Yateendra Mishra, and Gerard Ledwich. Market framework for local energy trading: A review of potential designs and market clearing approaches. *IET Generation, Transmission and Distribution*, 12(22):5899–5908, 2018.

[97] Yue Zhou, Jianzhong Wu, Chao Long, and Wenlong Ming. State-of-the-art analysis and perspectives for peer-to-peer energy trading. *Engineering*, 6(7):739–753, 2020.

[98] Chao Long, Jianzhong Wu, Yue Zhou, and Nick Jenkins. Peer-to-peer energy sharing through a two-stage aggregated battery control in a community Microgrid. *Applied Energy*, 226(May):261–276, 2018.

[99] Mohsen Khorasany, Yateendra Mishra, and Gerard Ledwich. Peer-to-peer market clearing framework for DERs using knapsack approximation algorithm. *2017 IEEE PES Innovative Smart Grid Technologies Conference Europe, ISGT-Europe 2017 - Proceedings*, 2018-January:1–6, 2017.

[100] Mohsen Khorasany, Yateendra Mishra, and Gerard Ledwich. A Decentralized Bilateral Energy Trading System for Peer-to-Peer Electricity Markets. *IEEE Transactions on Industrial Electronics*, 67(6):4646–4657, 2020.

[101] Md Habib Ullah and Jae Do Park. A Two-Tier Distributed Market Clearing Scheme for Peer-to-Peer Energy Sharing in Smart Grid. *IEEE Transactions on Industrial Informatics*, 3203(c), 2021.

[102] Zhiyi Li and Mohammad Shahidehpour. Privacy-Preserving Collaborative Operation of Networked Microgrids with the Local Utility Grid Based on Enhanced Benders Decomposition. *IEEE Transactions on Smart Grid*, 11(3):2638–2651, 2020.

[103] Stefano Lilla, Camilo Orozco, Alberto Borghetti, Fabio Napolitano, and Fabio Tossani. Day-Ahead Scheduling of a Local Energy Community: An Alternating Direction Method of Multipliers Approach. *IEEE Transactions on Power Systems*, 35(2):1132–1142, 2020.

[104] Wayes Tushar, Tapan Kumar Saha, Chau Yuen, Paul Liddell, Richard Bean, and H. Vincent Poor. Peer-to-Peer Energy Trading With Sustainable User Participation: A Game Theoretic Approach. *IEEE Access*, 6(c):62932–62943, 2018.

[105] Wayes Tushar, Tapan Kumar Saha, Chau Yuen, Thomas Morstyn, Malcolm D. McCulloch, H. Vincent Poor, and Kristin L. Wood. A motivational game-theoretic approach for peer-to-peer energy trading in the smart grid. *Applied Energy*, 243(March):10–20, 2019.

[106] Wayes Tushar, Tapan Kumar Saha, Chau Yuen, M. Imran Azim, Thomas Morstyn, H. Vincent Poor, Dustin Niyato, and Richard Bean. A coalition

formation game framework for peer-to-peer energy trading. *Applied Energy*, 261(January):114436, 2020.

[107] Zhenyuan Zhang, Haoyue Tang, Peng Wang, Qi Huang, and Wei Jen Lee. Two-Stage Bidding Strategy for Peer-to-Peer Energy Trading of Nanogrid. *IEEE Transactions on Industry Applications*, 56(2):1000–1009, 2020.

[108] Amrit Paudel, Kalpesh Chaudhari, Chao Long, and Hoay Beng Gooi. Peer-to-peer energy trading in a prosumer-based community microgrid: A game-theoretic model. *IEEE Transactions on Industrial Electronics*, 66(8):6087–6097, 2019.

[109] Chenghua Zhang, Jianzhong Wu, Yue Zhou, Meng Cheng, and Chao Long. Peer-to-Peer energy trading in a Microgrid. *Applied Energy*, 220(February):1–12, 2018.

[110] Rui Jing, Mei Na Xie, Feng Xiang Wang, and Long Xiang Chen. Fair P2P energy trading between residential and commercial multi-energy systems enabling integrated demand-side management. *Applied Energy*, 262(January):114551, 2020.

[111] Jaysson Guerrero, Archie C Chapman, and Gregor Verbič. Decentralized p2p energy trading under network constraints in a low-voltage network. *IEEE Transactions on Smart Grid*, 10(5):5163–5173, 2018.

[112] Jaysson Guerrero, Archie C Chapman, and Gregor Verbič. Local energy markets in lv networks: Community based and decentralized p2p approaches. In *2019 IEEE Milan PowerTech*, pages 1–6. IEEE, 2019.

[113] Kaixuan Chen, Jin Lin, and Yonghua Song. Trading strategy optimization for a prosumer in continuous double auction-based peer-to-peer market: A prediction-integration model. *Applied energy*, 242:1121–1133, 2019.

[114] Zibo Wang, Xiaodan Yu, Yunfei Mu, and Hongjie Jia. A distributed Peer-to-Peer energy transaction method for diversified prosumers in Urban Community Microgrid System. *Applied Energy*, 260(92):114327, 2020.

[115] Jema Sharin PankiRaj, Abdulsalam Yassine, and Salimur Choudhury. An auction mechanism for profit maximization of peer-to-peer energy trading in smart grids. *Procedia Computer Science*, 151(2018):361–368, 2019.

[116] Mohsen Khorasany, Yateendra Mishra, and Gerard Ledwich. Design of auction-based approach for market clearing in peer-to-peer market platform. *The Journal of Engineering*, 2019(18):4813–4818, 2019.

[117] Pablo Baez-Gonzalez, Enrique Rodriguez-Diaz, Miguel A. Ridao Carlini, and Carlos Bordons. A Power P2P Market Framework to Boost Renewable Energy Exchanges in Local Microgrids. *SEST 2019 - 2nd International Conference on Smart Energy Systems and Technologies*, 2019.

[118] Guodong Liu, Yan Xu, and Kevin Tomsovic. Bidding strategy for microgrid in day-ahead market based on hybrid stochastic/robust optimization. *IEEE Transactions on Smart Grid*, 7(1):227–237, 2016.

[119] Xinyue Chang, Yinliang Xu, and Hongbin Sun. Vertex scenario-based robust peer-to-peer transactive energy trading in distribution networks. *International Journal of Electrical Power and Energy Systems*, 138(December 2021):107903, 2022.

[120] Guanguan Li, Qiqiang Li, Xue Yang, and Ran Ding. International Journal of Electrical Power and Energy Systems General Nash bargaining based direct P2P energy trading among prosumers under multiple uncertainties. *International Journal of Electrical Power and Energy Systems*, 143(January):108403, 2022.

[121] Hossein Nezamabadi and Vahid Vahidinasab. Arbitrage Strategy of Renewable-Based Microgrids via Peer-to-Peer Energy-Trading. *IEEE Transactions on Sustainable Energy*, 12(2):1372–1382, 2021.

[122] Zheming Liang, Tao Chen, Hajir Pourbabak, and Wencong Su. Robust distributed energy resources management for microgrids in a retail electricity market. *2017 North American Power Symposium, NAPS 2017*, 2017.

[123] Yuanxing Xia, Qingshan Xu, Haiya Qian, and Li Cai. Peer-to-Peer energy trading considering the output uncertainty of distributed energy resources. *Energy Reports*, 8:567–574, 2022.

[124] Liudong Chen, Nian Liu, Chenchen Li, and Jianhui Wang. Peer-to-Peer Energy Sharing with Social Attributes: A Stochastic Leader-Follower Game Approach. *IEEE Transactions on Industrial Informatics*, 17(4):2545–2556, 2021.

[125] Jose Luis Crespo-Vazquez, Tarek Alskaif, Angel Manuel Gonzalez-Rueda, and Madeleine Gibescu. A Community-Based Energy Market Design Using Decentralized Decision-Making under Uncertainty. *IEEE Transactions on Smart Grid*, 12(2):1782–1793, 2021.

[126] Jiayong Li, Mohammad E. Khodayar, Jianhui Wang, and Bin Zhou. Data-driven Distributionally Robust Co-optimization of P2P Energy Trading and Network Operation for Interconnected Microgrids. *IEEE Transactions on Smart Grid*, 3053(c):1–1, 2021.

[127] Chun Wei, Zhuzheng Shen, Dongliang Xiao, Licheng Wang, Xiaoqing Bai, and Haoyong Chen. An optimal scheduling strategy for peer-to-peer trading in interconnected microgrids based on RO and Nash bargaining. *Applied Energy*, 295(April):117024, 2021.

[128] Mehdi Mehdinejad, Heidar Ali Shayanfar, Behnam Mohammadi-Ivatloo, and Hamed Nafisi. Designing a Robust Decentralized Energy Transactions Framework for Active Prosumers in Peer-to-Peer Local Electricity Markets. *IEEE Access*, 10:26743–26755, 2022.

[129] Yuanxing Xia, Qingshan Xu, Yu Huang, Yihan Liu, and Fangxing Li. Preserving Privacy in Nested Peer-to-Peer Energy Trading in Networked Microgrids Considering. 14(8), 2022.

[130] Luhao Wang, Yumin Zhang, Wen Song, and Qiqiang Li. Stochastic Cooperative Bidding Strategy for Multiple Microgrids with Peer-to-Peer Energy Trading. *IEEE Transactions on Industrial Informatics*, 18(3):1447–1457, 2022.

[131] Yuanxing Xia, Qingshan Xu, Siyu Tao, Pengwei Du, Yixing Ding, and Jicheng Fang. Preserving operation privacy of peer-to-peer energy transaction based on Enhanced Benders Decomposition considering uncertainty of renewable energy generations. *Energy*, 250:123567, 2022.

[132] Su Nguyen, Wei Peng, Peter Sokolowski, Damminda Alahakoon, and Xinghuo Yu. Optimizing rooftop photovoltaic distributed generation with battery storage for peer-to-peer energy trading. *Applied Energy*, 228:2567–2580, 2018.

[133] Alexandra Lüth, Jan Martin Zepter, Pedro Crespo del Granado, and Ruud Egging. Local electricity market designs for peer-to-peer trading: The role of battery flexibility. *Applied Energy*, 229:1233–1243, 2018.

[134] Weigang Hou, Lei Guo, and Zhaolong Ning. Local electricity storage for blockchain-based energy trading in industrial internet of things. *IEEE Transactions on Industrial Informatics*, 15(6):3610–3619, 2019.

[135] Thomas Morstyn, Alexander Teytelboym, and Malcolm D. Mcculloch. Bilateral contract networks for peer-to-peer energy trading. *IEEE Transactions on Smart Grid*, 10(2):2026–2035, 2019.

[136] Etienne Sorin, Lucien Bobo, and Pierre Pinson. Consensus-based approach to peer-to-peer electricity markets with product differentiation. *IEEE Transactions on Power Systems*, 34(2):994–1004, 2019.

[137] Fengji Luo, Zhao Yang Dong, Gaoqi Liang, Junichi Murata, and Zhao Xu. A distributed electricity trading system in active distribution networks based on multi-agent coalition and blockchain. *IEEE Transactions on Power Systems*, 34(5):4097–4108, 2019.

[138] Jiawen Kang, Rong Yu, Xumin Huang, Sabita Maharjan, Yan Zhang, and Ekram Hossain. Enabling localized peer-to-peer electricity trading among plug-in hybrid electric vehicles using consortium blockchains. *IEEE Transactions on Industrial Informatics*, 13(6):3154–3164, 2017.

[139] Zhetao Li, Jiawen Kang, Rong Yu, Dongdong Ye, Qingyong Deng, and Yan Zhang. Consortium blockchain for secure energy trading in industrial internet of things. *IEEE Transactions on Industrial Informatics*, 14(8):3690–3700, 2018.

[140] Ismael El-Samahy, Kankar Bhattacharya, Claudio Cañizares, Miguel F. Anjos, and Jiuping Pan. A procurement market model for reactive power services considering system security. *IEEE Transactions on Power Systems*, 23(1):137–149, 2008.

[141] Linquan Bai, Jianhui Wang, Chengshan Wang, Chen Chen, and Fangxing Li. Distribution Locational Marginal Pricing (DLMP) for Congestion Management and Voltage Support. *IEEE Transactions on Power Systems*, 33(4):4061–4073, 2018.

[142] Zhifang Yang, Haiwang Zhong, Anjan Bose, Tongxin Zheng, Qing Xia, and Chongqing Kang. A Linearized OPF Model with Reactive Power and Voltage Magnitude: A Pathway to Improve the MW-Only DC OPF. *IEEE Transactions on Power Systems*, 33(2):1734–1745, 2018.

[143] Zhifang Yang, Haiwang Zhong, Qing Xia, and Chongqing Kang. Solving opf using linear approximations: fundamental analysis and numerical demonstration. *IET Generation, Transmission & Distribution*, 11(17):4115–4125, 2017.

[144] Zhifang Yang, Haiwang Zhong, Anjan Bose, Qing Xia, and Chongqing Kang. Optimal power flow in ac–dc grids with discrete control devices. *IEEE Transactions on Power Systems*, 33(2):1461–1472, 2018.

[145] Yuntao Ju, Can Chen, Linlin Wu, and Hui Liu. General three-phase linear power flow for active distribution networks with good adaptability under a polar coordinate system. *IEEE Access*, 6:34043–34050, 2018.

[146] Parikshit Pareek and Ashu Verma. Piecewise linearization of quadratic branch flow limits by irregular polygon. *IEEE Transactions on Power Systems*, 33(6):7301–7304, 2018.

[147] X. J. Zeng, H. F. Zhai, M. X. Wang, M. Yang, and M. Q. Wang. A system optimization method for mitigating three-phase imbalance in distribution network. *International Journal of Electrical Power and Energy Systems*, 113(April):618–633, 2019.

[148] Salar Naghdalian, Turaj Amraee, and Sadegh Kamali. Linear daily UC model to improve the transient stability of power system. *IET Generation, Transmission and Distribution*, 13(13):2877–2888, 2019.

[149] Tohid Akbari and Mohammad Tavakoli Bina. A linearized formulation of AC multi-year transmission expansion planning: A mixed-integer linear programming approach. *Electric Power Systems Research*, 114:93–100, 2014.

[150] Michael D. Sankur, Roel Dobbe, Emma Stewart, Duncan S. Callaway, and Daniel B. Arnold. A Linearized Power Flow Model for Optimization in Unbalanced Distribution Systems. (June), 2016.

[151] Shouxiang Wang, Sijia Chen, Leijiao Ge, and Lei Wu. Distributed Generation Hosting Capacity Evaluation for Distribution Systems Considering the Robust Optimal Operation of OLTC and SVC. *IEEE Transactions on Sustainable Energy*, 7(3):1111–1123, 2016.

[152] Ragheb Rahmaniani, Shabbir Ahmed, Teodor Gabriel Crainic, Michel Gendreau, and Walter Rei. The benders dual decomposition method. *Operations Research*, 68(3):878–895, 2020.

[153] Jikai Zou, Shabbir Ahmed, and Xu Andy Sun. Stochastic dual dynamic integer programming. *Mathematical Programming*, 175(1):461–502, 2019.

[154] Martin N Hjelmeland, Jikai Zou, Arild Helseth, and Shabbir Ahmed. Nonconvex medium-term hydropower scheduling by stochastic dual dynamic integer programming. *IEEE Transactions on Sustainable Energy*, 10(1):481–490, 2018.

[155] Franco Quezada, Céline Gicquel, and Safia Kedad-Sidhoum. Combining polyhedral approaches and stochastic dual dynamic integer programming for solving the uncapacitated lot-sizing problem under uncertainty. *INFORMS Journal on Computing*, 34(2):1024–1041, 2022.

[156] Janina Struth, Matthias Leuthold, Astrid Aretz, and M Bost. PV-Benefit: a critical review of the effect of grid integrated PV-storage-systems. *8th International Renewable Energy Storage Conference and Exhibition*, (January 2015):1–10, 2013.

[157] Federal Energy Regulatory Commission. Order 2222: Participation of distributed energy resources aggregations in markets operated by RTO and ISO. 86(59):5–24, 2021.

[158] Giulia De Zotti, S. Ali Pourmousavi, Henrik Madsen, and Niels Kjolstad Poulsen. Ancillary Services 4.0: A Top-To-Bottom Control-Based Approach for Solving Ancillary Services Problems in Smart Grids. *IEEE Access*, 6:11694–11706, 2018.

[159] F Fran Li. *A Preliminary Analysis of the Economics of Using Distributed Energy as a Source of Reactive Power Supply First Quarterly Report for Fiscal Year 2006*. Number April. 2006.

[160] Yue Zhou, Jianzhong Wu, Chao Long, and Wenlong Ming. State-of-the-Art Analysis and Perspectives for Peer-to-Peer Energy Trading. *Engineering*, 6(7):739–753, 2020.

[161] Lahanda Purage Mohasha Isuru Sampath, Amrit Paudel, Hung D. Nguyen, Eddy Y.S. Foo, and Hoay Beng Gooi. Peer-to-Peer Energy Trading Enabled Optimal Decentralized Operation of Smart Distribution Grids. *IEEE Transactions on Smart Grid*, PP(c):1, 2021.

[162] Daryn Negmetzhanov, H. S.V.S.Kumar Nunna, Pierluigi Siano, and Suryanarayana Doolla. Peer-to-Peer Bundled Energy Trading with Game Theoretic Approach. *2021 IEEE Texas Power and Energy Conference, TPEC 2021*, (1):1–6, 2021.

[163] Adam Potter, Rabab Haider, and Anuradha M. Annaswamy. Reactive Power Markets for the Future Grid. pages 1–9, 2021.

[164] Qian Hu, Ziqing Zhu, Siqi Bu, Ka Wing Chan, and Fangxing Li. A multi-market nanogrid P2P energy and ancillary service trading paradigm: Mechanisms and implementations. *Applied Energy*, 293(December 2020):116938, 2021.

[165] Martha N. Acosta, Francisco Gonzalez-Longatt, Danijel Topić, and Manuel A. Andrade. Optimal microgrid–interactive reactive power management for day–ahead operation. *Energies*, 14(5):1–20, 2021.

[166] Meysam Doostizadeh, Mojtaba Khanabadi, and Masood Ettehadi. Reactive Power Provision from Distributed Energy Resources in Market Environment. *26th Iranian Conference on Electrical Engineering, ICEE 2018*, pages 1362–1367, 2018.

[167] Mansour Alramlawi, Erfan Mohagheghi, and Pu Li. Predictive active-reactive optimal power dispatch in PV-battery-diesel microgrid considering reactive power and battery lifetime costs. *Solar Energy*, 193(March):529–544, 2019.

[168] Cedrick Lupangu, Jackson J. Justo, and Ramesh C. Bansal. Model Predictive for Reactive Power Scheduling Control Strategy for PV-Battery Hybrid System in Competitive Energy Market. *IEEE Systems Journal*, 14(3):4071–4078, 2020.

[169] Oscar Danilo Montoya and Walter Gil-González. Dynamic active and reactive power compensation in distribution networks with batteries: A day-ahead economic dispatch approach. *Computers and Electrical Engineering*, 85(40), 2020.

[170] Zhong Zhang, Ran Li, and Furong Li. A Novel Peer-to-Peer Local Electricity Market for Joint Trading of Energy and Uncertainty. *IEEE Transactions on Smart Grid*, 11(2):1205–1215, 2020.

[171] Pierluigi Siano and Dolatabadi Mohammad. MILP Optimization model for assessing the participation of distributed residential PV-battery systems in ancillary services market. *CSEE Journal of Power and Energy Systems*, 7(2):348–357, 2021.

[172] Hao Hsiang Wu and Simge Küçükyavuz. A two-stage stochastic programming approach for influence maximization in social networks. *Computational Optimization and Applications*, 69(3):563–595, 2018.

[173] Amin Safari, Pouya Salyani, and Mehdi Hajiloo. Reactive power pricing in power markets: a comprehensive review. *International Journal of Ambient Energy*, 41(13):1548–1558, 2020.

[174] Luca Mazzola, Alexander Denzler, and Ramon Christen. Towards a Peer-to-Peer Energy Market: an Overview. 2020.

[175] Chenghua Zhang, Jianzhong Wu, Meng Cheng, Yue Zhou, and Chao Long. A Bidding System for Peer-to-Peer Energy Trading in a Grid-connected Microgrid. *Energy Procedia*, 103(April):147–152, 2016.

[176] Sarineh Hacopian Dolatabadi, Maedeh Ghorbanian, Pierluigi Siano, and Nikos D. Hatziargyriou. An Enhanced IEEE 33 Bus Benchmark Test System for Distribution System Studies. *IEEE Transactions on Power Systems*, 36(3):2565–2572, 2021.

Appendix A

List of Publications

In this chapter, the list of publications both journals and conferences papers, derived from the development of the thesis are presented.

A.1 Journal articles

- García-Muñoz, F., Díaz-González, F., & Corchero, C. (2020). A Mathematical Model for the Scheduling of Virtual Microgrids Topology into an Active Distribution Network. Applied Sciences, 10(20), 7199, doi: 10.3390/app10207199.

- García-Muñoz, F., Díaz-González, F., & Corchero, C. (2021). A novel algorithm based on the combination of AC-OPF and GA for the optimal sizing and location of DERs into distribution networks. Sustainable Energy, Grids and Networks, 27, doi: 10.1016/j.segan.2021.100497.

- García-Muñoz, F., Díaz-González, F., & Corchero, C. (2022). A two-stage stochastic programming model for the sizing and location of DERs considering electric vehicles and demand response. Sustainable Energy, Grids and Networks, 100624, doi: 10.1016/j.segan.2022.100624.

- García-Muñoz, F., Díaz-González, F., & Corchero, C. (2022). P2P Energy Trading Model for a Local Electricity Community Considering Technical Constraints. ICSC-Cities 2021, CCIS 1555, pp. 1–12, 2022, doi: 10.1007/978-3-030-96753-620.

- García-Muñoz, F., Dávila, S., & Quezada, F. (2022). A Benders decomposition approach for solving a two-stage local energy market problem under uncertainty. Submitted to Applied Energy.

- García-Muñoz, F., Teng, F., Junyent-Ferré, A., & Díaz-González, F, & Corchero, C. (2022). Stochastic optimization-based community energy trading approach to offer reactive power from distributed energy resources for ancillary services market. Submitted to Sustainable Energy, Grids and Networks.

A.2 Conference articles

- F. García-Muñoz, F. Díaz-Gonzalez, C. Corchero and C. Nuñez-de-Toro, "Optimal Sizing and Location of Distributed Generation and Battery Energy Storage System," 2019 IEEE PES Innovative Smart Grid Technologies Europe (ISGT-Europe), 2019, pp. 1-5, doi: 10.1109/ISGTEurope.2019.8905609.

- F. García-Muñoz, F. Díaz-Gonzalez, C. Corchero, "Economic profit variability of photovoltaic-battery systems for distribution networks," World Sustainable Energy Days, Wels, Austria (2020).

A.3 Other publications

Within this section other relevant publications not directly related to the thesis are introduced.

- Fredes, H. V., Acosta, B., Olivares, M., García-Muñoz, F., Tobar, F., Toro, V., & Becker, C. (2021). Impact of Energy Price Stabilization Mechanism on Regulated Clients' Tariffs: The Case of Chile. Sustainability, 13(21), 11870, doi: 10.3390/su132111870.

- Verdejo, H.; Holz, M.; Becker, C.; García-Muñoz, F. Mechanism for Financing the Accumulated Debt of Utility Services Water, Electricity and Gas as a Result of the COVID-19. Sustainability 2022, 14, 3617, doi: 10.3390/su14063617.

- García-Muñoz, F.; Alfaro, M.; Fuertes, G.; Vargas, M. DC Optimal Power Flow Model to Assess the Irradiance Effect on the Sizing and Profitability of the PV-Battery System. Energies 2022, 15, 4408. https://doi.org/10.3390/en15124408

- Fredes, H. V., García-Muñoz, F. Tobar, F., Olivares. M., & Becker, C. (2022) Retail Electricity Market Liberalization: An overview of international experience and effects on the Chilean regulated tariff. Submitted to Energy Reports.